AFWAL-TR-80-1088 /

AD A094465

ESTIMATION AND STATISTICAL AVERAGING APPLIED TO
REDUNDANT STRAPPED DOWN INERTIAL SENSORS FOR
NAVIGATION AND FLIGHT CONTROL

Jack W. Bell

LEVEL II

September 1980

DTIC
ELECTE
FEB 0 3 1981
E

TECHNICAL REPORT AFWAL-TR-80-1088

Final Report for Period 1 August 1978 - 1 February 1980.

Approved for public release; distribution unlimited.

AVIONICS LABORATORY
AIR FORCE WRIGHT AERONAUTICAL LABORATORIES
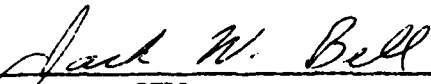AIR FORCE SYSTEMS COMMAND
WRIGHT-PATTERSON AIR FORCE BASE, OHIO 45433

81 2 03 032

JACK. W. BELL
Project Engineer
Advanced Aircraft Navigation

WILLIAM H. BLOCK, Major, USAF
Program Mgr. Adv Aircraft Navigation
System Avionics Division

FOR THE COMMANDER

RONALD L. RINGO, Chief
Reference Systems Branch
Systems Avionics Division

REPORT DOCUMENTATION PAGE		READ INSTRUCTIONS BEFORE COMPLETING FORM
1. REPORT NUMBER AFWAL-TR-80-1088	2. GOVT ACCESSION NO. AD-A094 465	3. RECIPIENT'S CATALOG NUMBER
4. TITLE (and Subtitle) ESTIMATION AND STATISTICAL AVERAGING APPLIED TO REDUNDANT STRAPPED DOWN INERTIAL SENSORS FOR NAVIGATION AND FLIGHT CONTROL		5. TYPE OF REPORT & PERIOD COVERED Final Report for Period 1 Aug 1978 — 1 Feb 1980
		6. PERFORMING ORG. REPORT NUMBER
7. AUTHOR(s) Jackie W. Bell		8. CONTRACT OR GRANT NUMBER(s) 143
9. PERFORMING ORGANIZATION NAME AND ADDRESS Avionics Laboratory (AFWAL/AAAN-1) Air Force Wright Aeronautical Laboratories(AFSC) Wright-Patterson Air Force Base, Ohio 45433		10. PROGRAM ELEMENT, PROJECT, TASK AREA & WORK UNIT NUMBERS 666A/03 36 03
11. CONTROLLING OFFICE NAME AND ADDRESS Avionics Laboratory (AFWAL/AAAN-1) Air Force Wright Aeronautical Laboratories (AFSC) Wright-Patterson Air Force Base, Ohio 45433		12. REPORT DATE September 1980
		13. NUMBER OF PAGES 144
14. MONITORING AGENCY NAME & ADDRESS(If different from Controlling Office)		15. SECURITY CLASS. (of this report) Unclassified
		15a. DECLASSIFICATION/DOWNGRADING SCHEDULE

16. DISTRIBUTION STATEMENT (of this Report)

Approved for public release; distribution unlimited.

17. DISTRIBUTION STATEMENT (of the abstract entered in Block 20, if different from Report)

18. SUPPLEMENTARY NOTES

19. KEY WORDS (Continue on reverse side if necessary and identify by block number)

Inertial Navigation, Strapped Down Inertial Sensors, Failure Detection, & Isolation

20. ABSTRACT (Continue on reverse side if necessary and identify by block number)

The concept of providing inertial data to satisfy on-board avionic functions from an integrated, strapped down, redundant inertial sensor reference system is presently receiving attention for military and commercial aircraft applications. Strapped down inertial sensors are well suited for flight control. However, in the highly dynamic environment of high-performance aircraft, the present accuracy provided by strapped down inertial reference systems (IRS) is insufficient to meet navigation and weapon delivery requirements. Performance

DD FORM 1473 EDITION OF 1 NOV 65 IS OBSOLETE
1 JAN 73

improvement of an IRS employing redundant strapped down inertial sensors of a specified ensemble is the subject of this study.

Two techniques to improve the performance are considered. One technique is to combine all redundant data from non-failed sensors, through a statistical average, into an orthogonal-triad inertial reference frame. This is accomplished by weighted-least-squares averaging.

A second technique is the use of an improved gyro and accelerometer output and output-rate estimation scheme. Estimation algorithms are developed using Kalman Filter theory, and evaluated in a highly dynamic environment.

Least-squares averaging of the redundant sensor data can significantly improve the navigation system performance. However, sensor misalignment errors must be minimized such that they are not the dominant sensor error source.

Improved estimates of the sensors output and output-rate were obtained. The sensor output estimates are beneficial in a failure detection and isolation algorithm for establishing and maintaining variable failure thresholds which are necessary in the highly dynamic environment of fighter aircraft. The output-rate estimates provide improved reference data for flight control and weapon delivery computation.

FOREWORD

Accession For	
NTIS GRA&I	☒
DTIC TAB	☐
Unannounced	☐
Justification	
By	
Distribution/	
Availability Codes	
Dist	Avail and/or Special
A	

AFWAL-TR-80-1088

TABLE OF CONTENTS

LIST OF ILLUSTRATIONS

LIST OF ILLUSTRATIONS (CONTINUED)

LIST OF ILLUSTRATIONS (CONTINUED)

LIST OF ILLUSTRATIONS (CONTINUED)

LIST OF ILLUSTRATIONS (CONTINUED)

LIST OF ILLUSTRATIONS (CONCLUDED)

LIST OF TABLES

SECTION I

INTRODUCTION

Strapped down inertial reference systems are receiving considerable attention for aircraft, missile, and space applications. Included among the most recent publications in this area are those by Burns (Reference 1), Harrington, et al. (Reference 2), Kubatt (Reference 3), Elson (Reference 4), Johnson, et al. (Reference 5), Lipscomb, et al. (Reference 6), and Reynolds (Reference 7). Of particular interest are those systems incorporating strapped down inertial sensors in a redundant configuration. These systems are being developed to provide the combined kinematic data requirements of flight control, navigation, weapon delivery, and other on-board avionic functions. Development of this concept is directed toward providing a high probability of mission success and possible reduction in avionic system life cycle costs.

A high probability of mission success can be achieved through implementation of a fault tolerant system employing effective Failure Detection and Isolation (FDI) techniques, and Redundancy Management (RM) algorithms. Reduction in life cycle costs should be obtained through reduction of the number of inertial sensors required, and through commonality of these sensors and associated software resulting from utilization of redundant inertial reference sensors.

If this concept is to be successfully employed, the requirements of all avionic functions utilizing the inertial reference data must be satisfied. Present state-of-the-art strapped down inertial reference systems do not meet all requirements in the dynamic environment of a highly maneuvering, high-performance type aircraft. Specifically, the velocity and position performance for navigation and weapon delivery, in a highly maneuvering dynamic environment, is typically in excess of specified requirements.

In addition, establishing and maintaining realistic FDI threshold levels presents problems of some concern. To accomplish this, some type of filtering of the inertial sensor outputs is needed and variable FDI

threshold level algorithms are required. FDI algorithms have received, and are continuing to receive, considerable attention. Daly et al. (Reference 8), investigated FDI algorithms with constant level thresholds. Motyka and Bell (Reference 9), extended this investigation to include variable FDI thresholds for the high performance aircraft environment.

This technical report addresses the investigation of algorithms for filtering the inertial sensor outputs, estimating the time rate of change of the sensor outputs, and statistical averaging of data from a set of strapped down, redundant, inertial sensors in skewed configurations. Filtering and estimation of the inertial sensor output is accomplished by a two-state Kalman filter algorithm. One state variable provides an estimate of the sensor output in the presence of noise. This estimate can be utilized directly in an FDI algorithm for establishing and maintaining medium and soft failure threshold levels, and in the navigation, flight control, and weapon delivery functions. The second state variable provides an estimate of the inertial sensor output time rate of change for utilization in the flight control and weapon delivery functions. Statistical averaging of the redundant inertial sensor data is accomplished by a weighted least-squares algorithm to improve position and velocity performance for navigation and weapon delivery.

The estimation algorithms are discussed in Section II. Statistical averaging of the redundant inertial sensor data is discussed in Section III. The simulation program used during the conduct of this investigation is discussed in Section IV. A discussion of results and conclusions are presented in Section V.

SECTION II

ESTIMATION ALGORITHMS

1. GENERAL DISCUSSION

The need to improve upon strapped down inertial reference system performance in certain applications has become apparent. Specifically, improvement is needed to meet navigation and weapon delivery requirements for applications in highly maneuvering aircraft. This need has been verified by recent studies which were discussed in Section I. A need also exists in some flight control system applications for improved methods of estimating the time rate of change of vehicle angular rates and body accelerations.

Velocity errors derive from specific force measurement error due to accelerometer bias, scale factor error, input axis misalignment, some higher order errors, and to imperfect attitude matrix computation. Attitude and attitude rate errors derive from gyro errors including drift, scale factor error, and input axis mislaignment. Drift errors are dependent upon the type of gyro being used. Laser gyro drift, termed g-insensitive drift, is not influenced by gravity (g). On the other hand, rotating mass gyro drift includes g-insensitive, g-sensitive, and g^2-sensitive components. Of the gyro and accelerometer errors, all are random with the exception of input axis misalignment. The input axis misalignment error is random only in the sense of inability to achieve initially accurate sensor alignment and repeatable alignment due to maintenance procedures.

To satisfy the inertial reference needs of navigation and weapon delivery, the strapped down inertial reference system must perform the functions depicted in Figure 1. These functions are to determine a body attitude matrix which contains the relative angular information between the body coordinate frame and the navigation coordinate frame, and to resolve the compensated velocity changes through this transformation matrix. The navigation algorithm then calculates velocity and position in the navigation frame.

3
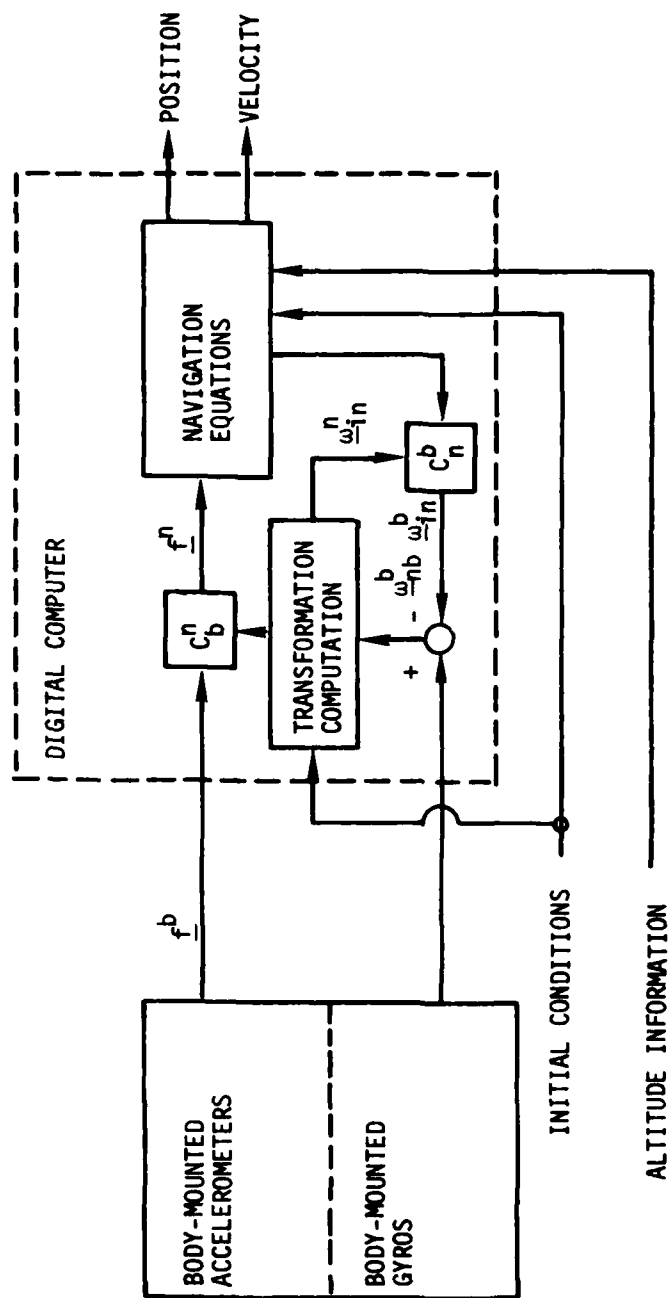
Figure 1. Strapped Down Geographic Local-Level Navigation System Mechanization

4

The attitude matrix is derived and updated through measurements of the gyro outputs. Several algorithms have been developed over the years to accomplish the attitude matrix functions. Two of these are implemented in the simulation program used for this investigation. They are the classical direction cosine mechanization and a quaternion mechanization. The quaternion mechanization is used in most state-of-the-art strapped down inertial navigation systems because of its reported capabilities of smaller computational errors, and reduced processing time and storage requirements. The rate of updating the transformation matrix is of prime importance when considering system performance. However, for this investigation it is not one of the factors considered. An in-depth analysis of inertial navigation systems is presented by Britting (Reference 10).

The transformation matrix mechanization utilizes the gyro outputs to establish and update the body attitude matrix. However, the gyro outputs are angular changes and not angular rates as required for this computation. Thus, the angular rates must be estimated from the gyro incremental angular output. The typical method of estimating the angular rates ω_i from the incremental angular changes $\Delta\theta_i$ is by piecewise constant outputs as follows.

$$\hat{\omega}_i(t) = \frac{\Delta\theta_i(t_n)}{\Delta t} = \frac{\theta_i(t_n)-\theta_i(t_{n-1})}{t_n-t_{n-1}} \tag{1}$$

where

i = x, y, z, gyro axes

t = time and $t_{n-1} < t \le t_n$

t_n = time of nth update

$\Delta t = t_n - t_{n-1}$ is the sampling interval

$\hat{\omega}_i$ = x, y, z gyro axes estimated rates

Possible areas of improving the strapped down inertial reference system to meet the accuracy and stability requirements (placed on attitude, attitude rate, and body accelerations by state-of-the-art flight control and navigation requirements) are: by improving the inertial sensors; by improving the estimation of sensor outputs; by improving the system mechanization; or by a combination of all three. Improvement through improved estimates of the time rate of change of noisy, sampled data using measurements from redundant sensors of a specified ensemble is the prime concern of this investigation. The intent is not to estimate the inertial sensor errors, but rather to obtain an improved estimate of sensor output and output-rate for utilization in the functions of flight control, navigation, and weapon delivery. Hereafter in this text, references to sensor output estimation will imply estimation of both the sensor output and output-rate.

Previous investigations have sought to improve reference system performance through integration of independent position and velocity sensors with an inertial system using some type of optimal filtering method. These efforts have generally been computer limited and error modeling has been relegated to system errors considered most important, such as position, velocity, and attitude. Some of these investigations have considered modeling of inertial sensor randon errors to estimate the errors magnitude for system update and error correction. Typically, these errors are given only a cursory glance, with gyro random bias estimation being the only error seriously investigated.

Failure to implement the random error sources in these hybrid systems has not been due to lack of interest nor desire to do so. Instead, the primary reason is the computational load involved, and typically utilization of a single general-purpose computer. Addition of the gyro and accelerometer random error sources causes the number of state variables to grow extensively, approximately by a power of three when considering full modeling of all sensors.

6

Due to significant advances in digital computer technology and computational techniques over the last few years, the computation problem should no longer be a limiting factor in modeling of the inertial sensor random errors. Avionics designers are also moving more toward distributed processing throughout the on-board avionics. Thus, one or more micro-processors can be utilized for dedicated inertial sensor and/or reference system computation. Their computational speed, small size, and relatively low cost make extensive modeling of inertial sensor random errors to accomplish optimal estimation of the sensor's output and output-rate a viable concept.

As discussed in Section I, integration of inertial sensors for flight control, navigation, and weapon delivery into a single inertial reference assembly results in a set of redundant inertial sensors. This is due to the fact that most aircraft employ redundant inertial sensors for flight control to meet flight safety requirements. Thus, data from the redundant gyros and accelerometers is available for utilization in the navigation and weapon delivery functions as well. Optimal estimation techniques are utilized to investigate the possibility of improving upon the estimate of the time rate of change of noisy vehicle angular rates and body accelerations. The estimated outputs of these redundant inertial sensors are then combined and transformed into the orthogonal-triad body reference frame through a weighted-least-squares estimator as shown by Figure 2.

It is possible to combine the sensor output estimation and weighted-least-squares estimation into one process. However, a relatively high computational rate is required for sensor output estimation while the weighted-least-squares transformation can be accomplished at a much lower rate. These two estimation processes lead to a local global processing scheme shown in Figure 3. The local processor is operated at a high data rate while the global processor is operated at some lower data rate. This technique also allows separate microprocessors for local and global processing if so desired.

7
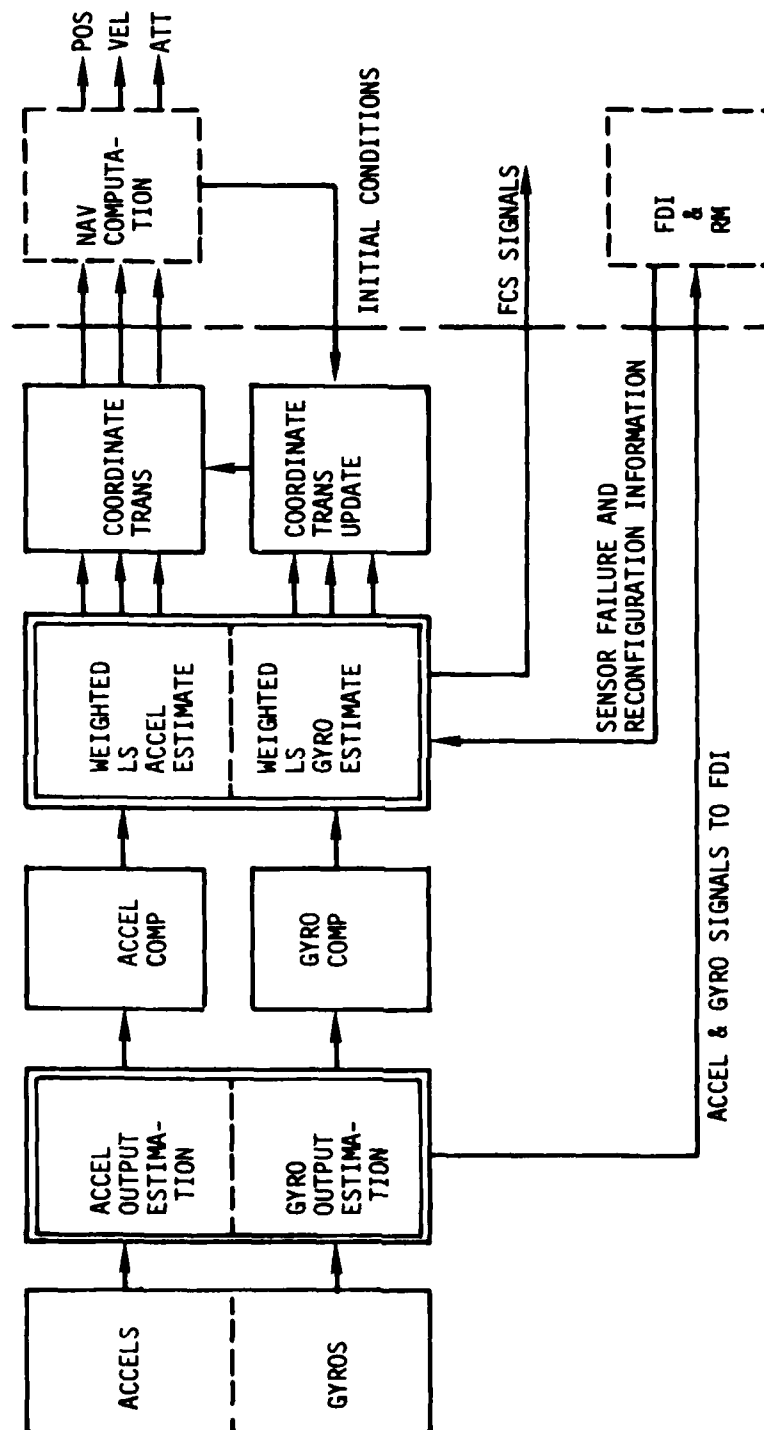
Figure 2. Redundant Sensor Output Estimation Block Diagram
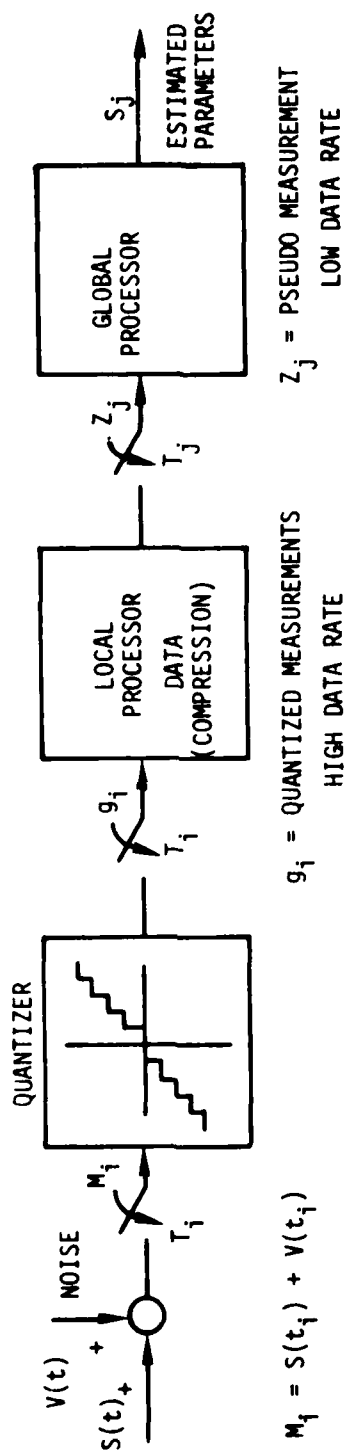
Figure 3. Estimation Algorithm Processing

9

2. SENSOR ESTIMATION ALGORITHMS

To apply optimal estimation to the inertial sensors, a model describing the inertial sensor dynamics must be developed. In view of the similarity of the gyro and accelerometer error models, one would expect to see a similarity in the dynamic models describing the sensors. As it turns out, the sensors can be represented by quite similar models. The method chosen to model the inertial sensor random errors is through combinations of the random process models presented in the Appendix.

3. GYRO MODEL

The dynamics of a gyro can be modeled by a combination of a random constant, a random ramp, and exponentially correlated random errors (Markov Processes). Block diagrams of these common random processes are shown in Figure 4. Two Markov processes deserve consideration. One has a short correlation time measuring in seconds while the second has a long correlation time measuring in minutes or hours.

The state vector differential equations of the models are as follows:

Random Constant

$$\dot{x} = 0 \tag{2}$$

Random Ramp

$$\dot{x}_1 = x_2$$

$$\dot{x}_2 = 0 \tag{3}$$

Markov Processes

Short Correlation Time Constant

$$\dot{x} = \frac{1}{\tau_1}x + u \tag{4}$$

Long Correlation Time Constant

$$\dot{x} = \frac{1}{\tau_2}x + u \tag{5}$$

where u = White Noise

τ_1, τ_2 = Short and long correlation time constant, respectively

10
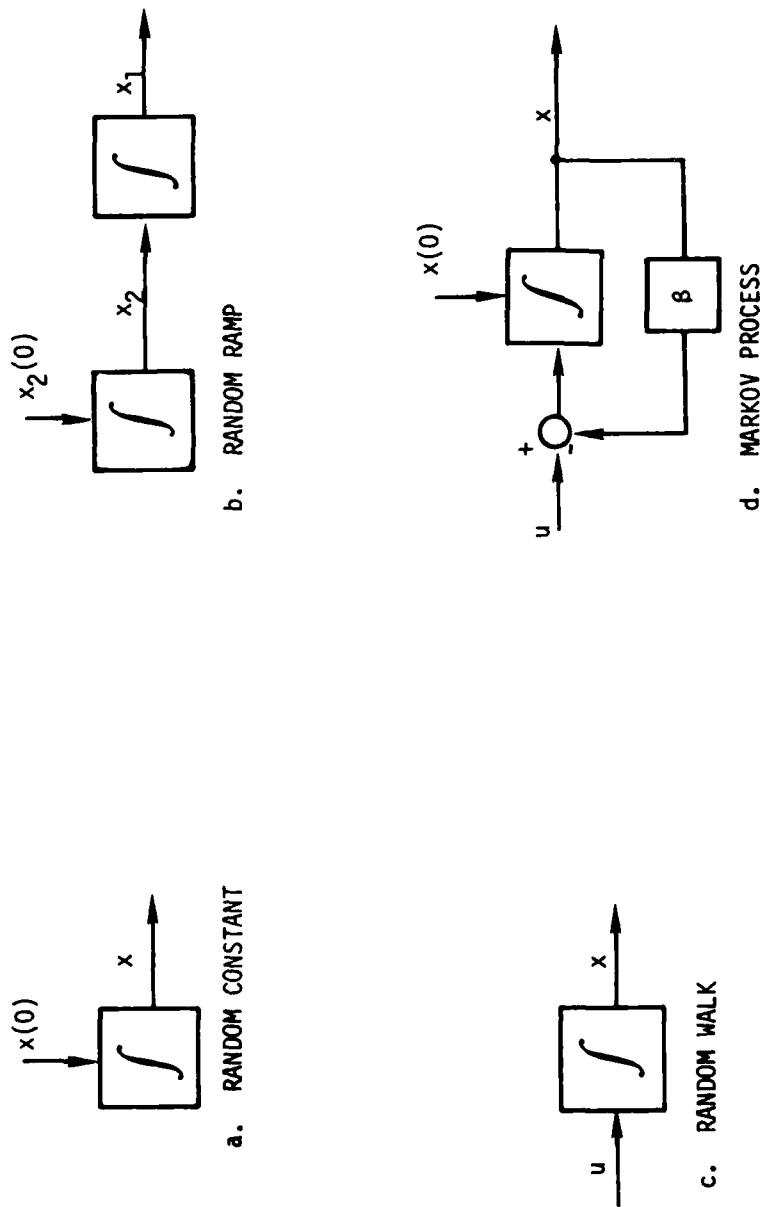
Figure 4. Common Random Process Model Block Diagrams

11

There are a number of ways these models can be combined. One way is simply to sum all of them together to form the gyro dynamic model shown in Figure 5. However, this would result in a state vector containing five state variables for each gyro.

$$\dot{x}_1 = 0$$

$$\dot{x}_2 = x_3$$

$$\dot{x}_3 = 0$$

$$\dot{x}_4 = -\alpha x_4 + u_4$$

$$\dot{x}_5 = -\beta x_5 + u_5$$

(6)

where

$$\alpha = \frac{1}{\tau_1}$$

$$\beta = \frac{1}{\tau_2}$$

The model as it stands, would result in considerable computation when redundant sensors are considered. Thus, an attempt to reduce the number of state variables in the gyro model seems in order. This results in a suboptimal estimator but the computational load and storage requirement saved when considering redundant sensors could be considerable.

Simplification can be obtained by observing the first three state variables in Equation 6, along with their appropriate block diagrams given in Figure 4, and recognizing that these three state variables can be combined into a form requiring only two state variables. Thus, a random bias and random ramp can be represented by two state variables as shown in Figure 6. The state vector differential equations for this combination are

$$\dot{x}_1 = x_2$$

$$\dot{x}_2 = 0$$

(7)
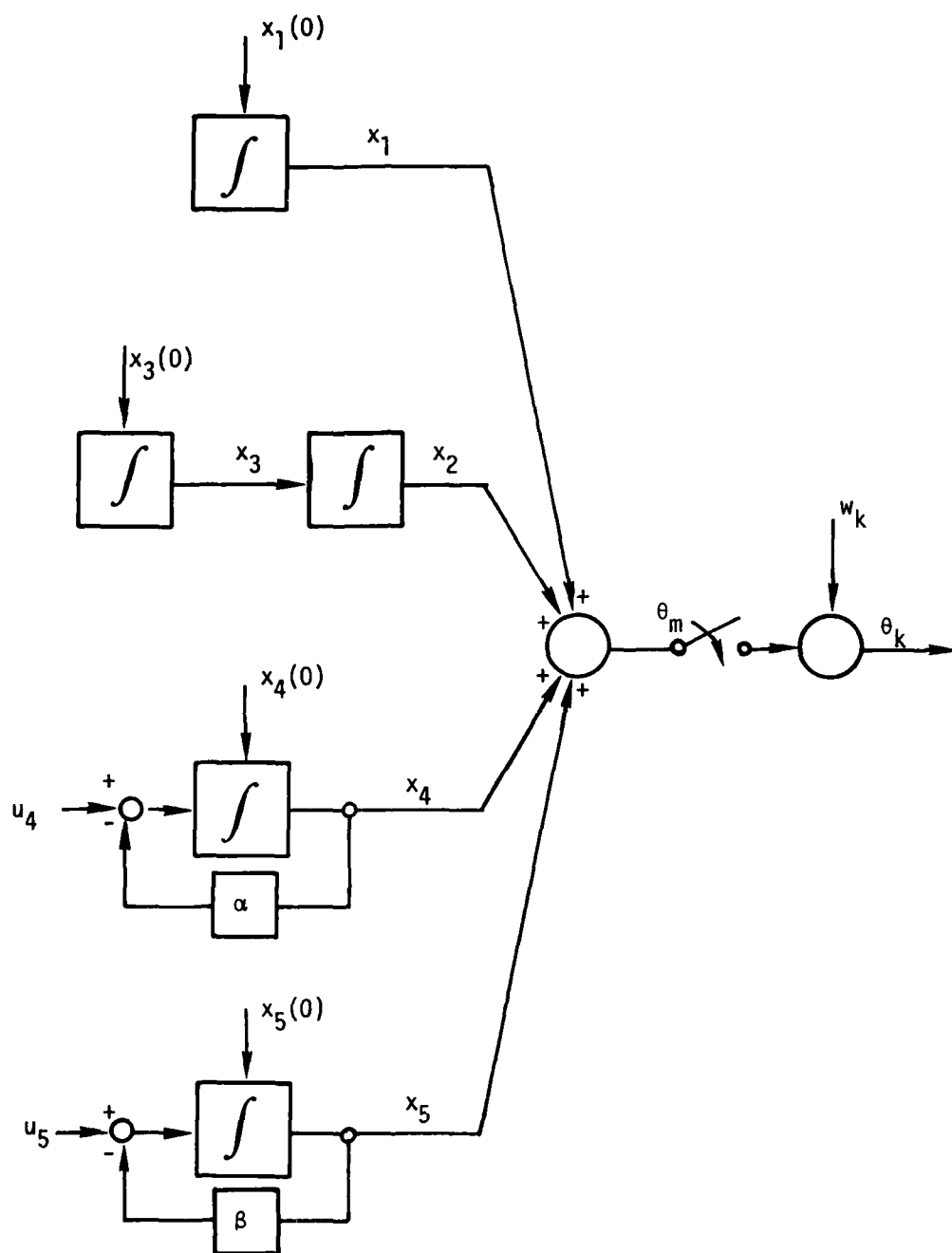
Figure 5. Five-State-Variable Model Block Diagram

13
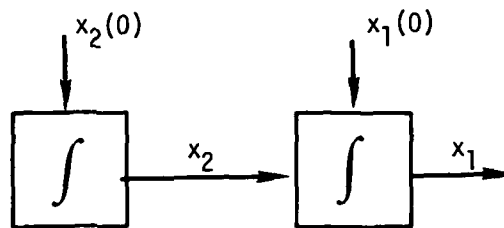
Figure 6. Random Constant and Random Ramp Block Diagram

The gyro model has now been reduced from a state vector with five state variables to one with four state variables without any loss in estimation accuracy. A block diagram of this model is shown in Figure 7. The state vector differential equations are

$$\dot{x}_1 = x_2$$

$$\dot{x}_2 = 0$$

$$\dot{x}_3 = -\alpha x_3 + u_3$$

$$\dot{x}_4 = -\beta x_4 + u_4 \tag{8}$$

Now the exponentially correlated random error with long correlation time is examined. The state differential equation for this error is given by:

$$\dot{x}_L = -\beta x_L + u_L \tag{9}$$

where

$$u_L = \text{White Noise}$$

$$\beta = \frac{1}{\tau_2}$$

$$\tau_2 = \text{Long correlation time constant}$$
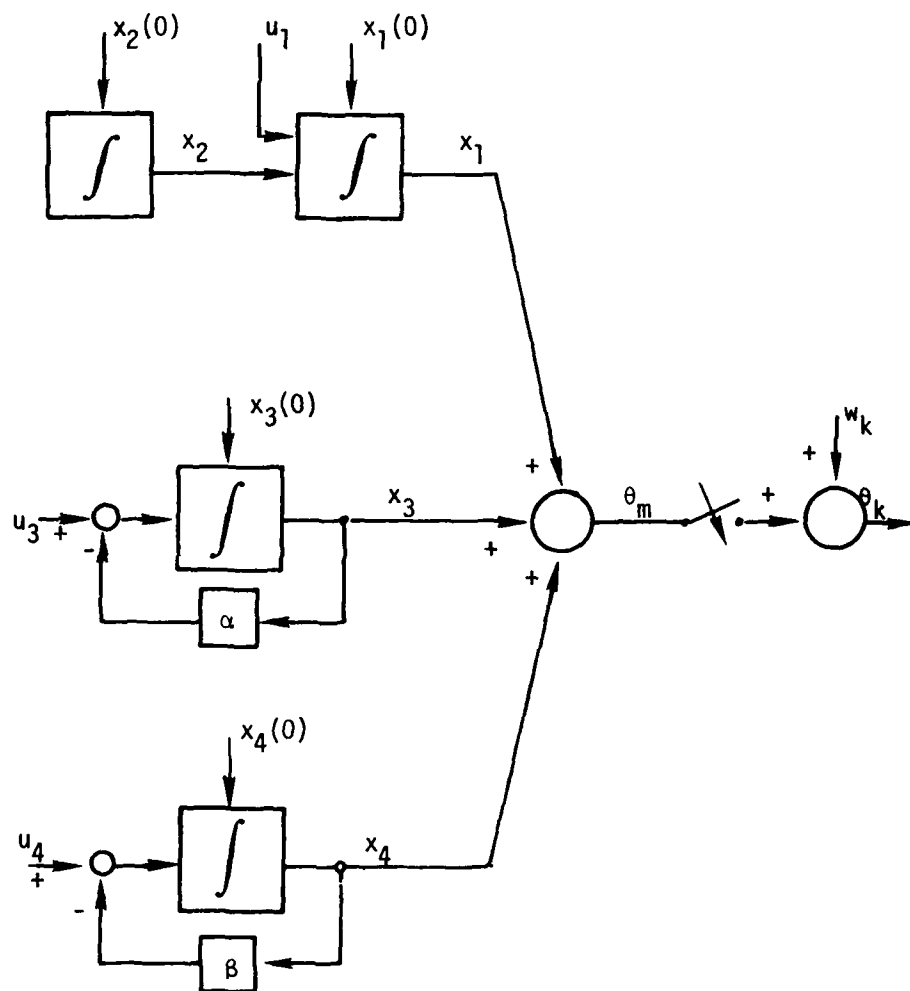
Figure 7. Four-State-Variable Model Block Diagram

15

As the correlation time constant is made large, Equation 9 assumes a
similarity with the random walk model. The random walk differential
equation is given by

$$\dot{x}_{RW} = u_{RW} \tag{10}$$

Thus, if τ_2 is very large then Equation 9 can be represented by

$$\dot{x}_L = u_L \tag{11}$$

In reality, the correlation time constant of the gyro exponentially
correlated random error is not infinite but is relatively large. Since
the time constant is large then this exponentially correlated random
error can be modeled by a random walk.

Now some equality must be established between the Power Spectral
Density (PSD) of the exponentially correlated random error white noise u_L
and the random walk white noise u_{RW}. Wauer and Bucy (Reference 11)
states that through error analysis it has been empirically found that the
best performance is obtained when the PSD amplitude of the random walk
white noise is

$$Q_{RW} = \frac{\sigma_L^2}{\tau_2} \tag{12}$$

If the exponentially correlated random error with long correlation
time constant is modeled by a random walk, then the gyro model is sub-
optimal. Even though the model is not exact, it does result in error
statistics which tend to account for unmodeled errors.

The random walk model can be combined with the random bias and
random ramp with the three random errors modeled by only two state
variables. The suboptimal gyro model block diagram is shown in
Figure 8 and the state variable differential equations are

$$\dot{x}_1 = x_2 + u_c$$

$$\dot{x}_2 = 0$$

$$\dot{x}_3 = -\alpha x_3 + u_3 \tag{13}$$

16
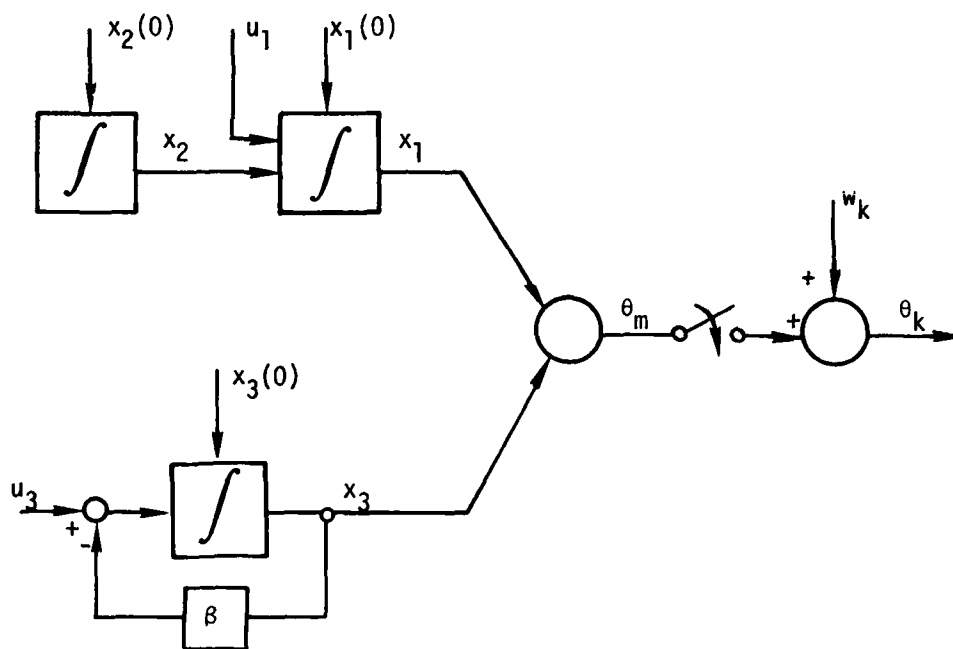
Figure 8. Three-State-Variable Model Block Diagram

where

$$u_c \text{ is white noise representing } u_1 \text{ and } \beta \sigma_L^2 \qquad (14)$$

The exponentially correlated random error with short correlation time has a variance of σ_s and white noise u_3 with PSD

$$Q_s = 2\sigma_s^2 \tau_1 \qquad (15)$$

The PSD of an exponentially correlated random error is given by

$$S(\omega) = \cfrac{\cfrac{2\sigma_s^2}{\tau_1}}{\omega^2 + \left[\cfrac{1}{\tau_1}\right]^2} \qquad (16)$$

The PSD functions for a Markov process and for white noise are given in Figure 9. Examination of these two functions indicate they are similar for frequencies between the cutoff frequencies. If zero frequency is considered, Equation 16 becomes

$$S(0) = 2\sigma_s^2 \tau \qquad (17)$$

This is exactly the PSD of the white noise process for this error source. Thus, if the correlation time is short compared to the system natural frequency, then the exponentially correlated random error can be modeled by white noise. In particular, for an inertial system the natural (Schuler) frequency is

$$\omega_s = \frac{2\pi}{T} \qquad (18)$$

where

ω_s = Schuler frequency

T = Schuler period (84.2 minutes)

$$\omega_s = \frac{2\pi}{84.2 \times 60} = \frac{1}{804.02} \text{ seconds} \qquad (19)$$

18
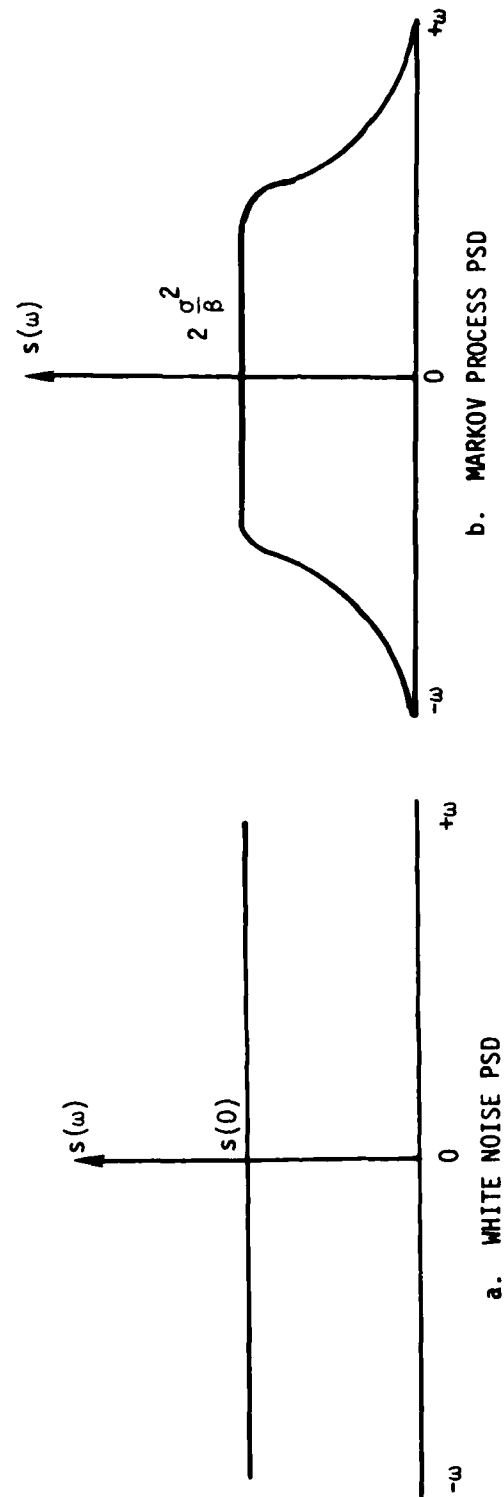
Figure 9. White Noise and Markov Process Power Spectral Density

19

Rounding off, this gives

$$\frac{1}{\omega_s} \fallingdotseq 800 \text{ seconds} \tag{20}$$

Then for

$$\tau_s < \frac{1}{\omega_s} \tag{21}$$

or equivalently

$$\tau_s < 800 \text{ seconds} \tag{22}$$

a white noise model can be used.

An error source modeled by white noise does not require the addition of a state variable to the state vector. The white noise amplitude can simply be added to the system noise. The suboptimal estimator now only requires two state variables to model the gyro. A block diagram of the reduced order model is shown in Figure 10. The state vector differential equations are

$$\dot{x}_1 = x_2 + u_T$$
$$\dot{x}_2 = 0 \tag{23}$$

where
u_T is white noise representing u_c and $\sigma_s^2 \tau_1$

$$x_1(0) = \sigma_s + \sigma_L$$

$$x_2(0) = \text{Random bias error drift rate}$$
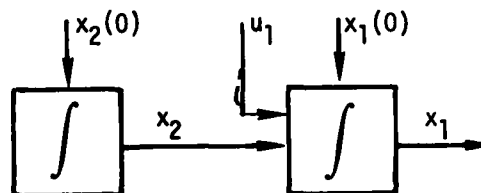
Figure 10. Two-State-Variable Model Block Diagram

Equations 8, 13, and 23 are now put into state space equation form.

$$\underline{\dot{x}} = F\underline{x} + G\underline{u} \qquad (24)$$

where

$\underline{x}$ = System state vector

F = System distribution or description matrix

G = System driving function matrix

u_1 = System driving function (white noise) vector

For Equation 8, these vectors and matrices are

$$\underline{x} = \begin{bmatrix} x_1 \\ x_2 \\ x_3 \\ x_4 \end{bmatrix} \qquad (25)$$

$$F = \begin{bmatrix} 0 & 1 & 0 & 0 \\ 0 & 0 & 0 & 0 \\ 0 & 0 & -\alpha & 0 \\ 0 & 0 & 0 & -\beta \end{bmatrix} \qquad (26)$$

$$G = \begin{bmatrix} 0 & 0 & 0 \\ 0 & 0 & 0 \\ 0 & 1 & 0 \\ 0 & 0 & 1 \end{bmatrix} \qquad (27)$$

$$u = \begin{bmatrix} 0 \\ 0 \\ u_3 \\ u_4 \end{bmatrix} \tag{28}$$

From Figure 7, the measurement equation is given by

$$z = H\underline{x} + \underline{v}_k \tag{29}$$

where

H = Measurement distribution matrix

$\underline{v}_k$ = Measurement noise (white noise)

$\underline{z}$ = Measurement vector

$H = [1 \quad 0 \quad 1 \quad 1]$

Since these equations are linear, a linear estimation scheme is sought to optimally estimate the gyro output angle and angle rate. The best unbiased linear minimum-error-variance estimation algorithm is the Kalman filter. The discrete Kalman equations of concern are listed below. A full development of these equations has been accomplished by Kalman and Bucy (Reference 12), Jazwinski (Reference 13), Sage and Melsa (Reference 14), Meditch (Reference 15), Papoulis (Reference 16), and Gelb (Reference 17).

22

System Model

$$\underline{x}(k + 1) = \phi(k + 1,k)\underline{x}(k) + \Gamma(k)\underline{u}(k) \tag{31}$$

where

$x(k)$ = System state vector at the kth interval

$\phi(k + 1,k)$ = System state transition matrix

$\Gamma(k)$ = System noise distribution matrix

$u(k)$ = System noise vector

Measurement Vector

$$\underline{z}(k) = H(k)\underline{x}(k) + \underline{v}(k) \tag{32}$$

where

$z(k)$ = Measurement vector

$H(k)$ = Measurement distribution matrix

$v(k)$ = Measurement noise vector

The system noise vector and measurement noise vector are zero mean, white noise processes with respective covariances

$$\text{Cov}\left[\underline{u}(k),\underline{u}(j)\right] = Q(k)\delta_k(k-j) \tag{33}$$

$$\text{Cov}\left[\underline{v}(k),\underline{v}(j)\right] = R(k)\delta_k(k-j) \tag{34}$$

Filter State Estimate Update

$$\hat{x}(k) = \hat{\underline{x}}(k-1) + K(k)\left[\underline{z}(k) - H(k)\hat{\underline{x}}(k-1)\right] \tag{35}$$

Kalman Gain

$$K(k) = P_x^-(k)H^T(k)\left[H(k)P_x^-(k)H^T(k) + R(k)\right]^{-1} \tag{36}$$

Covariance Update

$$P_x^-(k) = \left[I - K(k)H(k)\right]P_x^-(k,k-1) \tag{37}$$

State Estimate Propagation

$$\hat{\underline{x}}(k+1,k) \quad = \quad \phi(k+1,k)\hat{\underline{x}}(k) \tag{38}$$

Error Covariance Propagation

$$P_x^{\sim}(k + 1, k) = \phi(k + 1, k)P_x^{\sim}(k)\phi^T(k + 1), k)$$

$$+ \Gamma(k)Q(k) \Gamma^T(k) \tag{39}$$

where

I = Identity matrix

T = Transpose of a matrix or vector

$\hat{}$ = Estimate quantity

$\sim$ = Error quantity

$( )^{-1}$ = Inverse of a matrix

To apply the discrete Kalman equations, the continuous state equations must be expressed in discrete form. *The procedure for discretizing these equations are described in the literature and are not presented here.* The resulting discrete form of the equations are:

Transition Matrix

$$\phi \quad = \quad \begin{bmatrix} 1 & \Delta t & 0 & 0 \\ 0 & 1 & 0 & 0 \\ 0 & 0 & e^{-\alpha\Delta t} & 0 \\ 0 & 0 & 0 & e^{-\alpha\Delta t} \end{bmatrix} \tag{40}$$

Covariance Propagation

$$P_{11}(k+1) = P_{11}(k) + \left[P_{12}(k)+P_{21}(k)\Delta t\right] + P_{22}(k)(\Delta t)^2$$

$$P_{12}(k+1) = P_{12}(k) + P_{22}(k)\Delta t$$

$$P_{13}(k+1) = \left[P_{13}(k) + P_{23}(k)\Delta t\right]e^{-\alpha\Delta t}$$

$$P_{14}(k+1) = \left[P_{14}(k) + P_{24}(k)\Delta t\right]e^{-\beta\Delta t}$$

$$P_{22}(k+1) = P_{22}(k)$$

$$P_{23}(k+1) = P_{23}(k)e^{-\alpha\Delta t}$$

$$P_{24}(k+1) = P_{24}(k)e^{-\beta\Delta t}$$

$$P_{33}(k+1) = \left[P_{33}(k) - \frac{\sigma_a^2}{2\alpha}\right]e^{-2\alpha\Delta t}$$

$$P_{34}(k+1) = P_{34}(k)e^{-(\alpha+\beta)\Delta t}$$

$$P_{44}(k+1) = \left[P_{44}(k) - \frac{\sigma_a^2}{2\beta}\right]e^{-2\beta\Delta t} \tag{41}$$

The reduced order state equation models result in subsets of the fourth order model, are developed by Bell (Reference 18), but are not presented here.

In the preceding development, the system is the model of a gyro which senses vehicle motion in a noisy dynamic environment. The vehicle motion sensed is angular velocity, with the output being the angular change which occurs between sampling intervals. Thus, a natural choice for system noise would be the vehicle angular acceleration. For small sampling periods the angular acceleration can be considered constant. Now assuming that the acceleration is uncorrelated between sampling periods, the system noise statistics can be represented by

$$a_k = \text{constant for } t_k \le T \le T_{k+1}$$

$$E\left[a_k a_j\right] = \sigma_a^2 \qquad \text{for } k = j \tag{42}$$
$$= 0 \qquad \text{for } k \ne j$$

25

Thus, a_k is considered to be a zero mean random variable with covariance σ_a^2. Since the noise parameters represented by Equation 28 all stem from the same source, they can be considered identical. Assuming this to be true, then

$$u_3 = u_4 = u$$

and

$$\underline{u} = \begin{bmatrix} 0 \\ 0 \\ u \\ u \end{bmatrix} \tag{43}$$

The measurement noise of the gyro is due to the random pickoff error of the output incremental angle $\Delta\theta$. The measurement noise is assumed to be uncorrelated between measurement intervals with zero mean and covariance σ_θ^2.

The set of equations for the two-state variable gyro model are similar to those suggested by Friedland (Reference 19), wherein somewhat different system dynamics were assumed and a fixed gain filter was formulated. The filter equations are summarized as follows:

System Dynamics

$$x_1(k+1) = x_1(k) + x_2(k) \, \Delta t + a_n \frac{(\Delta t)^2}{2} \tag{44}$$

$$x_2(k+1) = x_2(k) + a_n \Delta t$$

$$\underline{x} = \begin{bmatrix} x_1 \\ x_2 \end{bmatrix} \tag{45}$$

$$\phi = \begin{bmatrix} 1 & \Delta t \\ 0 & 1 \end{bmatrix} \tag{46}$$

26

$$\Gamma Q \Gamma^T = \begin{bmatrix} \dfrac{(\Delta t)^4}{4} & \dfrac{(\Delta t)^3}{2} \\ \dfrac{(\Delta t)^3}{2} & (\Delta t)^2 \end{bmatrix} \times \sigma_a^2 \qquad (47)$$

$$R = \sigma_\theta^2 \qquad \text{Measurement noise variance} \qquad (48)$$

$$Q = \sigma_a^2 \qquad \text{System random acceleration noise variance}$$

$$H = \begin{bmatrix} 1 & 0 \end{bmatrix}$$

State Estimate Propagation Equations

$$\hat{x}_1(k+1) = \hat{x}_1(k) + \hat{x}_2(k) \, \Delta t$$

$$\hat{x}_2(k+1) = \hat{x}_2(k) \qquad (49)$$

State Estimate Update Equations

$$\hat{x}_1(k+1) = \hat{x}_1(k) + K_1(k+1) \left[z - \hat{x}_1(k) \right]$$

$$\hat{x}_2(k+1) = \hat{x}_2(k) + K_2(k+1) \left[z - \hat{x}_1(k) \right] \qquad (50)$$

This filter algorithm was developed as a constant gain filter rather than a time-varying Kalman filter which implies a statistical steady state process, or stationary Kalman filter. This formulation is equivalent to the Wiener filter and is valid only if: the system and measurement models are linear and time invarient (F, G, and H are constant matrices); are at least wide-sense stationary (Q and R are constant matrices); and a steady state can be reached. This last requirement is satisfied if complete observability can be shown.

If these requirements are all met then the Kalman gain is constant, the state vector estimate is stationary, and the error covariance matrix (p) is constant. The continuous equations for the error covariance, Kalman Gain, and filter estimate are

$$0 = FP(0) + P(o)F^T - P(o)H^TR^{-1}HP(o) + \Gamma Q\Gamma^T$$

$$K(o) = P(o)H^TR^{-1}$$

$$\underline{\hat{x}}(t) = F\underline{\hat{x}}(t) + K(o)\left[z(t)-H\underline{\hat{x}}(t)\right] \tag{51}$$

where

$$P(t) = P(o) = \text{Constant Covariance}$$

Direct solution of the first equation in 108 is very difficult and tedious for all but low-order filters. Even the second order filter being described requires considerable matrix manipulation and algebraic calculations. Thus, only the final equations that are programmed in the simulation are presented here.

$$P(1,1) = \frac{\sigma_\theta^2}{r^2}d(d+1)^2$$

$$P(1,2) = \frac{\sigma_\theta\sigma_a\Delta t}{2r}(d+t)^2 \tag{52}$$

$$P(2,2) = \frac{\sigma_a^2(\Delta t)^2}{2}(d+1)$$

Filter Constant Gains

$$K_1 = \frac{1}{r^2}d(d-1)^2 \tag{53}$$

$$K_2 = \frac{2}{r^2\Delta t}(d-1)^2$$

where

$$r = \frac{4\sigma_\theta}{\sigma_a (\Delta t)^2}$$

$$d = \sqrt{1 + 2r}$$

$$\hat{x}_1(k+1) = (1-K_1-K_2\Delta t)\hat{x}_1(k) + \Delta t\hat{x}_2(k)$$

$$+ (K_1+K_2\Delta t)z(k)$$

$$\hat{x}_2(k+1) = K_2 \left[z(k)-z(k-1) \right] + (2-K_1-K_2\Delta t)$$

$$\hat{x}_2(k-1) - (1-K_1)\hat{x}_2(k-2) \tag{54}$$

For simplification and ease in further discussion the four-state-variable model will be termed Algorithm A, the three-state-variable model will be termed Algorithm B, the two-state-variable model will be termed Algorithm C, the Kalman filter model represented by Equations 44 through 51 will be termed Algorithm D, and the fixed gain model of Algorithm D will be termed Algorithm E.

4.   ACCELEROMETER MODEL

The accelerometer can be satisfactorily modeled by a combination of a random bias, a random ramp, and two Markov processes as was done for the gyro. The short correlation-time error can be modeled by white noise and the long correlation-time error can be modeled as a random walk.

Thus, the estimation models developed for the gyros can also be used for the accelerometers. The only changes required are in the initial conditions, system and measurement driving noise statistics, and correlation time constants. These are all obtained from gyro and accelerometer test data and known behavior of different types of inertial sensors.

Accelerometer bias is significant for two reasons in strapped down inertial systems. When the inertial system is aligned prior to flight, system errors are correlated. However, during flight the inertial system deviates from its original orientation and some errors are no longer correlated. Specifically, if the aircraft executes a ninety-degree turn, a step of acceleration equal to the bias magnitude is introduced into the system. The second reason the accelerometer bias is significant, and the one of interest for this investigation, is that the bias is a random error and not a constant. Bias is typically the most dominant of the random accelerometer errors. Particularly, for short duration flights of less than two hours, the bias rms value is one to two orders of magnitude larger than that of other random errors.

SECTION III

REDUNDANT SENSOR DATA AVERAGING

Redundant inertial sensors in skewed configurations were discussed previously. While many different configurations are possible, only a few provide increased benefits and are practical for application as aircraft inertial reference systems. A study by Burns (Reference 1) resulted in three of the most promising configurations. These three candidates are designated as a single aligned quint, a dual skewed triad, and a dual reversed double triad. The transformation matrices of four configurations, including the three mentioned above, are given below. These configurations were all used in this study and are designated Configuration 1 through Configuration 4. The geometry for Configuration 1, the dual skewed triad, is depicted in Figure 11. A sixth gyro has been added to the quint, Configuration 2, for comparison with the other for configurations

$$
\begin{bmatrix}
1 & 0 & 0 \\
0 & 1 & 0 \\
0 & 0 & 1 \\
2/3 & 2/3 & -1/3 \\
-1/3 & 2/3 & 2/3 \\
-2/3 & 1/3 & 2/3
\end{bmatrix}
\qquad
\begin{bmatrix}
1 & 0 & 0 \\
0 & 1 & 0 \\
0 & 0 & 1 \\
\frac{1}{\sqrt{3}} & \frac{1}{\sqrt{3}} & \frac{1}{\sqrt{3}} \\
-\frac{\sqrt{2}}{\sqrt{3}} & \frac{\sqrt{2}}{\sqrt{3}} & \frac{\sqrt{2}}{\sqrt{3}} \\
0 & \frac{\sqrt{6}}{2\sqrt{3}} & -\frac{\sqrt{6}}{2\sqrt{3}}
\end{bmatrix}
$$

Configuration 1   Configuration 2

$$\frac{\sqrt{3}}{6} \begin{bmatrix} \sqrt{6} & \sqrt{2} & -2 \\ -\sqrt{6} & \sqrt{2} & \overline{-2} \\ 0 & -2\sqrt{2} & -2 \\ -\sqrt{6} & -\sqrt{2} & -2 \\ \sqrt{6} & -\sqrt{2} & -2 \\ 0 & 2\sqrt{2} & -2 \end{bmatrix} \qquad \begin{bmatrix} 0.97204 & 0 & -0.23482 \\ -0.60075 & -0.77653 & -0.18997 \\ 0 & 0.47992 & 0.87731 \\ 0 & -0.47992 & 0.87731 \\ -0.60075 & 0.77653 & -0.18997 \\ 0 & 0 & 0 \end{bmatrix}$$

Configuration 3   Configuration 4
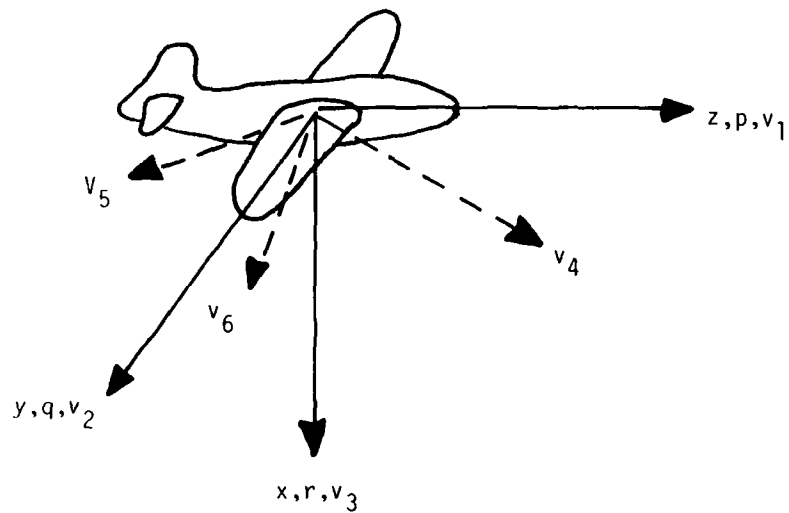
Figure 11. Dual Skewed-Triad Sensor Input Axes Diagram

If properly mixed, or averaged, the redundant inertial sensor information can result in improved system performance. The method chosen to perform this averaging is by weighted least squares estimation. This method was chosen for its simplicity and estimating capability. No stochastic assumptions are required and the estimation can be treated as a deterministic optimization problem. As a result, the estimate will be a statistical average of the redundant inertial sensor data, for each axis of an orthogonal triad, in body coordinates.

The least-squares estimator is based upon an estimate $\hat{\underline{x}}_k$ of $\underline{x}$ which will minimize the quadratic measure

$$J(\hat{\underline{x}}_k) = \frac{1}{2}(\underline{z}_k - H_k\hat{\underline{x}}_k)^T R_k^{-1}(\underline{z}_k - H_k\hat{\underline{x}}_k) \tag{56}$$

where

$$J(\hat{\underline{x}}_{k_{LS}}) \leq J(\hat{\underline{x}}_k)$$

$\hat{\underline{x}}_{k_{LS}}$ = Least-squares estimate of $\underline{x}_k$

$\underline{z}_k$ = M X 1 vector of measurements

H_k = M X N measurement of matrix

$\hat{\underline{x}}_k$ = N X 1 vector of parameters to be established

R_k^{-1} = M X N positive definite and symmetric weighting matrix

T = Transpose of vector or matrix

A^{-1} = Inverse of matrix A

33

Linear measurements corrupted by zero-mean noise with constant variance of the form

$$\underline{z}_k = H_k \underline{x} + \underline{v}_k \qquad (57)$$

are made where $\underline{v}_k$ is an M X 1 vector of measurement noise.

If it exists, the least-squares estimate is obtained by setting the partial differential of the quadratic measure equal to zero. Thus,

$$\left. \frac{\partial J(\underline{\hat{x}}_k)}{\partial \hat{x}_k} \right|_{\underline{\hat{x}}_k = \underline{\hat{x}}_{k_{LS}}} = H_k R_k^{-1}(\underline{z}_k - H_k \underline{x}_{k_{LS}}) = 0 \qquad (58)$$

which results in the desired solution

$$\underline{\hat{x}}_{k_{LS}} = (H_k^T R_k^{-1} H_k)^{-1} H_k^T R_k^{-1} \underline{z}_k \qquad (59)$$

If the weighting matrix R, in the least-squares estimator is made equal to the variance matrix for the measurement noise, the least-squares estimator is identical to the linear minimum variance estimator. If the measurement errors are uncorrelated the measurement matrix R is diagonal. Further, if all errors have equal variance, then Equation 59 reduces to the least-squares estimator.

$$\underline{\hat{x}}_{k_{LS}} = (H_k^T H_k)^{-1} H_k^T \underline{z}_k \qquad (60)$$

A full development of the least-squares estimator is given by Sage and Melsa (Reference 14). A sequential form of the least-squares estimator is possible. However, in this investigation, batch measurements are processed and the sequential form is not required.

By comparing Equation 60 with the defining equation of the pseudo-inverse, it can be seen that $(H^T H)^{-1} H^T$ is the pseudoinverse of the matrix H which has more rows than columns. This is the overdetermined case in the solution of linear equations with more equations than unknowns. The solution of Equation 60 is the best solution in a least-squares sense. Thus, the 6 X 3 sensor input matrix given in Equation 55 can be assumed as the measurement matrix H for the least-squares estimator. The six inertial sensor outputs are transformed through a statistical weighted average to the body frame reference triad.

For this investigation, six angle-degree-of-freedom gyros and six single-axis accelerometers are modeled. When two-degree-of-freedom gyros are used, then six axes of information are utilized. A vector $\underline{x}$ is used for each set of six sensors. One for the gyros and one for the accelerometers. The elements making up each vector consist of the individual sensor outputs as estimated by the selected sensor estimation algorithm. Thus, for the gyros $\underline{x}_G$ is the 6 X 1 vector.

$$\underline{\hat{x}}_G = \begin{bmatrix} \Delta\hat{\theta}_1 \\ \Delta\hat{\theta}_2 \\ \Delta\hat{\theta}_3 \\ \Delta\hat{\theta}_4 \\ \Delta\hat{\theta}_5 \\ \Delta\hat{\theta}_6 \end{bmatrix} \qquad (61)$$

and for the accelerometers

$$\underline{\hat{x}}_A = \begin{bmatrix} \hat{\Delta}v_1 \\ \hat{\Delta}v_2 \\ \hat{\Delta}v_3 \\ \hat{\Delta}v_4 \\ \hat{\Delta}v_5 \\ \hat{\Delta}v_6 \end{bmatrix}$$

(62)

The H and R matrices for this application are time invariant. Thus, the weighted least-squares estimator can be represented by

$$\underline{\hat{x}}_{k_{LS}} = T_{k_{LS}} \underline{z}$$

(63)

where $T_{k_{LS}}$ is a time invariant least-squares transformation matrix of dimension 3 X 6 and $\underline{x}_{k_{LS}}$ is a 3 X 1 vector representing the orthogonal set of estimated sensor outputs in body coordinates.

Assuming that the measurement errors are uncorrelated, the measurement matrix is diagonal. Further, assuming that all measurements do not have equal variance, then the measurement matrix for the set of six gyros or six accelerometers is given by

$$R = \begin{bmatrix} \sigma_1^2 & & & & & \\ & \sigma_2^2 & & & & \\ & & \sigma_3^2 & & & \\ & & & \sigma_4^2 & & \\ & & & & \sigma_5^2 & \\ & & & & & \sigma_6^2 \end{bmatrix}$$

(64)

36

where the σ_i^2 represent the relative measurement error weighting values for each individual sensor.

For the sensors with input axis aligned along a body axis, no geometry change is made. Thus, no dynamically induced error effects, not present in a typical three axis strapped down inertial system, are incurred by these sensors. However, sensors with input axis skewed with respect to the body axes will generally exhibit deteriorated performance due to the dynamically induced errors. This is especially true of gyros with rotating mass, whereas most accelerometers are affected to a lesser degree, and ring laser gyros are affected very little. Ring laser gyros and quartz-flexure accelerometers are the inertial sensors considered in this investigation. Since the statistical effects (in a dynamic flight environment) of skewing these sensors is not available, the error magnitudes are inferred from laboratory test data. As of this time (to the author's knowledge) no reliable flight testing of skewed configuration strapped down inertial sensors in a high dynamic aircraft environment has been accomplished.

The diagonal elements of the weighting matrix are assigned a range of weights, with different values selected, and evaluated by simulation. Further discussion on selected of weights is contained in Section V.

SECTION IV

SIMULATION PROGRAM DESCRIPTION

The simulation used in the conduct of this investigation permits
the evaluation of strapped down inertial reference systems over arbitrary
flight profiles. The total simulation consists of two units which will
be referred to as the Data Base and Sensor Reference Simulator, and the
Estimation Algorithm Simulator. The two units can be run independently
if desired, but for this investigation the Estimation Algorithm Simulator
was structured as a subprogram to the Data Base and Sensor Reference
Simulator. The total simulation is controlled by the Data Base and
Sensor Reference Simulator, while the Estimation Algorithm Simulator
has control of its own individual subroutines.

The total simulation is configured for both open loop operation and
for closed loop feedback control operation. In the open loop mode, the
Data Base and Sensor Reference Simulator provides the necessary sensor
and dynamic information to the Estimation Algorithms. The Estimation
Algorithm Simulator computes a "best estimate" of the inertial sensor
information which is then compared with a set of truth data provided by
the Data Base and Sensor Reference Simulator. The estimation errors are
computed by differencing the estimated values from the truth values.
These estimation errors are output via printouts and plots for analysis
and evaluation. In the closed loop mode the inertial sensor "best
estimates," as computed by the Estimation Algorithm Simulator are fed
back to the Data Base and Sensor Reference Simulator and used in the
navigation computation in place of the normal inertial sensor outputs.
The navigation system outputs are differenced from a set of truth data
to provide the navigation system errors. These error parameters are
then output via printouts and plots for analysis and evaluation.

Both simulators are completely digital and are coded in FORTRAN IV
computer language. The computation for this investigation was accomplished
on a CYBER-175/CYBER-74 series digital computer facility.

1.   DATA BASE AND SENSOR REFERENCE SIMULATOR

The Data Base and Sensor Reference Simulator is used primarily for program control, for generating flight profile and vehicle dynamics, flight control, navigation, and for providing the sensor and dynamic information to the Estimation Algorithm Simulator. For each simulation run, the Data Base and Sensor Reference Simulator is executed over a specified flight profile. Time histories of all inertial sensor information, navigation parameters, and a set of truth parameter information are recorded on tape. All required data is also passed to the Estimation Algorithm Simulator.

The Data Base and Sensor Reference Simulator is a significantly remodeled version of a simulation developed by the Charles Stark Draper Laboratory. It contains the model of a high performance aircraft represented by nonlinear six-degree-of-freedom equations of motion and nonlinear aerodynamics. Turbulence and winds are modeled to provide a more realistic environment. Models of three lateral, and three longitudinal-directional structural modes, and a flight control system representative of this type of aircraft are included. The inertial sensors, which provide kinematic data for utilization in navigation, flight control, and other avionic systems are also modeled.

The inertial sensors modeled in this simulation represent state-of-the-art technology. Both two-degree-of-freedom tuned rotor gyros and ring laser gyros are modeled. Either type of gyro can be selected for any simulation run along with a set of accelerometers. The accelerometers modeled are of the single-axis pendulous force-rebalance type. The program is structured such that random selection of the gyro and accelerometer bias and scale factor errors is accomplished at the beginning of each simulation run. The option of utilizing a known input value for the bias and scale factor errors is also available. This provides the capability of making either deterministic simulation runs or a Monte Carlo simulation over an ensemble of runs.

39

The strapped down configuration of inertial sensors considered in this investigation must be capable of providing the kinematic data required to perform the functions of flight control and navigation, as well as other avionic functions onboard an aircraft. For safety-of-flight considerations most aircraft in both civilian and military environments require redundancy in the flight control system. Thus, in this simulation six gyros and six accelerometers have been modeled to provide a strapped down inertial reference with redundant capabilities. However, no attempt has been made toward incorporating any Failure Detection and Isolation (FDI) or Redundancy Management (RM) capabilities in the simulation.

The sensors can be placed at any desired location within the aircraft, either singly or co-located, thus allowing evaluation of sensor configuration and location effects. The location effects of interest consist of these resulting from lever arms and aircraft structural modes.

The simulation contains a local-vertical wander-azimuth whole-value model and an error model of a strapped down inertial navigation system. The whole-value model includes the effects of model and computation errors, thus reflecting the expected performance of an actual strapped down inertial navigation system in a realistic environment. Utilizing both models allows assessment of the magnitude of these errors.

Feedback of the estimated inertial sensor information from the Estimation Algorithm Simulator into the navigation system mechanization allows evaluation of the estimation algorithms and their effect upon total navigation system performance. The estimated inertial sensor information can also be fed back to the flight control system to evaluate effects of the estimation algorithms upon the aircraft flight control.

A block diagram of the system is presented in Figure 12. Switches S11 and S12 represent the capability of adding or deleting the Estimation Algorithm Simulator to the Data Base and Sensor Reference Simulator. Switches S21 and S22 represent the capability of using either an orthogonal triad set of sensors or switching in the "best estimate" of an

Figure 12. Simulation Block Diagram

41

orthogonal triad from the optimal combination of all the redundant
inertial sensors. Switch S31 represents the capability of using the
normal flight control system gyros or the estimated inertial navigation
sensor information in the flight control system.

2. ESTIMATION ALGORITHM SIMULATOR

The Estimation Algorithm Simulator consists of a number of
algorithms for estimating the outputs of a set of redundant gyros and
accelerometers in the noisy and dynamic environment of the strapped down
inertial reference system. These estimation algorithms are developed and
discussed in detail in Section II.

The Estimation Algorithm Simulator was developed for use in con-
junction with the Data Base and Sensor Reference Simulator, but can be
adapted for stand-alone simulation. When utilized in this fashion, the
simulator operates on inertial sensor information and dynamic data which
is input from a magnetic tape. However, since no navigation routine is
incorporated in this simulator, no feedback capability exists.

Numerous options are incorporated in the simulator. All, or any
combination, of the algorithms can be selected for estimating the gyro
and accelerometer outputs during any simulation run. Feedback of the
estimated outputs of either the gyros or the accelerometers, or both,
can be selected. The filter update rates are variable and all parameters
are easily changed by computer input cards. Any parameter can be
selected, up to a maximum of one hundred, for recording on magnetic tape
and/or printing and plotting.

The redundant sensors output data are statistically averaged and
transformed into an orthogonal triad set of inertial data by a weighted
least-squares estimation algorithm. The simulator is mechanized to use
up to eight axes of gyro and eight axes of accelerometer data with the
number of gyros and accelerometers selected for each simulation run.
The weighting parameter for each individual sensor is also selectable.

42

SECTION V

RESULTS AND CONCLUSIONS

A whole value simulation was chosen for this investigation since the primary purpose was to evaluate and compare alternative estimation algorithms in a realistic environment. Evaluation of absolute strapped down inertial reference system errors was not the intent. However, a comparison of the relative error performance between the various algorithms was a primary concern. Thus, an error simulation was not utilized in the actual evaluation, but was run in parallel with the whole value simulation as an aid in analysis.

Both Deterministic and Monte Carlo simulations were utilized throughout the investigation. However, due to the amount of computer time required for the whole value simulation, insufficient runs were made to establish a statistical base with the Monte Carlo simulation. Simulation runs were made to determine system performance with the various estimation algorithms from random error source inputs. Whole value, deterministic simulation runs were used primarily for analysis and evaluation of the relative performance of the various algorithms.

A covariance analysis simulation was not utilized since an evaluation of effects of the various algorithms on the total strapped down inertial reference system was desired rather than a sensitivity analysis. However, a covariance analysis simulation would be desired for establishing sensitivities of the various algorithms and inertial sensor error parameters.

No attempt was made to optimize any of the algorithms by selectively changing the statistical parameters. A range of values for each parameter, based upon known sensor characteristics and upon expected aircraft dynamics, were used to establish performance capability. Optimization of the estimation algorithms would require a complete sensitivity analysis, since these parameters are dependent upon sensor configuration, sensor location within the aircraft, and aircraft dynamics.

1.   SENSOR OUTPUT ESTIMATION

The capabilities of five algorithms in estimating the inertial sensor
output were evaluated. These algorithms were discussed in Section II.
Of these algorithms, two were found to be superior, and will be the only
ones discussed further. The algorithms to be discussed are Algorithm D,
a Kalman Filter mechanization, and Algorithm E, a constant gain mech-
anization of Algorithm D. Algorithm C gave fair performance in some
areas, but did not perform as well as Algorithms D and E. For evaluation
purposes, the simulation was run using flight profiles ranging from
thirty seconds to thirty minutes. The profile used for most of the
simulation runs is represented by Figure 13. The time between maneuvers
for the shorter runs was simply reduced, and some maneuvers were
eliminated for these profiles. For each simulation run the aircraft is
initially trimmed to straight and level flight at an altitude of 5000
feet, a heading of zero degrees, and a velocity of Mach 0.5.

Table 1 lists the parameter values assumed for the accelerometers,
Table 2 lists the parameter values assumed for ring-laser gyros, and
Table 3 lists the parameter values assumed for two-degree-of-freedom
gyros during the evaluation.

For this part of the evaluation an orthogonal set of three ring-
laser gyros and three accelerometers were simulated. This configuration
is shown in Figure 14 with sensor input axes as indicated.

Algorithms D and E provide approximately the same performance.
However, Algorithm E gives a slightly better performance during high
dynamic aircraft maneuvers. The capability of these two algorithms in
estimating the gyro output can be seen by observing Figure 15 through
Figure 17.

These figures are all error plots. The sensor outputs and the
estimates of sensor outputs are differenced from the true sensor input
generated by the simulation. Figure 15 is a plot of the pitch-axis laser
gyro output error. Figure 16 is a plot of the error in estimating the
pitch-gyro output by Algorithm D, and Figure 17 is a plot of the error
in estimating the pitch-gyro output by Algorithm E. The mean-squared

1800 —

1610 — 145° Heading

Loiter
2-1/2 Revolutions at a 30° Bank Angle

1000 —
960 —
Climb to H = 14,500 ft.

Decrease Speed to MACH = 0.5

700 —

600 — 360° Roll

500 — Evasive Maneuver - 4.5 g Rolling-Pullup, 45° Heading

450 — 360° Roll

350 — Weapon Delivery - 3.5 g Pull-Up

250 — 360° Roll - Maximum Normal Acceleration is 4.5 g

225 —

Descent at H = 500 ft., MACH = 0.75

100 —

Cruise at H = 5000 ft., MACH = 0.5, North Heading

0 —
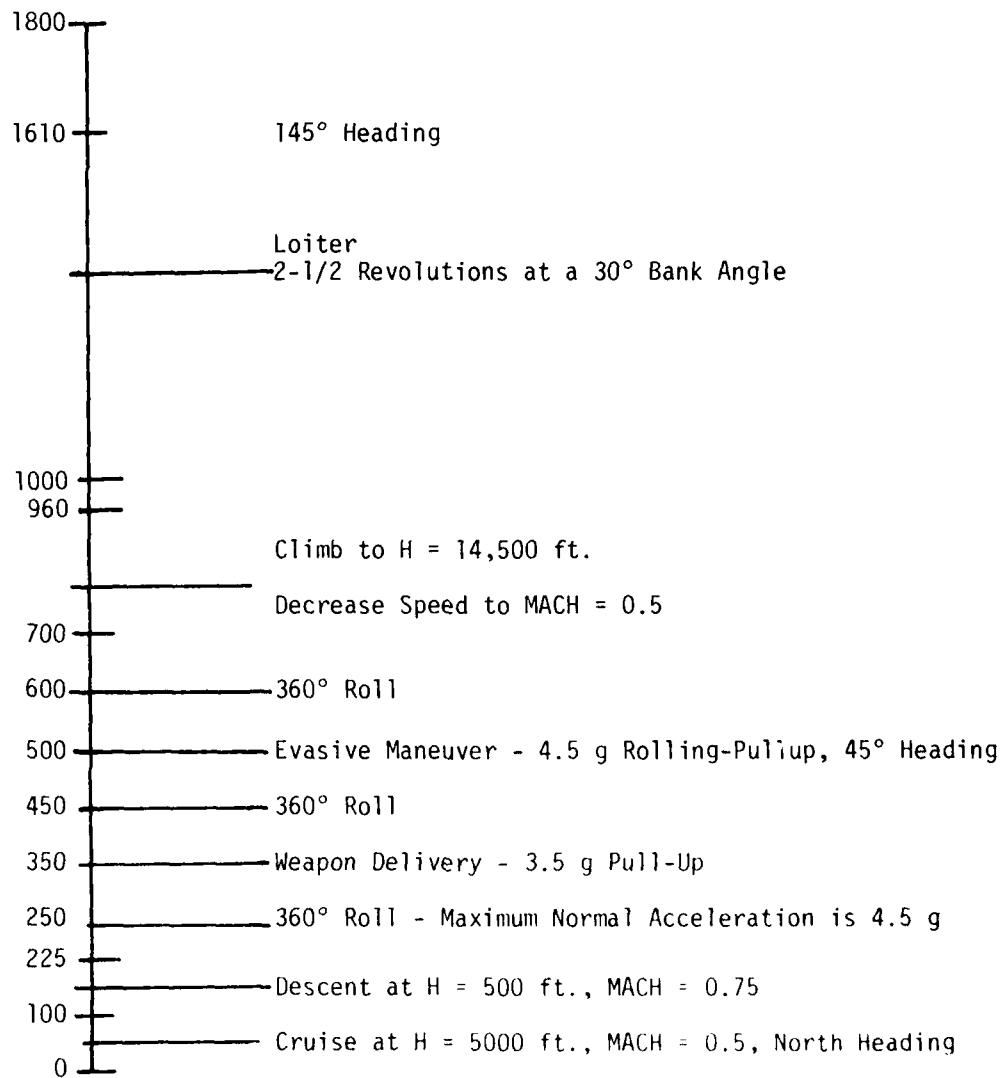
Figure 13. Flight Profile

TABLE 1

ACCELEROMETER PARAMETERS

Parameter	Value	Units
Bias	50	Micro-g
Scale Factor	$32(10^3)$	(Pulses/sec)/g
Scale Factor Error	100	PPM
Scale Factor Non-Linearity	40	Micro-g/g^2
Misalignment Errors	$5(10^{-5})$	Radians
Cross-Coupling Errors	$1.96(10^{-5})$	Radian/g

TABLE 2

RING-LASER GYRO PARAMETERS

Parameter	Value	Units
Fixed Bias	0.01	Deg/Hour
Wideband Random Noise	0.002-0.007	Deg/ $\sqrt{\text{Hour}}$
Scale Factor	1.57	Arc-Sec/Pulse
Scale Factor Error	5	PPM
Misalignment Errors	$5(10^{-5})$	Radians

TABLE 3

TWO-DEGREE-OF-FREEDOM GYRO PARAMETERS

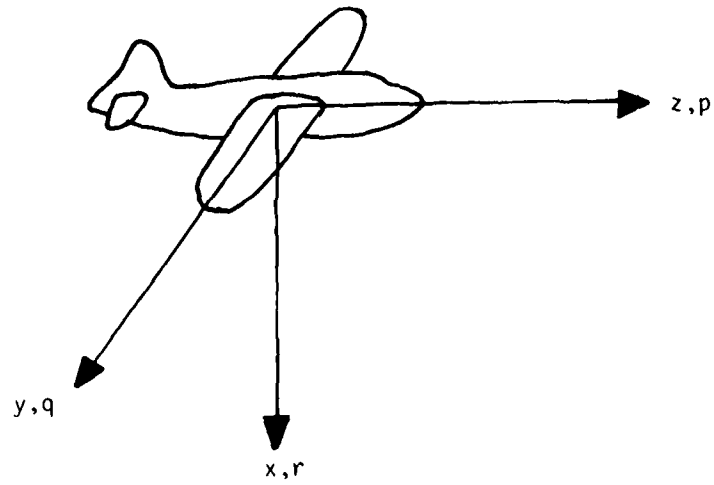| Parameter	X-Axis	Source	Y-Axis	Units
Bias	0.01		0.01	Deg/Hour
Scale Factor	1.57		1.57	Arc-Sec/ Pulse
Scale Factor Error	50		50	PPM
Misalignment Errors	10^{-4}		10^{-4}	Radians
g-Dependent	0.02	g_x	0.04	
Errors	0.04	g_y	0.02	Deg/Hour/g
	0.01	g_z	0.01	
g^2-Dependent	0.02	g_x	0.00	
Errors	0.00	g_y	0.02	Deg/Hour/g^2
	0.005	g_z	0.005	
gxg-Dependent	0.01	g_x, g_y	0.01	
Errors	0.04	g_y, g_z	0.04	Deg/Hour/g^2
	0.04	g_x, g_z	0.04	
ωxω-Dependent	0.0	ω_x, ω_y	0.0	
Errors	80	ω_y, ω_z	20	$\dfrac{\text{Deg/Hour}}{(\text{Rad/Sec})^2}$
	20	ω_z, ω_x	80	

Figure 14. Orthogonal-Triad Inertial Reference Coordinate Frame
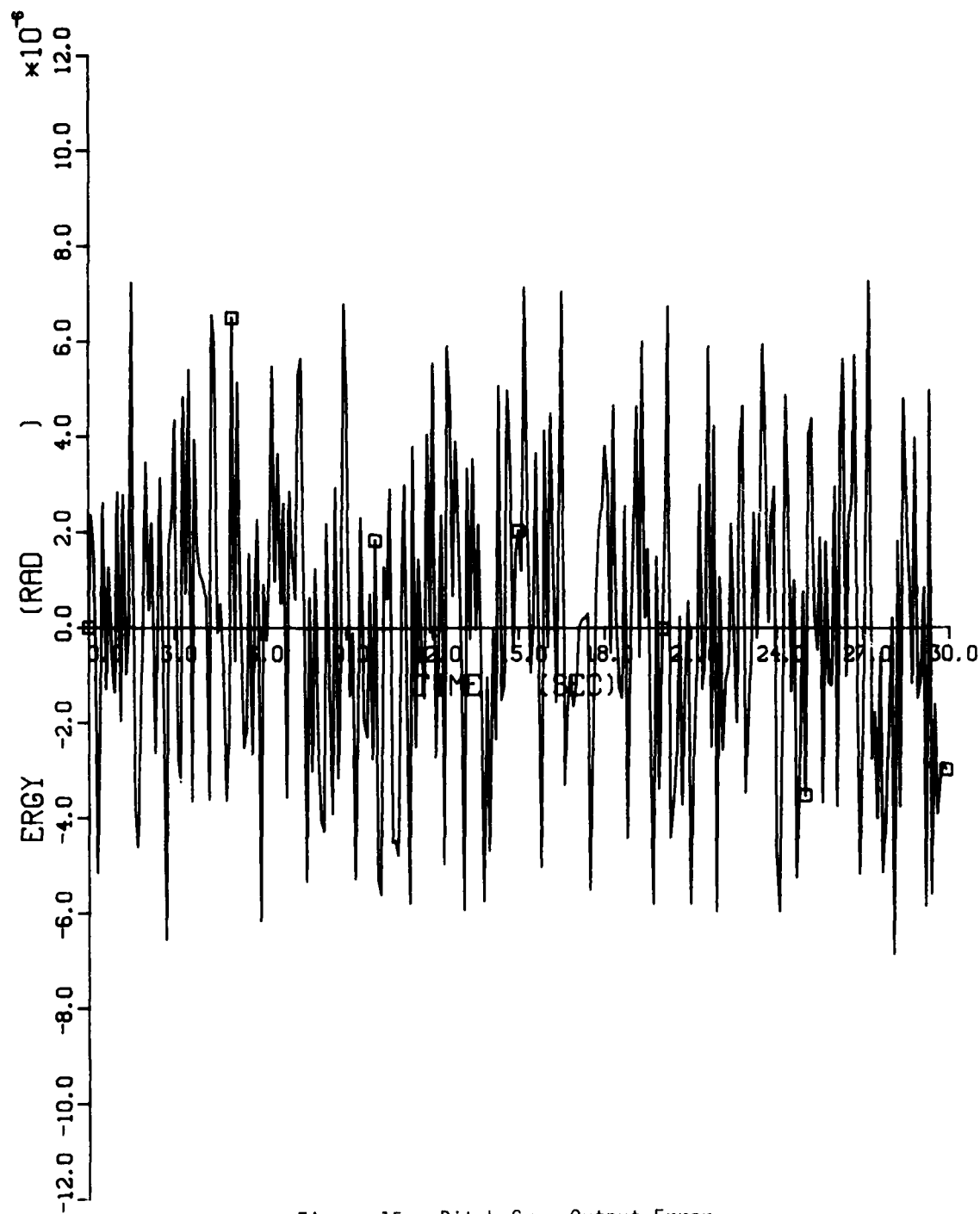
RSDIRS PERFORMANCE IMPROVEMENT

Figure 15.   Pitch-Gyro Output Error

49

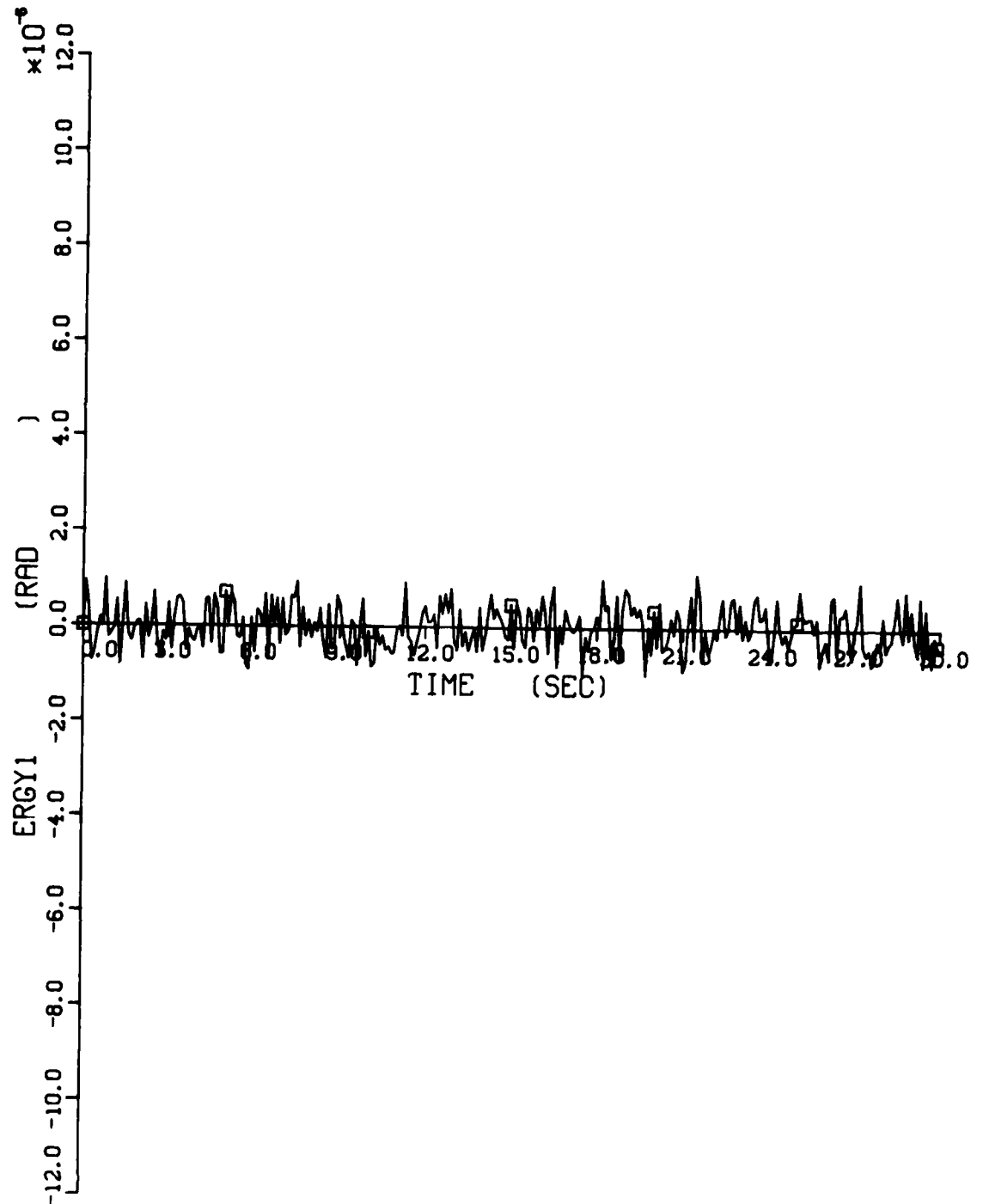# RSDIRS PERFORMANCE IMPROVEMENT

Figure 16.   Algorithm D Pitch-Gyro Output Estimation Error

50

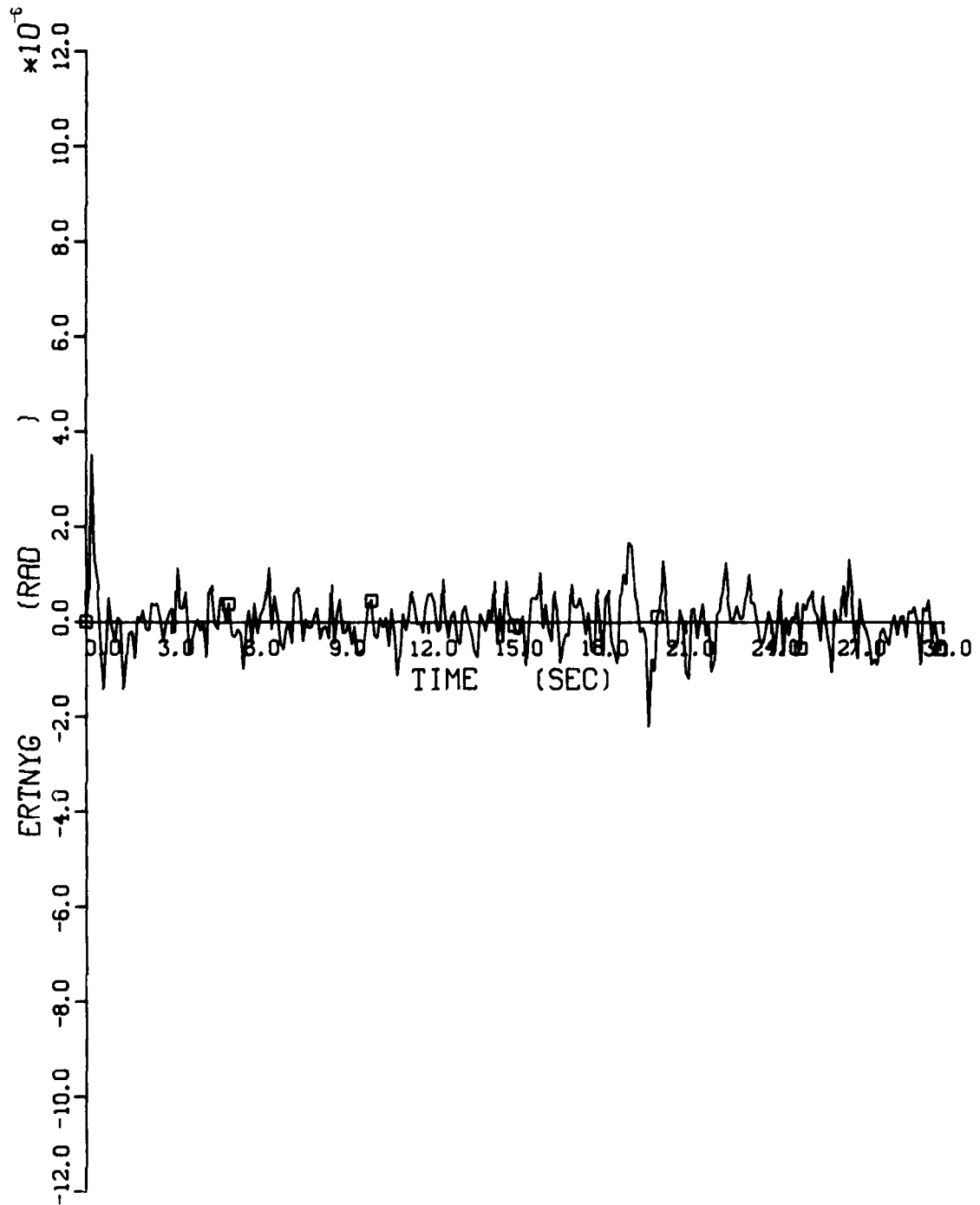# RSDIRS PERFORMANCE IMPROVEMENT

Figure 17.   Algorithm E Pitch-Gyro Output Estimation Error

51

error in the estimates are shown in Figure 18 through Figure 20.
Comparing Figure 19 and Figure 20 with Figure 18 shows that reduction in
the mean-squared error obtained with either Algorithm D or Algorithm E is
nearly the same. However, Algorithm D is somewhat better. The acceleration
noise level, measurement error, and computation interval for these plots
are

$$\sigma_a = 1.0 \text{ Deg/sec}^2 \quad \text{Acceleration Noise Level}$$

$$\sigma_\theta = 3.0 \text{ Arc-Sec} \quad \text{Measurement Error}$$

$$\Delta t = 0.0025 \text{ Sec} \quad \text{Computation Interval}$$

For these parameter magnitudes, Algorithms D and E both exhibit
approximately an order of magnitude improvement in estimating the gyro
output. Similar results were obtained in estimating the output of the
roll and azimuth gyros.

These improved sensor output estimates are very useful in the
application of failure detection and isolation. This is particularly
important in establishing and maintaining sensor failure threshold levels
in the highly dynamic environment of high-performance aircraft. The
estimated sensor output can be used directly in the FDI and RM algorithms.
The need for filtering the inertial sensor outputs was established and
discussed by Motyka and Bell (Reference 9).

The improvement obtained by these algorithms in estimating the
accelerometer output can be observed by comparing Figure 21 with Figure 22
for Algorithm D, and with Figure 22 for Algorithm E.

As was the case for the gyros, this performance improvement is
important in establishing and maintaining sensor failure threshold levels
for failure detection and isolation. However, the mean-squared error
in estimating the accelerometer output is important for a different
reason than for the gyros. The gyro output estimates are utilized to
establish an accurate transformation from a body coordinate frame, in
which the sensor measurements are taken, to a navigation coordinate frame
in which the navigation computation is accomplished. The accelerometer
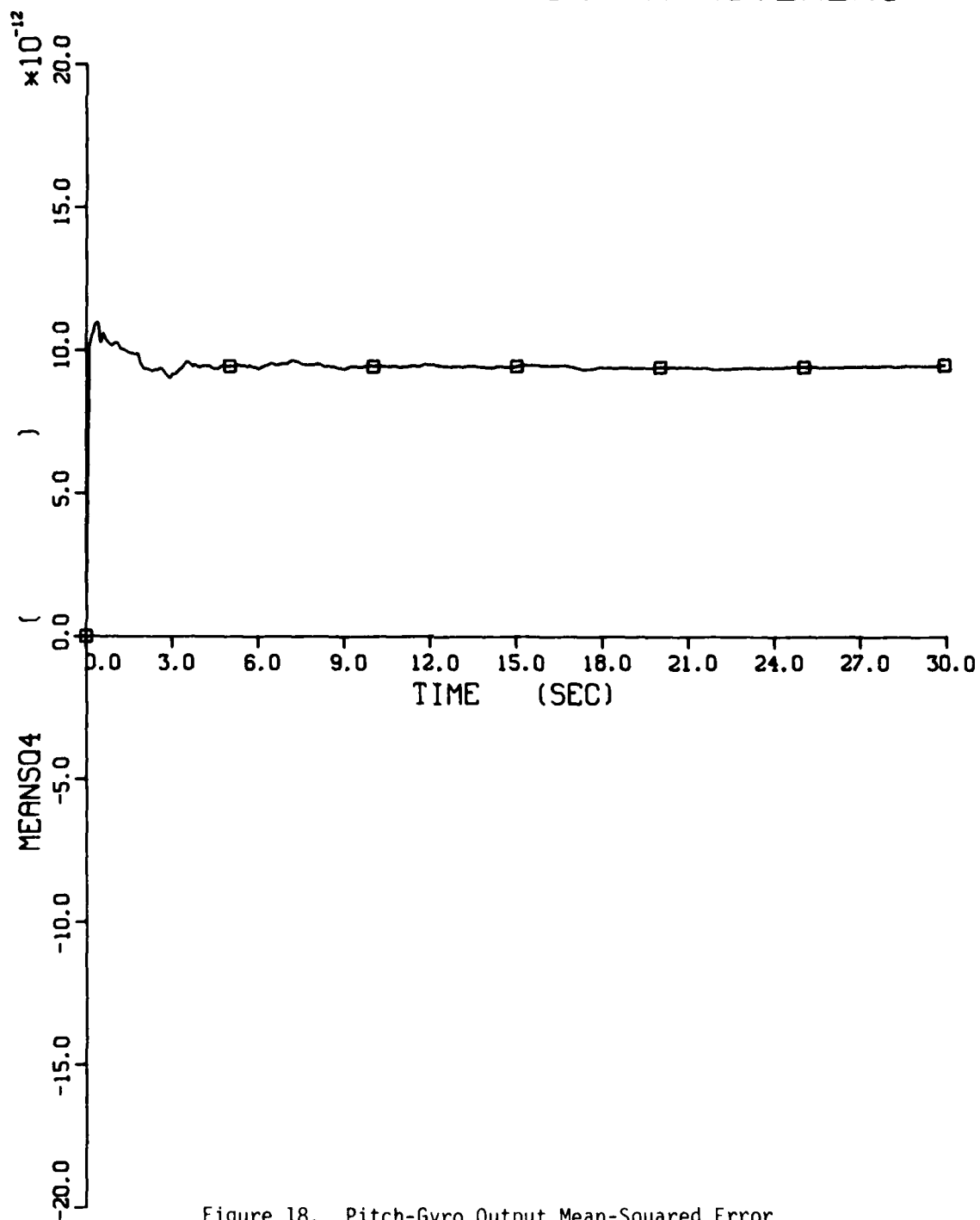
52

RSDIRS PERFORMANCE IMPROVEMENT

Figure 18.   Pitch-Gyro Output Mean-Squared Error
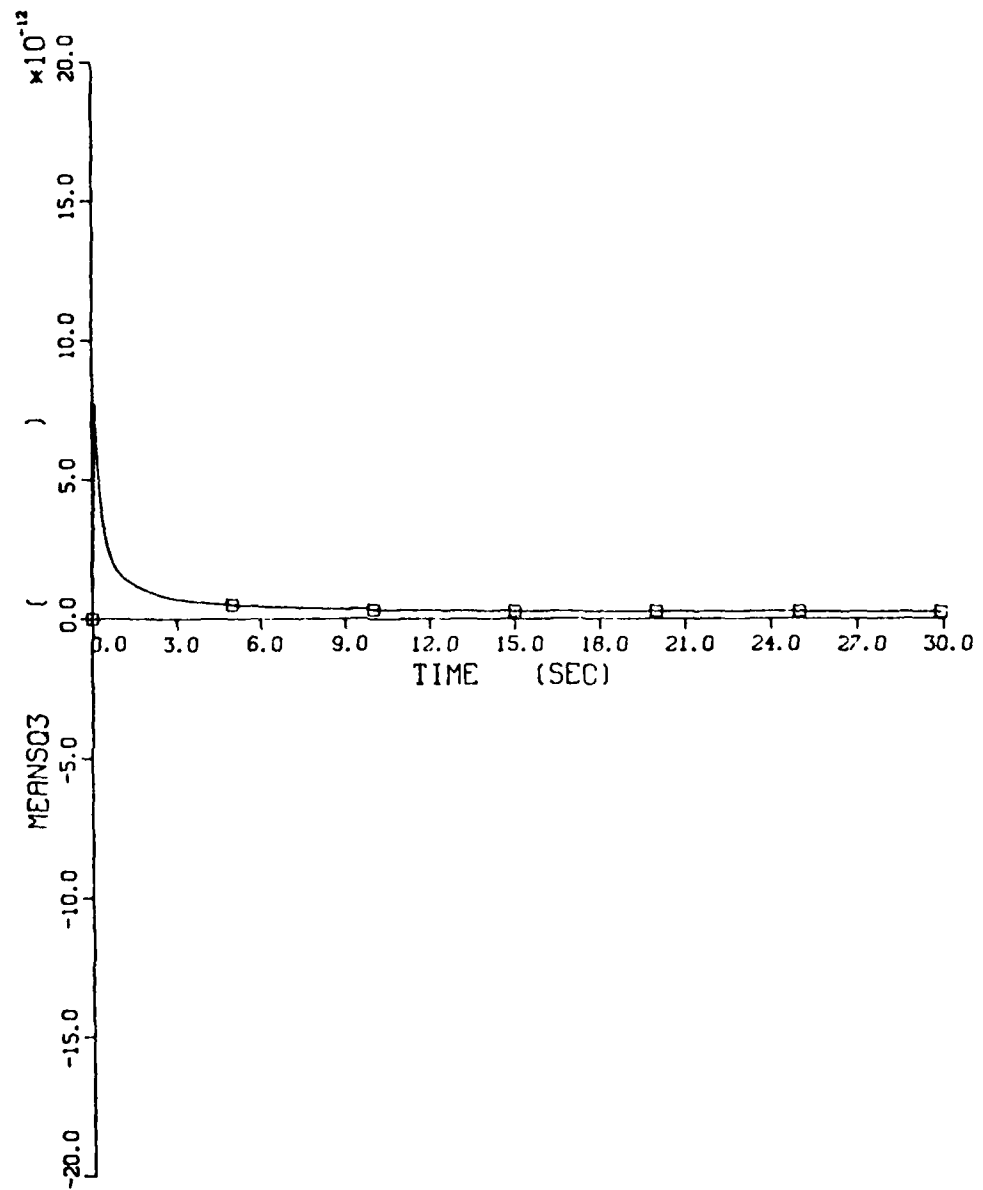
53

RSDIRS PERFORMANCE IMPROVEMENT

Figure 19.   Algorithm D Pitch-Gyro Output Estimation Mean-
Squared Error

54
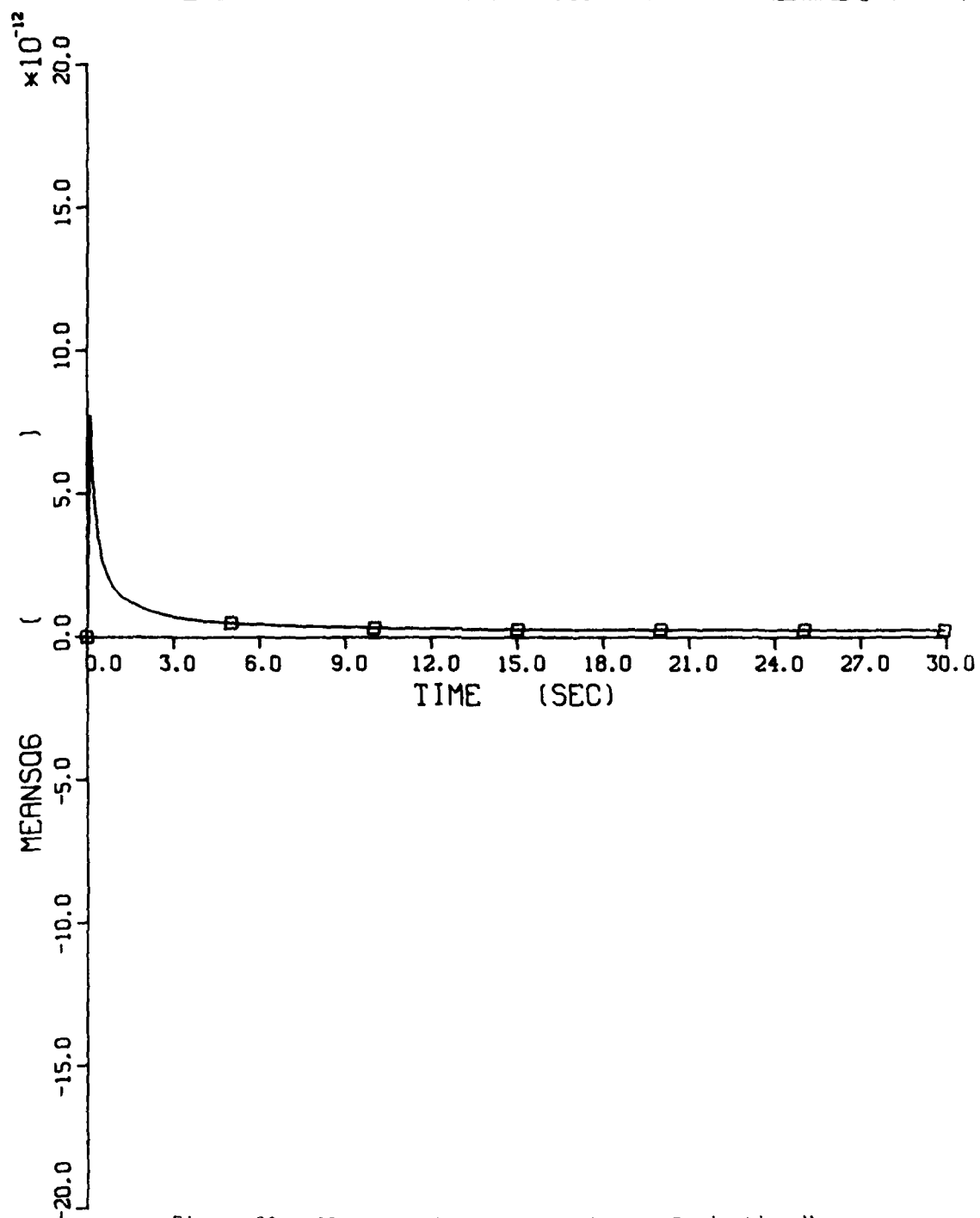
Figure 20.   Algorithm E Pitch-Gyro Output Estimation Mean-
Squared Error

RSDIRS PERFORMANCE IMPROVEMENT

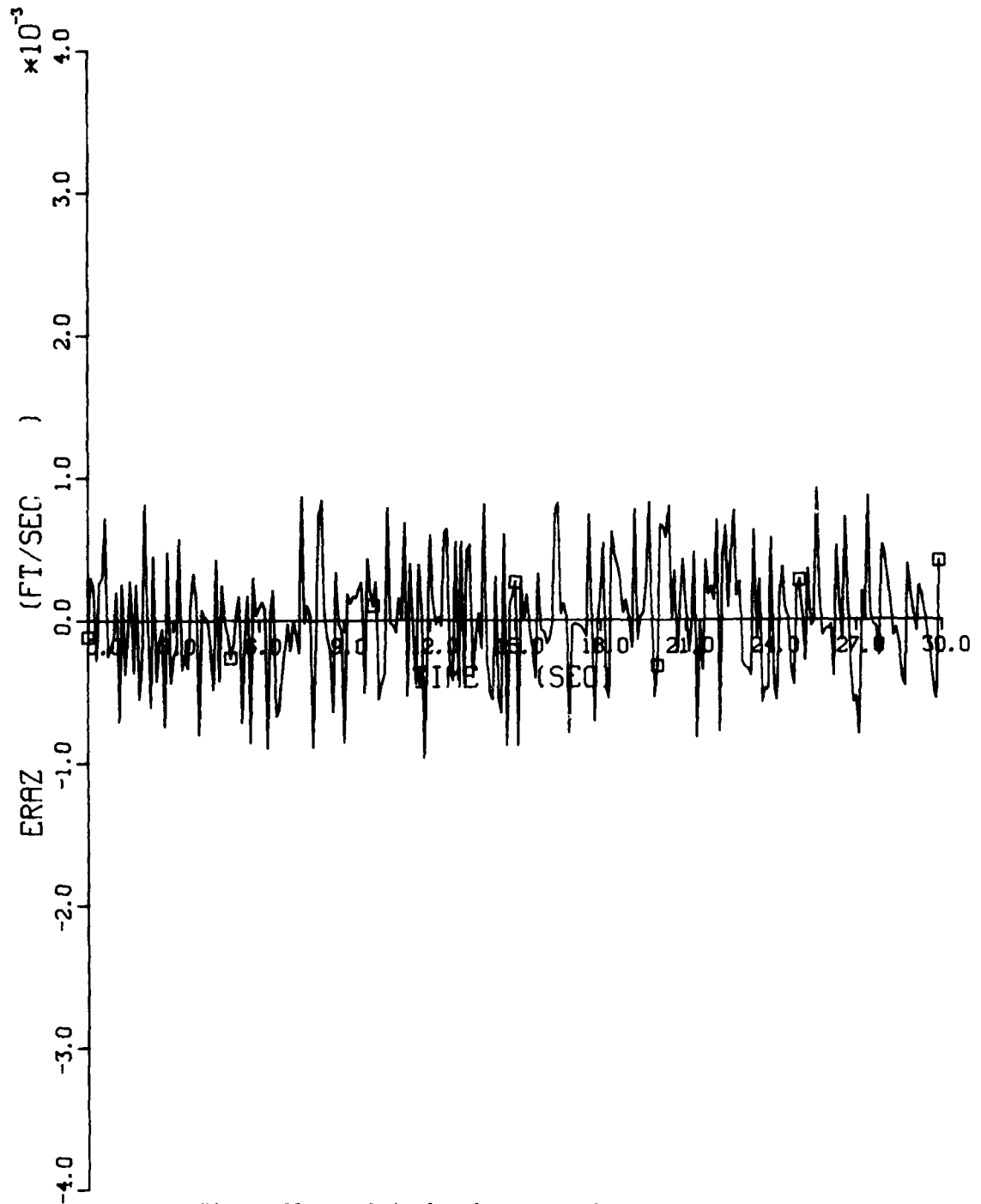
Figure 21.   Z-Axis Accelerometer Output Error

56

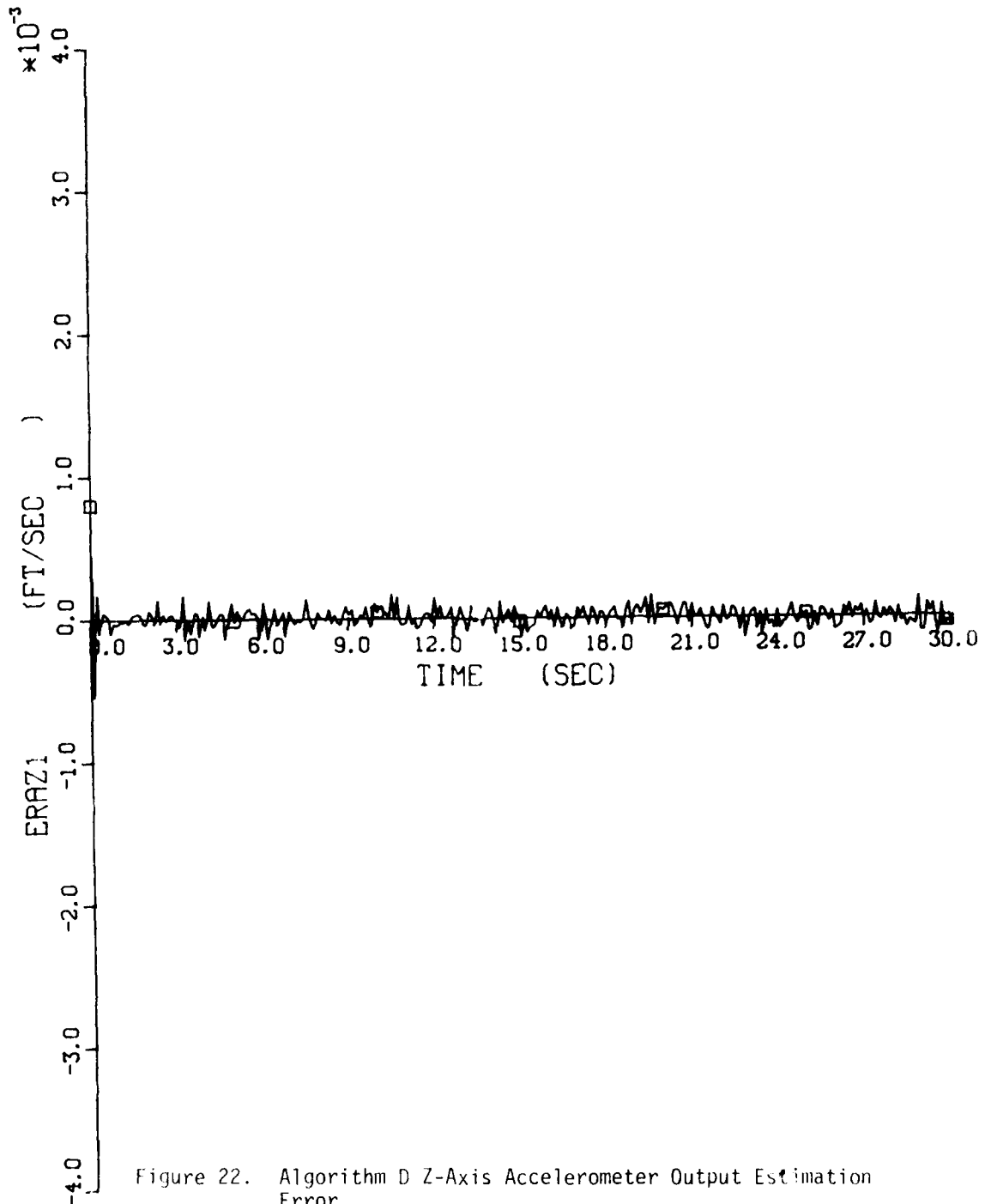# RSDIRS PERFORMANCE IMPROVEMENT

Figure 22.   Algorithm D Z-Axis Accelerometer Output Estimation
Error

RSDIRS PERFORMANCE IMPROVEMENT
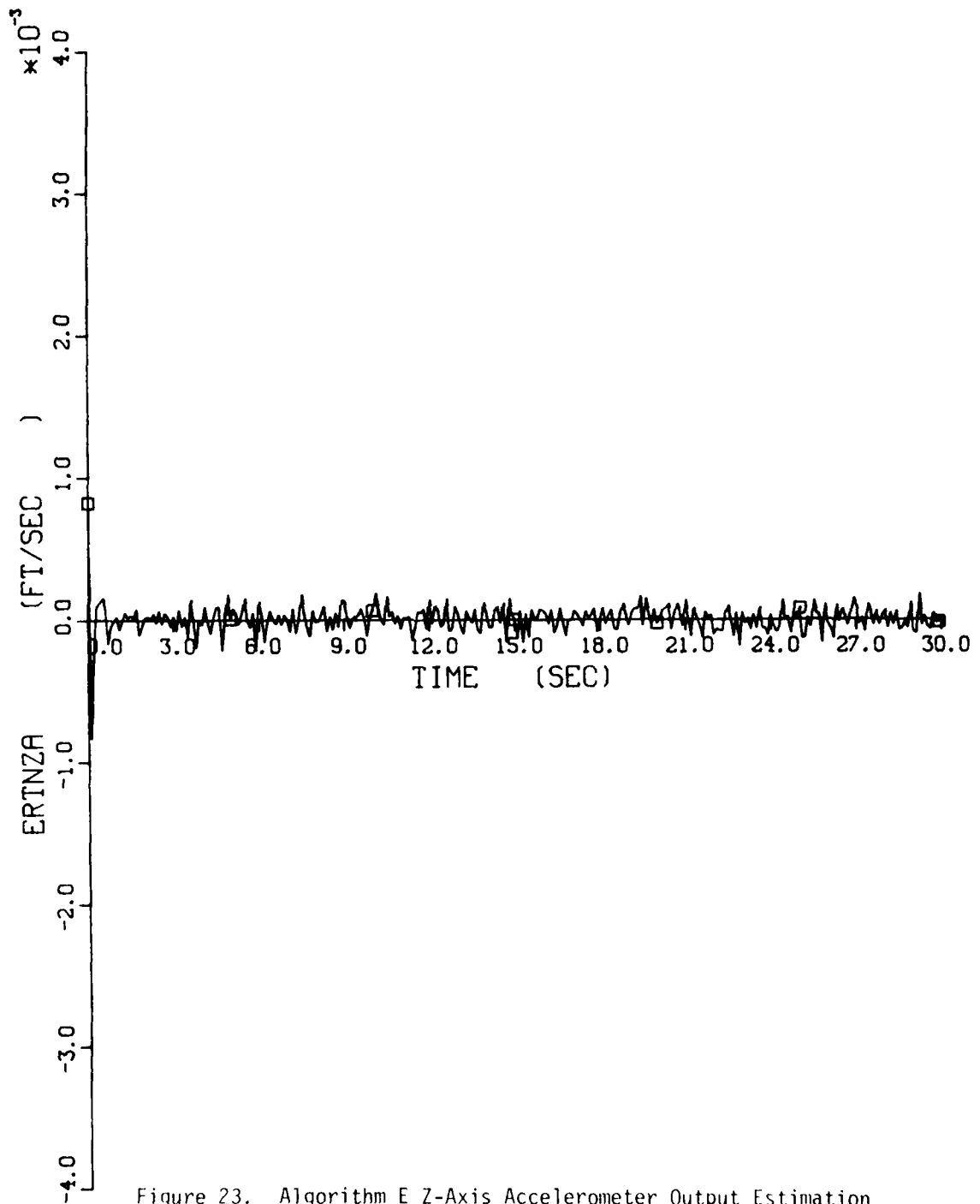

Figure 23. Algorithm E Z-Axis Accelerometer Output Estimation
             Error

output estimates are transformed by this transformation into the navigation coordinate frame and processed to compute vehicle velocity. The mean-squared error in estimating the output of the accelerometers are determining factors in vehicle velocity accuracy. Decreased mean-squared error in estimation for each algorithm can be observed by comparing Figure 24 with Figure 25 for Algorithm D, and with Figure 26 for Algorithm E.

2. SENSOR OUTPUT-RATE ESTIMATION

The output-rates of the gyros and the accelerometers are used in an integrated inertial reference assembly for the functions of flight control and weapon delivery. The flight control system uses the gyro output-rates for angular-rate information and the accelerometer output-rates for linear-acceleration information.

For sensor output-rate estimation both Algorithms D and E perform nearly the same in most instances. As discussed by Friedland (Reference 19), up to twenty-five percent improvement in estimating gyro output-rate can be obtained with Algorithm E. This is also true of Algorithm D. The improvement obtained is dependent upon sensor accuracy and aircraft dynamics. No attempt was made to optimize the algorithms and evaluation was accomplished with similar statistical parameters.

Sensor output-rate estimation improvement was obtained for all sensors. Since no optimization was accomplished for sensor orientation or location, the percentage of improvement for each sensor was different. Figure 27 shows an example of the output-rate estimation obtained for an accelerometer.

3. WEIGHTED-LEAST-SQUARES AVERAGING

The sensor configurations used for this part of the study are those discussed in Section III. The majority of simulation runs were made with the inertial sensors arranged in a quint configuration plus an additional gyro and accelerometer (Configuration 2). Six ring-laser gyros (RLG's) and six accelerometers were mechanized, all located at the same position within the aircraft. The majority of simulation runs were accomplished with the sensors located at flight station FS313 within the aircraft,

59
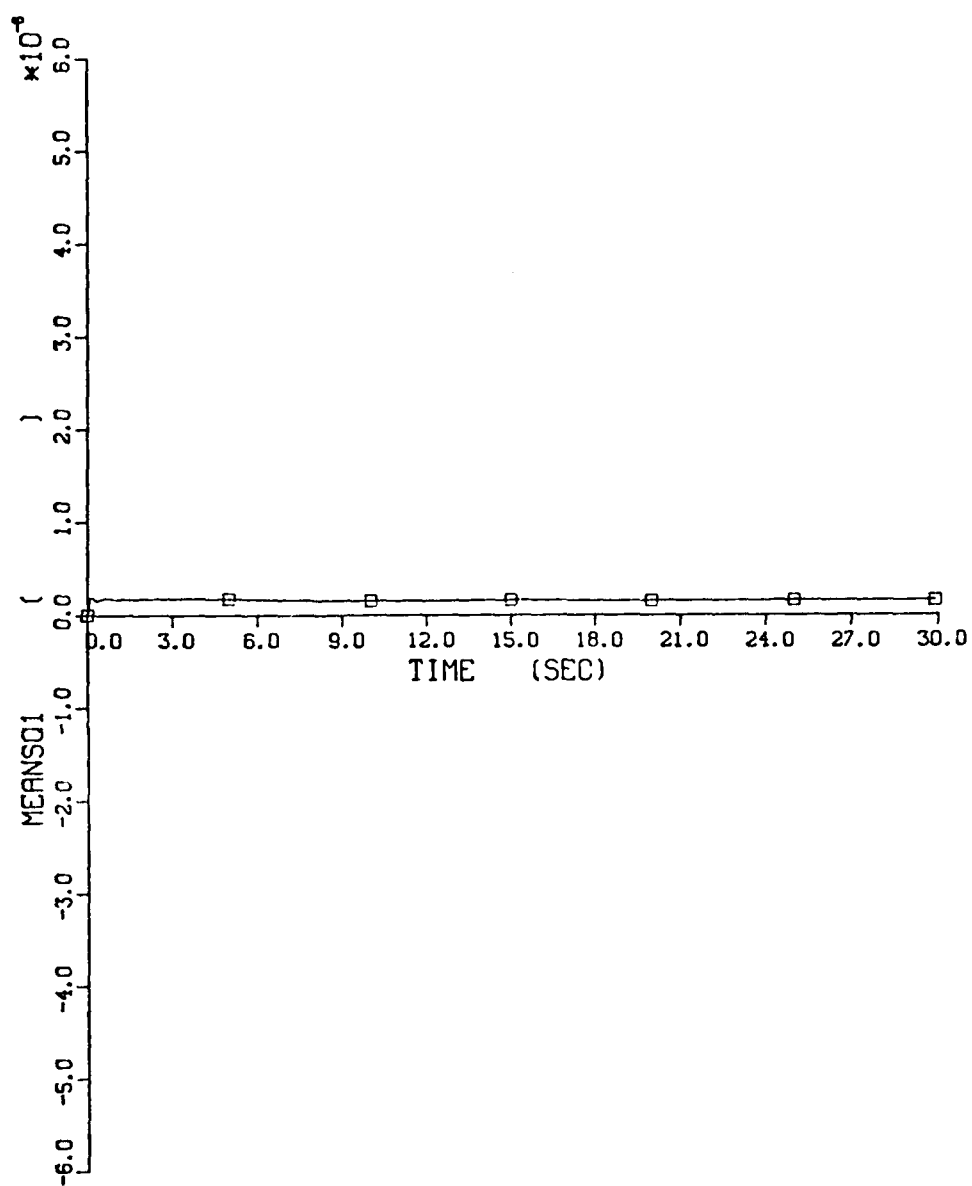
RSDIRS PERFORMANCE IMPROVEMENT

Figure 24. Z-Axis Accelerometer Output Mean-Squared Error
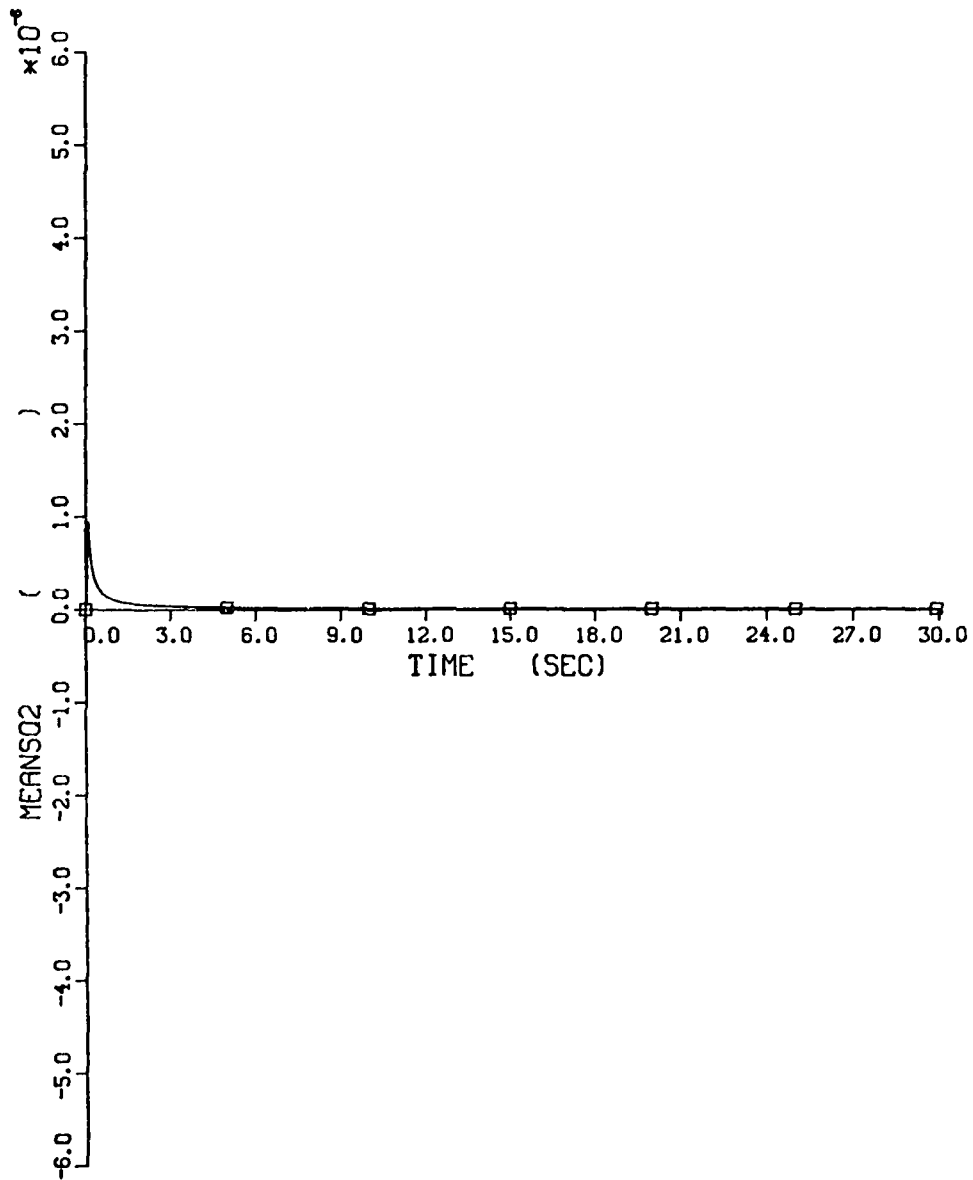
RSDIRS PERFORMANCE IMPROVEMENT

Figure 25. Algorithm D Z-Axis Accelerometer Output Estimation
Mean-Squared Error
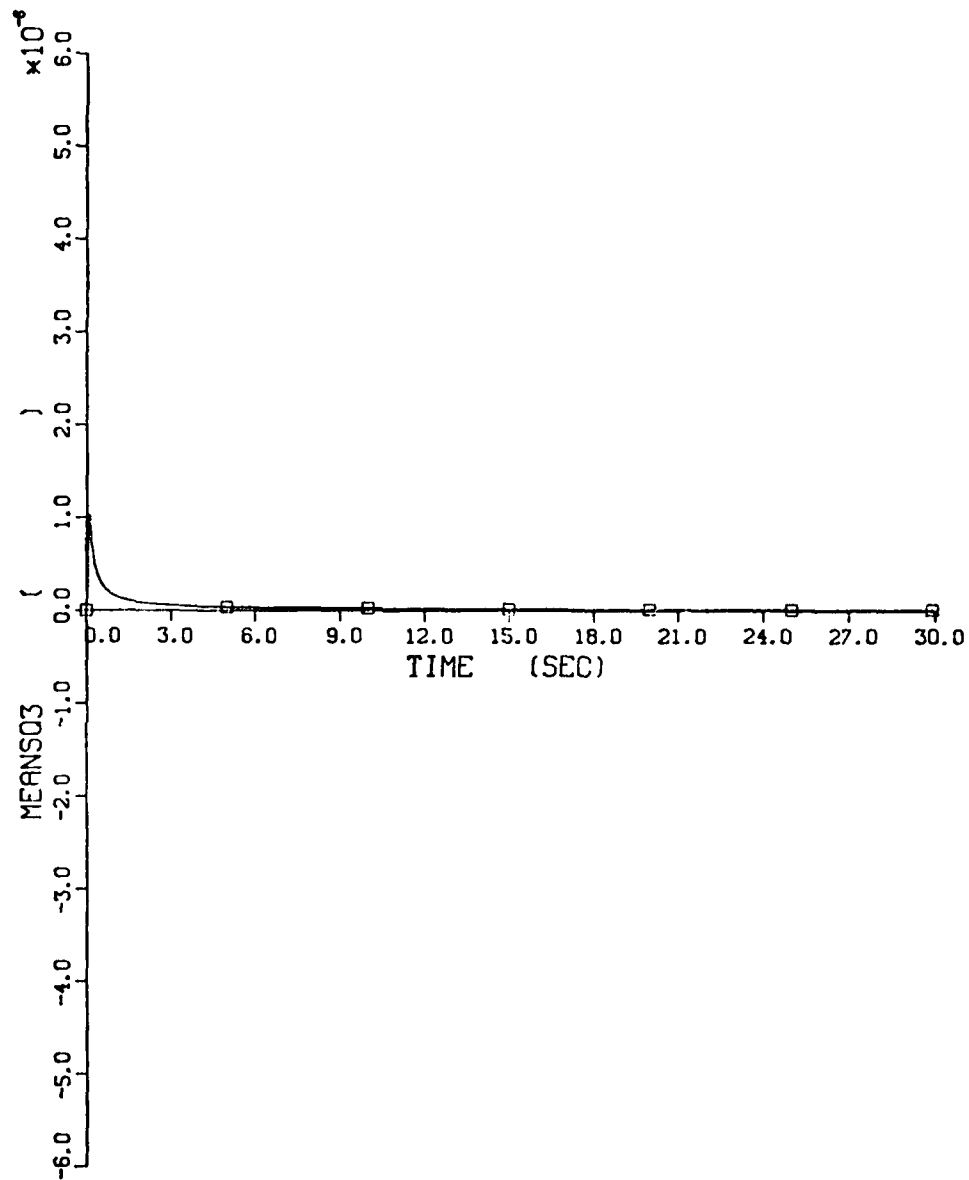
61

RSDIRS PERFORMANCE IMPROVEMENT

Figure 26. Algorithm E Z-Axis Accelerometer Output Estimation
Mean-Squared Error
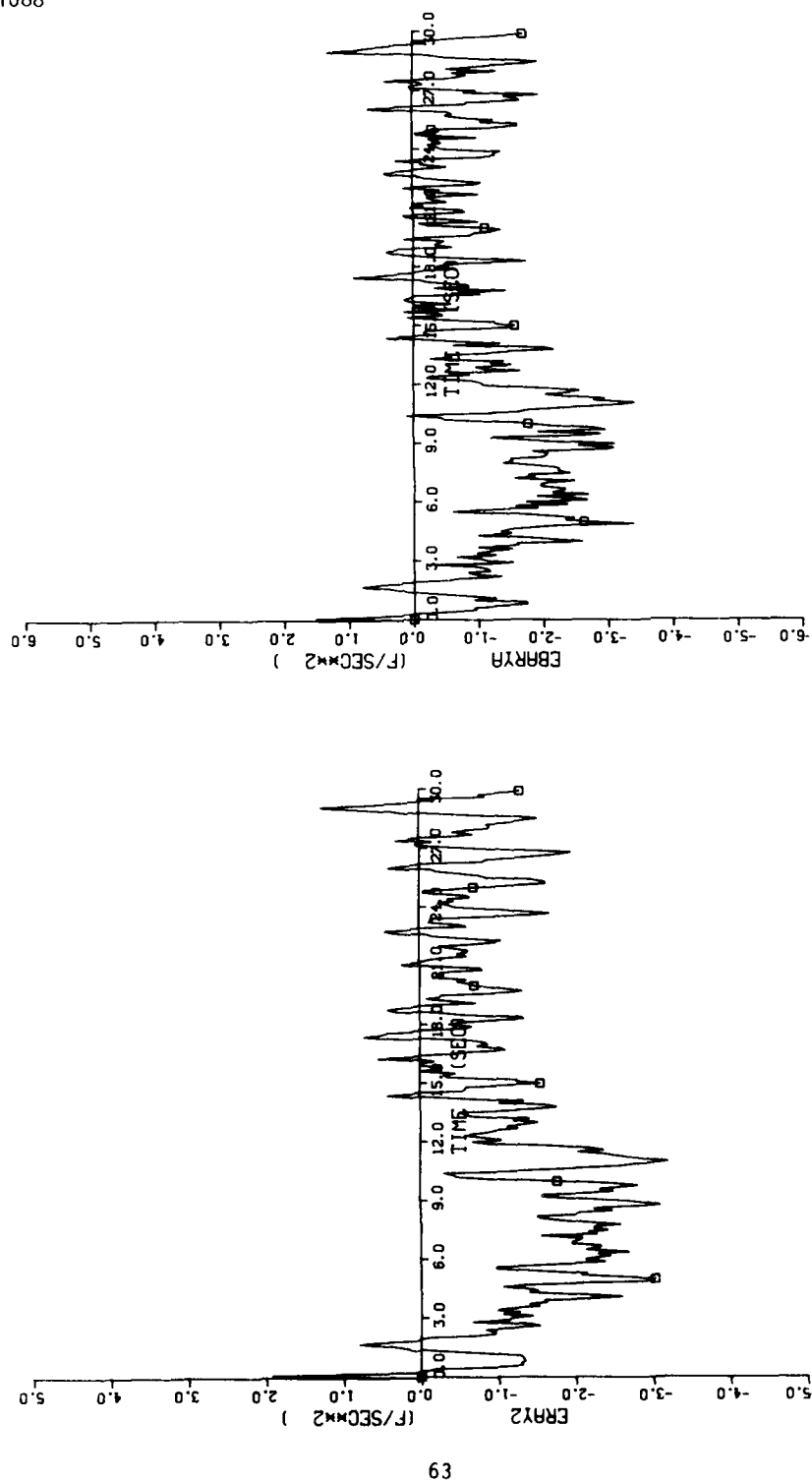
62

RSDIRS PERFORMANCE IMPROVEMENT

Figure 27. Y-Axis Accelerometer Output-Rate Error and Algorithm
a. Y-Axis Accelerometer Output-Rate Estimation Error

just aft of the pilot's station. Others were made with the sensors located
at FS77, which is forward of the pilot's station. The parameters used for
the deterministic simulation runs are given in Table 1 and Table 2 for
the accelerometers and ring-laser gyros respectively. The parameter
amplitudes were each set identical for each of the gyros and acceler-
ometers; however, the algebraic sign of the parameters were not all the
same.

Simulation runs over the flight profile shown in Figure 13 were
made with and without weighted-least-squares averaging mechanized for
the inertial reference assembly. Simulation runs were made using:
least-squares averaging of the redundant gyro data only; least-squares
averaging of the redundant accelerometer data only; and least-squares
averaging of both, redundant gyro and accelerometer data. The results
discussed in this section are all from deterministic simulation runs
to facilitate detailed comparative analysis of total system errors.

The inertial navigation system (INS) position, velocity, and
altitude errors, for sensor Configuration 2 located at FS313, are shown
in Figure 28, Figure 29, and Figure 30 respectively. During this
simulation run the effects of accelerometer lever-arm are included, but
the aircraft structural mode effects are not included for any of the
sensors. The dashed curves represent the errors resulting from an
orthogonal-triad of inertial sensors aligned relative to the aircraft
cardinal axes as shown by Figure 11. The solid curves represent
navigation system errors resulting from least-squares averaging of the
redundant inertial sensor data from the same orthogonal-triad of sensors
plus an additional orthogonal-triad of sensors which is skewed with
respect to the first triad.

For this case, the accelerometer data was obtained from an ortho-
gonal-triad of sensors aligned relative to the aircraft cardinal axes,
while the least-squares data averages of all six gyros were utilized.
As can be observed from Figure 28, a significant decrease in position
error can be obtained by utilizing the redundant gyro data. A corre-
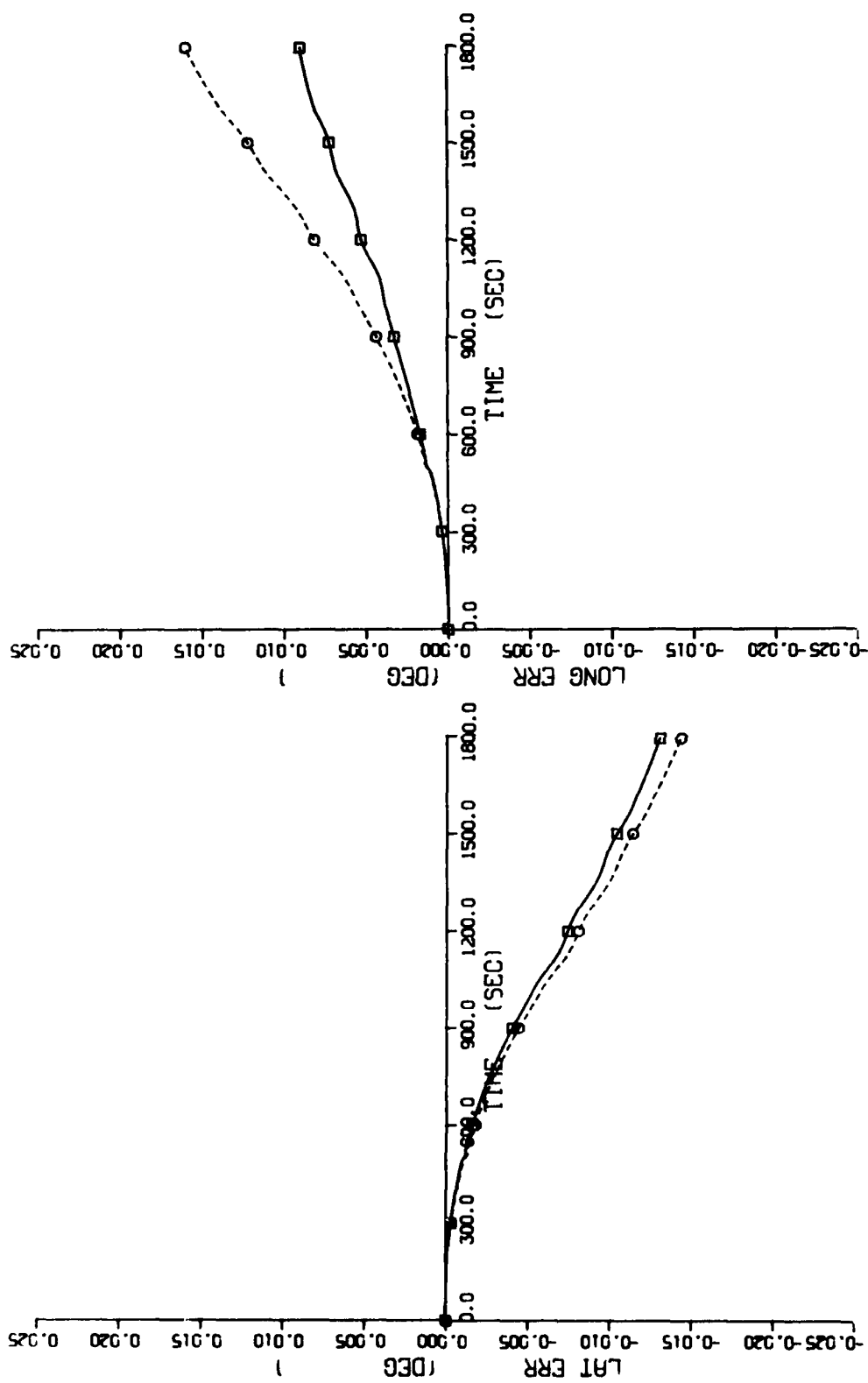sponding decrease in velocity error is also apparent in Figure 29.

Figure 28. Latitude and Longitude Errors, With and Without
Least-Squares Averaging of Redundant Gyro Data,
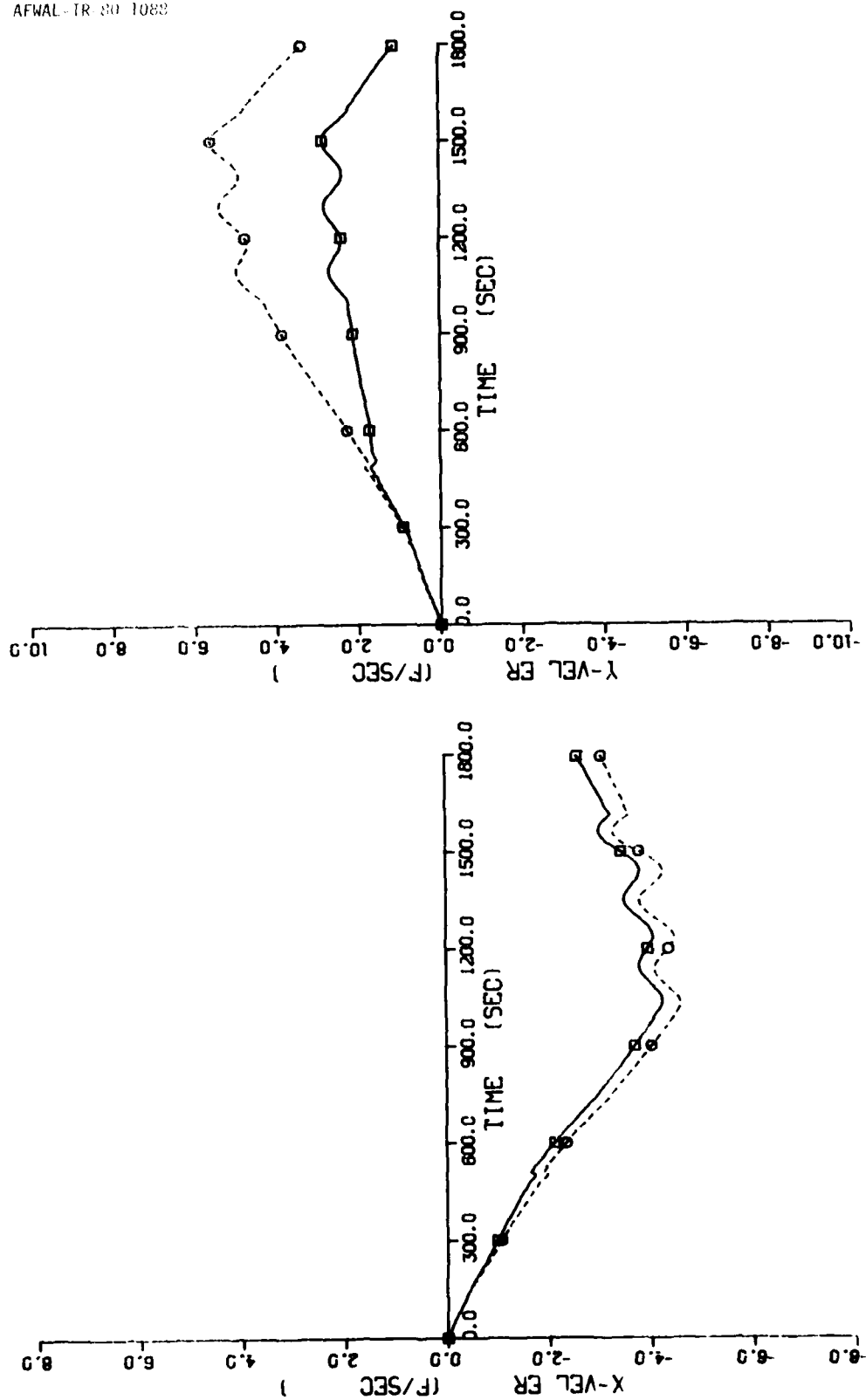For Sensor Configuration 2

Figure 29. X and Y Velocity Errors, With and Without Least-Squares Averaging of Redundant Gyro Data, For Sensor Configuration 2
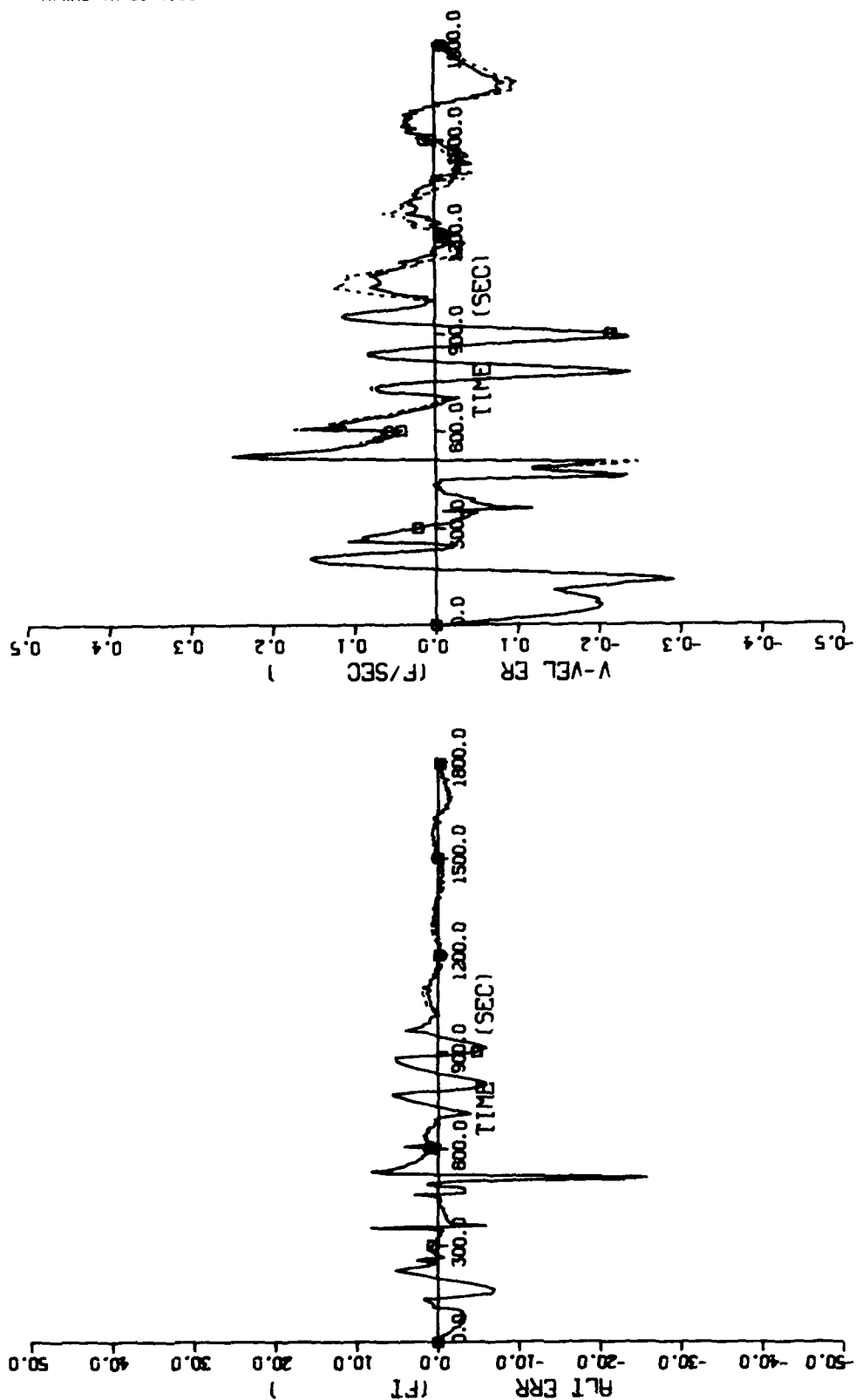
Figure 30. Altitude and Vertical Velocity Errors, With and
Without Least-Squares Averaging of Redundant
Gyro Data, For Sensor Configuration 2

Some points of interest on the curves of Figure 29 can be noted. After approximately 500 seconds an evasive maneuver consisting of a 4.5-g rolling-pullup and a change from zero to forty-five degree heading was accomplished. The abrupt change in Y-Velocity error with least-squares averaging is due, almost entirely, to gyro misalignment errors and the interaction of these errors with least-squares averaging of gyro data.

A loiter maneuver was initiated at approximately 1000 seconds. No significant difference was noted between the error propagation with and without least-squares averaging of gyro data. The sine-wave component of error during this maneuver is due to a combination of sensor errors including bias, scale factor, misalignment, and attitude computation. The attitude computation is accomplished by a third-order quaternion algorithm.

Following the loiter maneuver, aircraft heading was changed from the previous 45 degrees to a new heading of 145 degrees. The abrupt change in velocity error, with and without least-squares averaging of gyro data, is due primarily to accelerometer bias errors, and secondarily to gyro bias errors along with gyro and accelerometer scale factor and misalignment errors.

Altitude and vertical velocity errors are presented in Figure 30. Some improvement in vertical velocity accuracy with least-squares averaging of gyro data can be noted during the evasive maneuver at 500 seconds and during the loiter maneuver. Improvement in altitude accuracy appears to be minimal and noticeable only during the loiter maneuver. A third-order damping loop is used to damp the inertial navigation system vertical channel.

Figure 31 through Figure 33 show the navigation system errors, with and without least-squares averaging of the redundant accelerometer data. In this case the gyro data was obtained from an orthogonal-triad of sensors aligned relative to the aircraft cardinal axes. All other parameters remain the same as for the previous case.
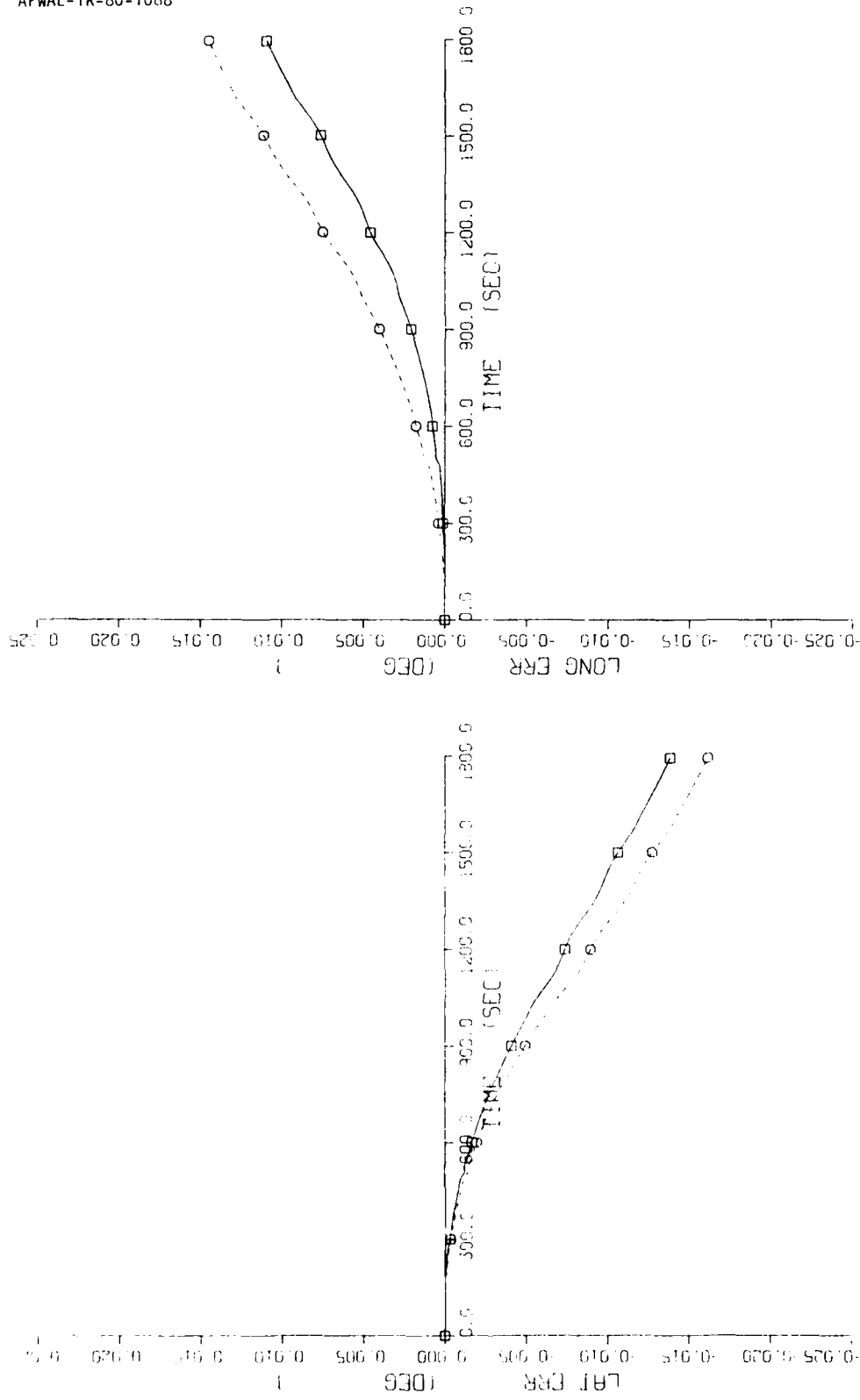
Figure 31. Latitude and Longitude Errors, With and Without
Least-Squares Averaging of Redundant Accelerometer
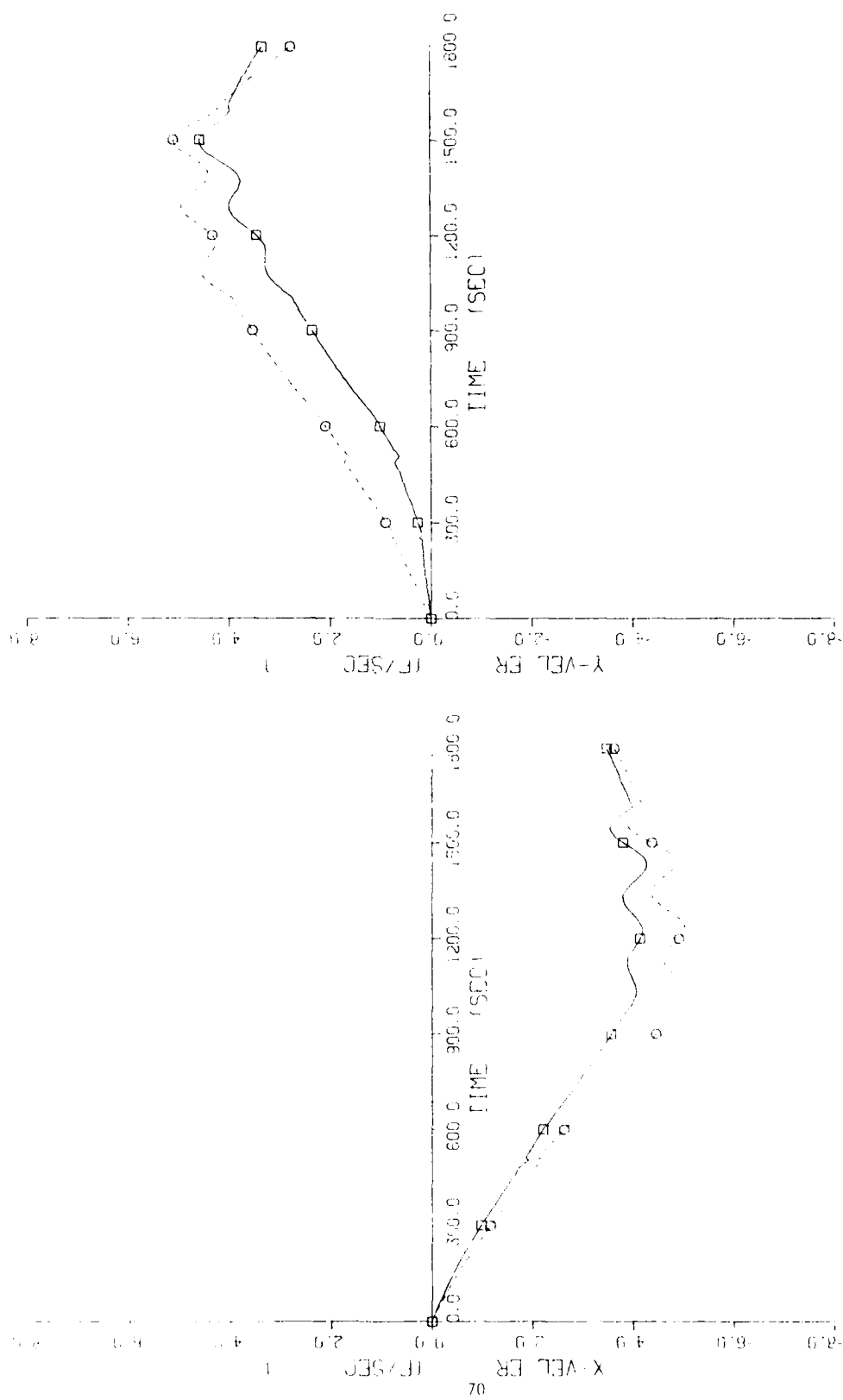Data, For Sensor Configuration 2

Figure 32. X and Y Velocity Errors, With and Without Least-
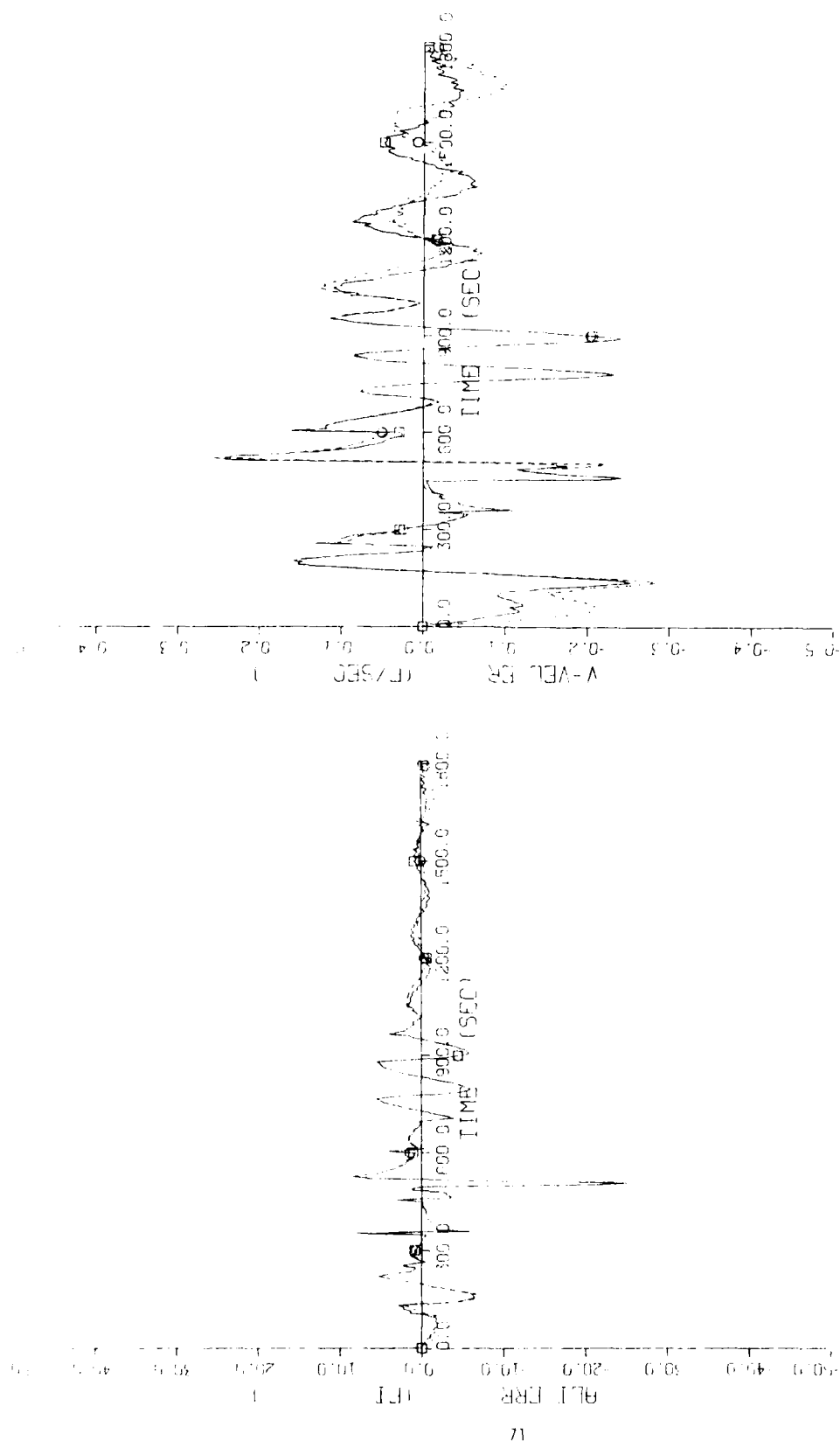Squares Averaging of Redundant Accelerometer Data,
For Sensor Configuration 2

Figure 33. Altitude and Vertical Velocity Errors, With and
Without Least-Squares Averaging of Redundant
Accelerometer Data, For Sensor Configuration 2

Observation of Figure 31 indicates that a significant decrease in position error can be realized by employing least-squares averaging of accelerometer data. Figure 32 indicates a corresponding decrease in velocity error. Except for the effect of gyro misalignment on the Y-Velocity error during the evasive maneuver, position and velocity error propagation resulting from least-squares averaging of gyro data was similar to that obtained from least-squares averaging of accelerometer data.

Comparison of Figure 33 with Figure 30 indicates that least-squares averaging can result in smaller altitude and vertical velocity errors when using redundant data from the accelerometers than from the gyros.

Figure 34 through Figure 36 show the reduction in navigation system errors which can result when redundant data from both, gyros and accelerometers, are averaged by the least-squares method. For this case, a significant decrease in position and velocity errors resulted. However, there is very little difference between the errors in altitude and vertical velocity resulting from averaging the gyro and accelerometer data, as compared with averaging the accelerometer data only. The navigation system performance resulting from least-squares averaging of both, gyro and accelerometer redundant data, is essentially the sum of error differences resulting from least-squares averaging of redundant gyro data only and redundant accelerometer data only.

Figure 37 through Figure 42 show the results obtained for sensor Configuration 1. During the simulation runs all other parameters and dynamics remained the same as those used for sensor Configuration 2. Comparison of Figure 28 with Figure 37, Figure 29 with Figure 38, and Figure 30 with Figure 39 shows similar results for the two sensor configurations when least-squares averaging of redundant gyro data is used. However, some differences do occur and can be observed in the plots. The dashed curves will be the same for both configurations as they represent the results obtained from an orthogonal-triad of sensors aligned relative to the aircraft cardinal axes.
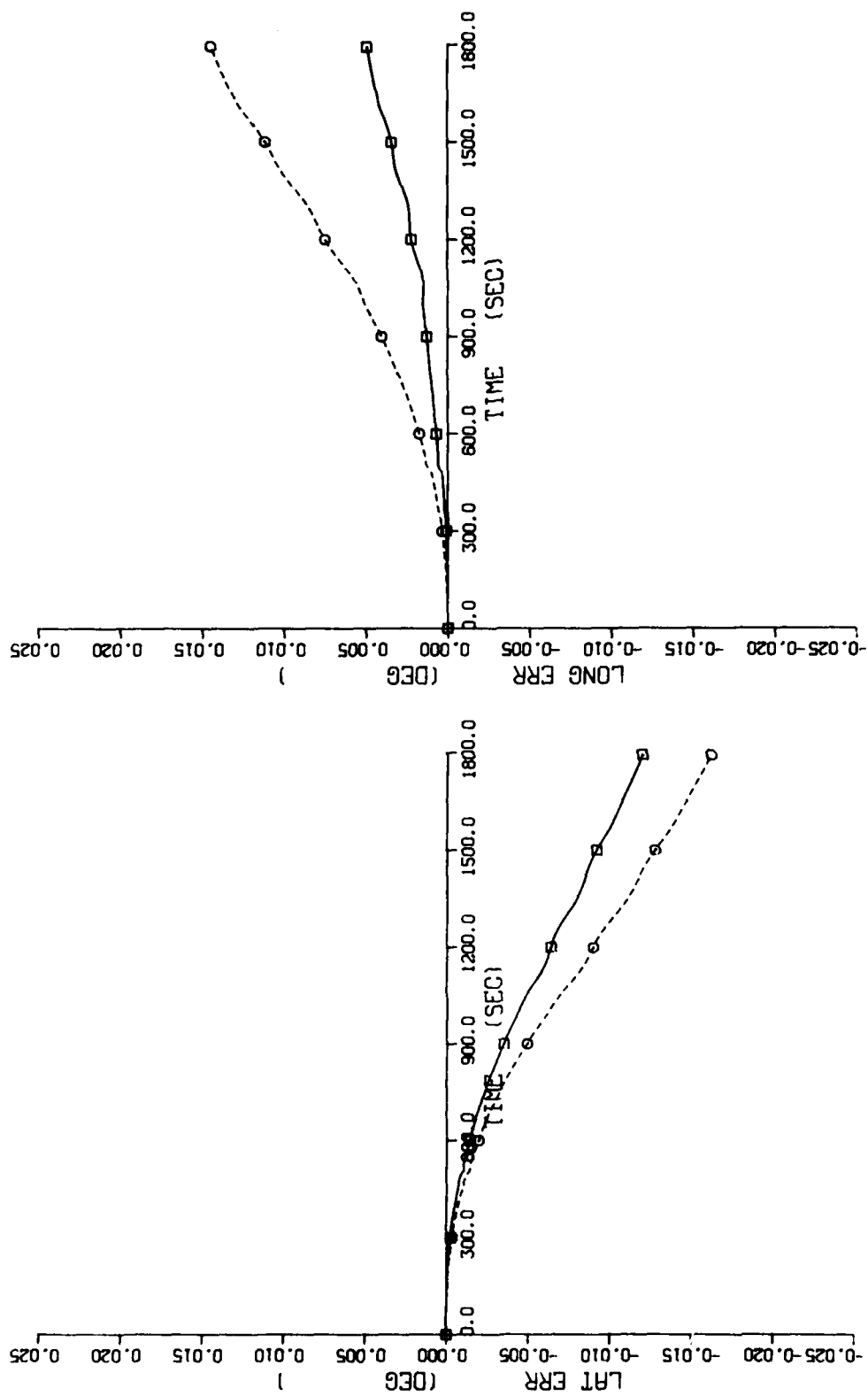
Figure 34. Latitude and Longitude Errors, With and Without Least-Squares Averaging of Redundant Gyro and Accelerometer Data, For Sensor Configuration 2
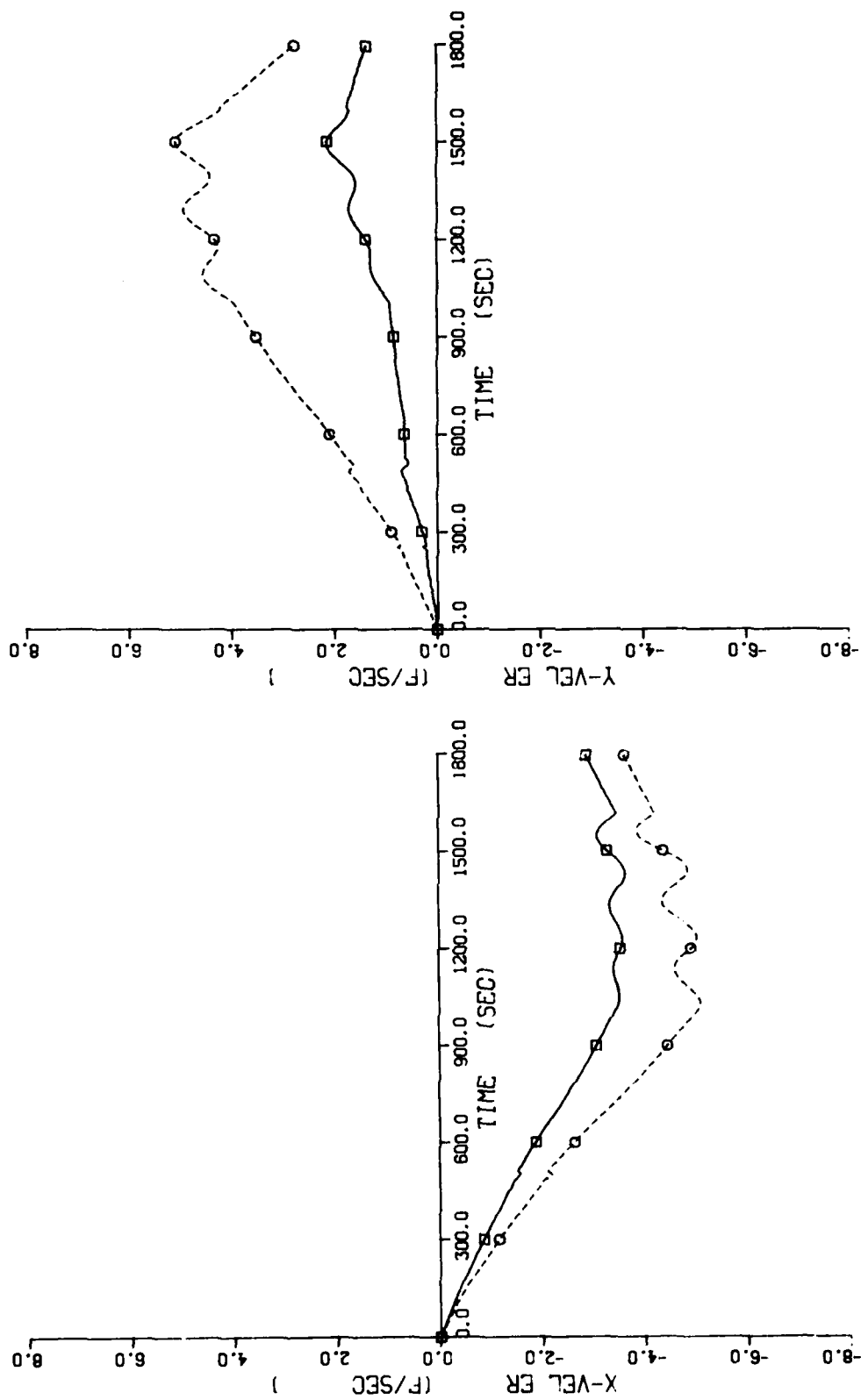
Figure 35. X and Y Velocity Errors, With and Without Least-Squares Averaging of Redundant Gyro and Accelerometer Data, For Sensor Configuration 2
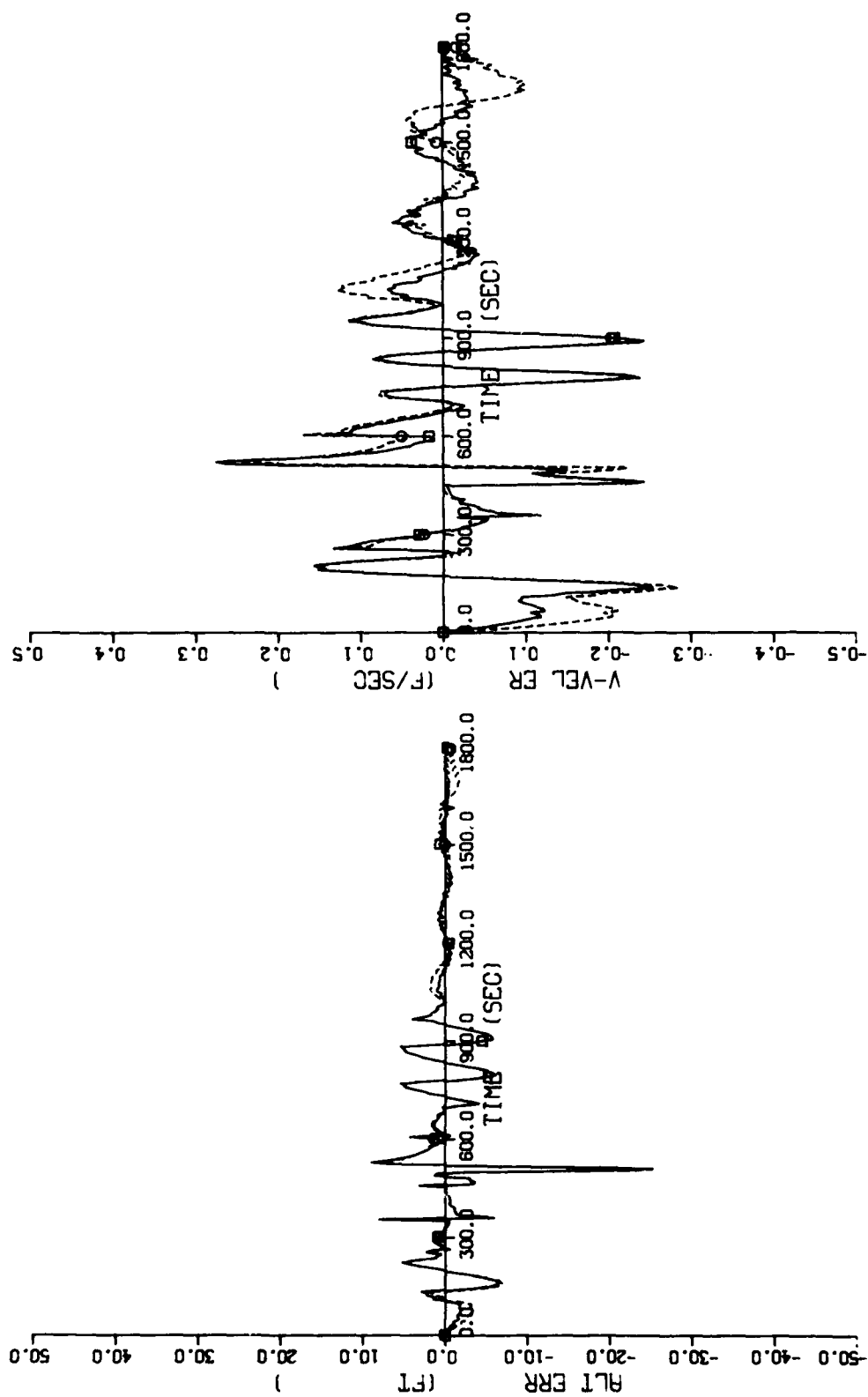
Figure 36. Altitude and Vertical Velocity Errors, With and Without Least-Squares Averaging of Redundant Gyro and Acceler- ometer Data, For Sensor Configuration 2
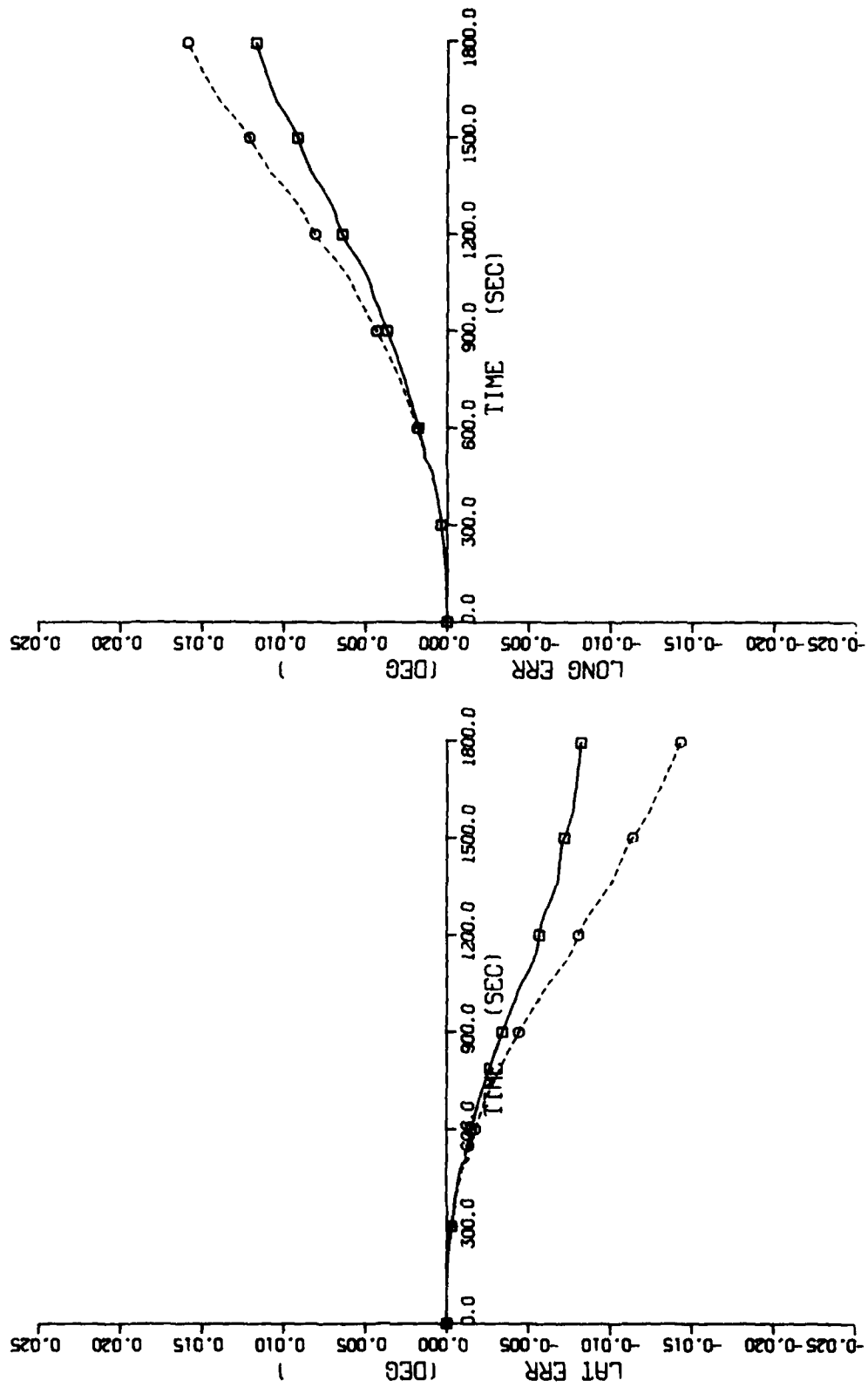
Figure 37. Latitude and Longitude Errors, With and Without Least-Squares Averaging of Redundant Gyro Data, For Sensor Configuration 1

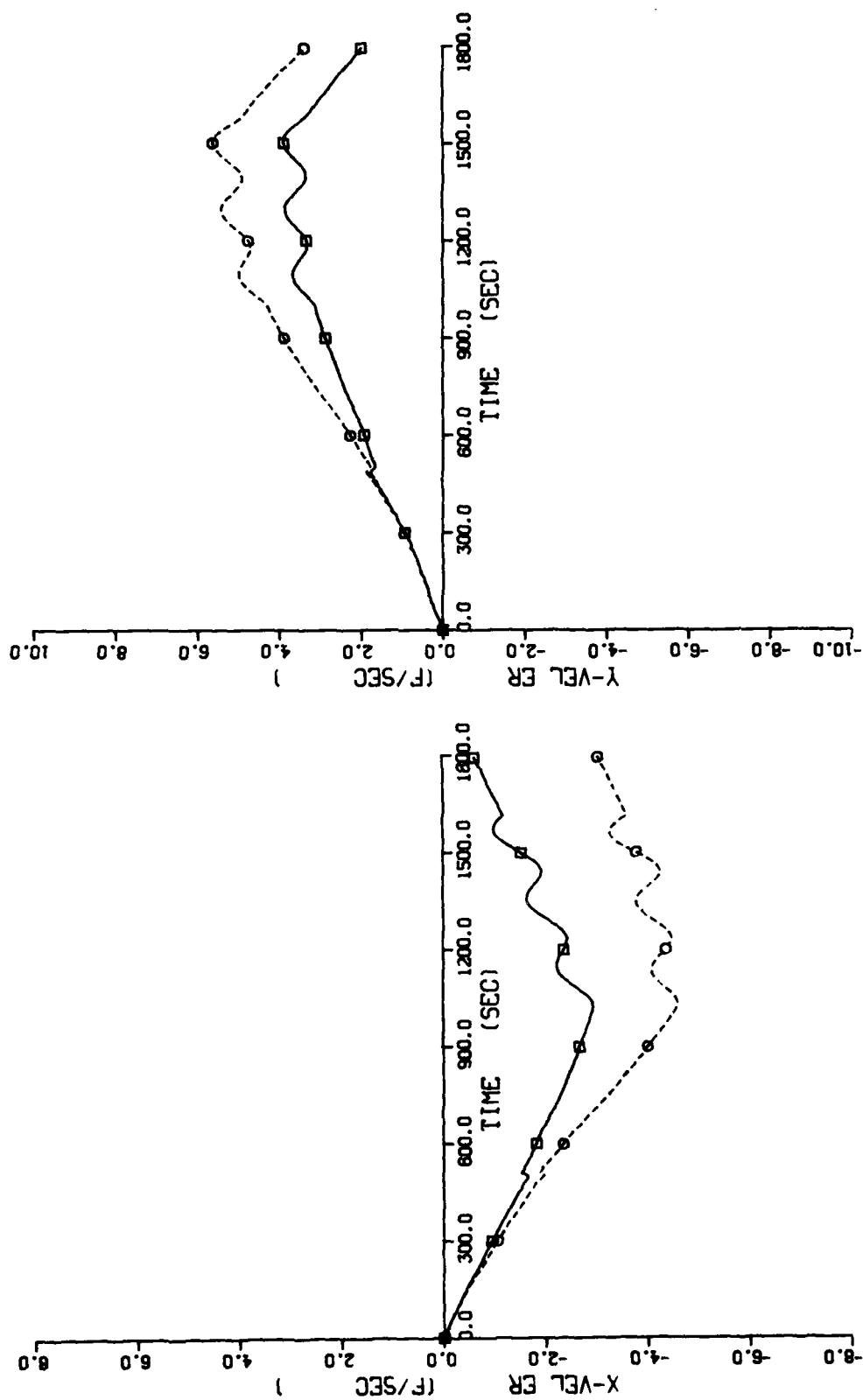Figure 38. X and Y Velocity Errors, With and Without Least-Squares Averaging of Redundant Gyro Data, For Sensor Configuration 1

Figure 39. Altitude and Vertical Velocity Errors, With and Without Least-Squares Averaging of Redundant Gyro Data, For Sensor Configuration 1

Figure 40. Latitude and Longitude Errors, With and Without
Least-Squares Averaging of Redundant Accelerometer
Data, For Configuration 1

Figure 41. X and Y Velocity Errors, With and Without Least-Squares Averaging of Redundant Accelerometer Data, For Configuration 1
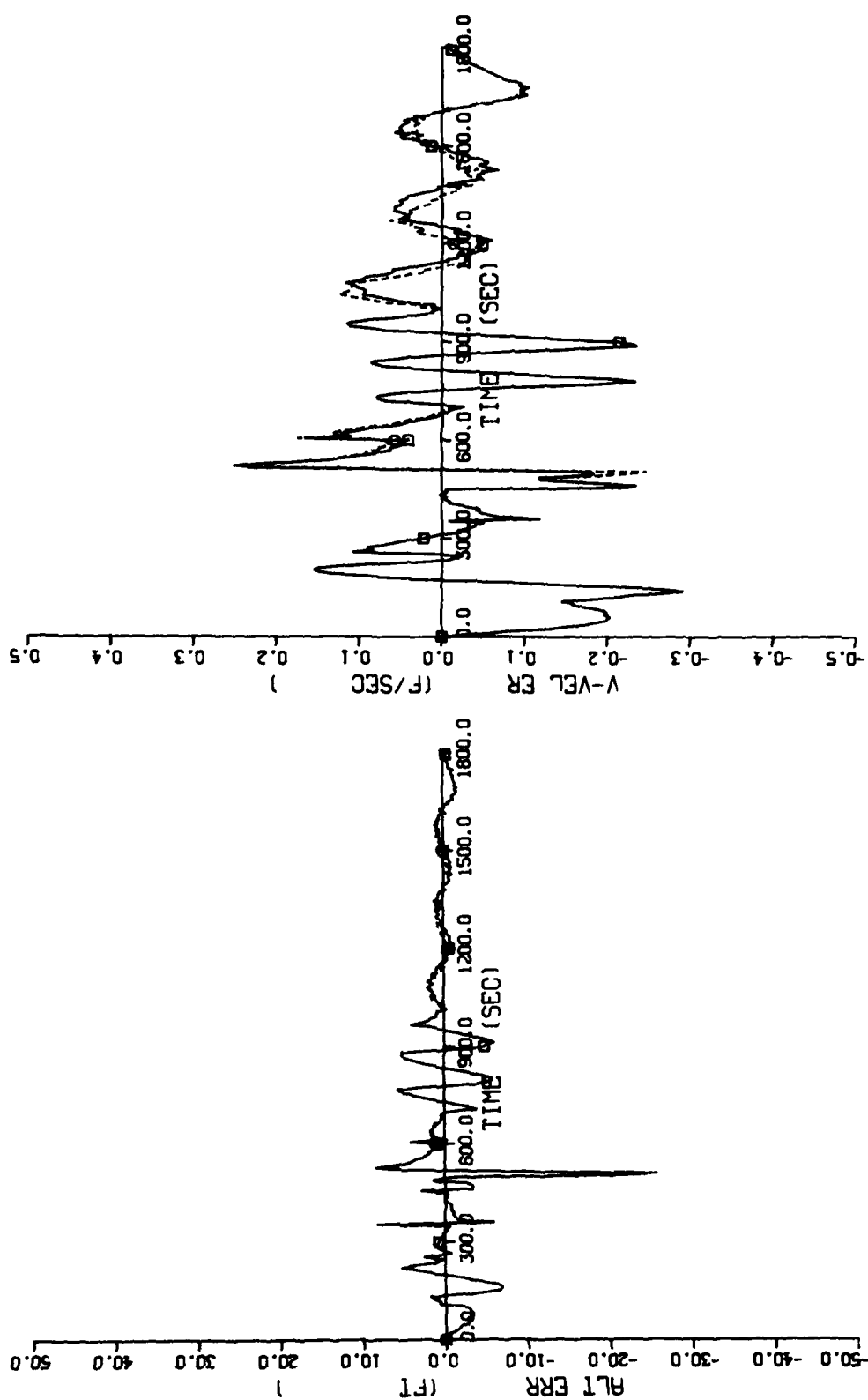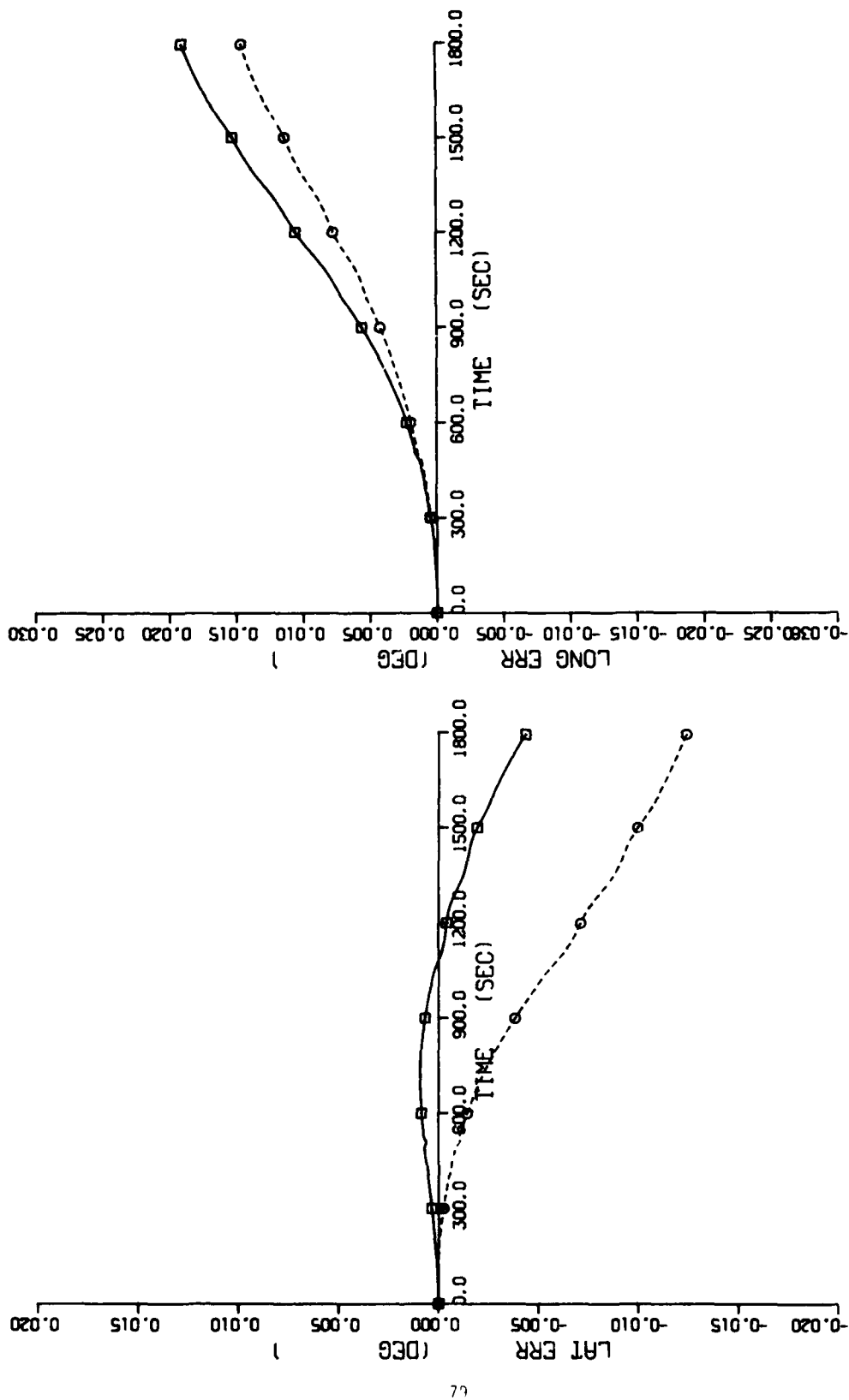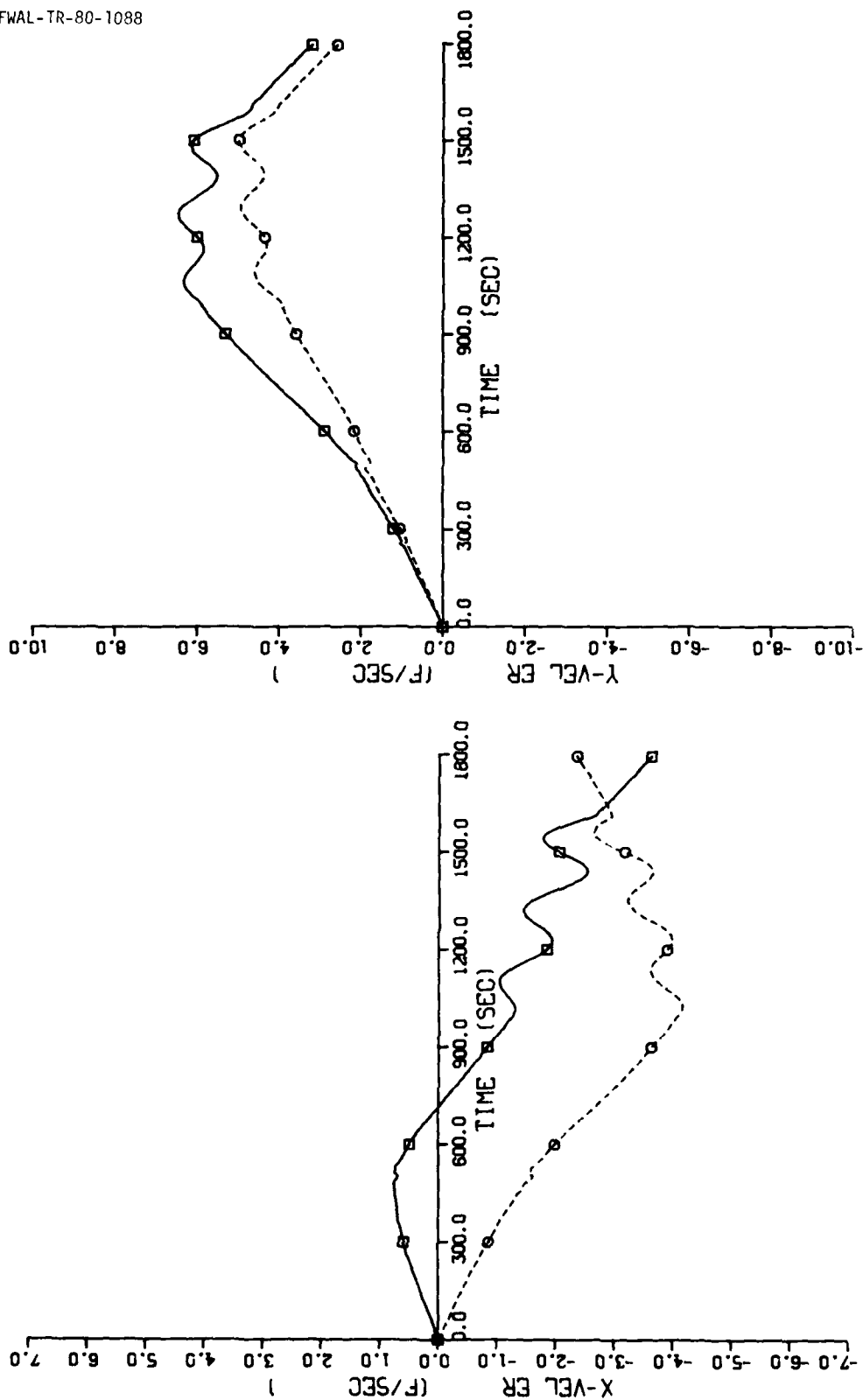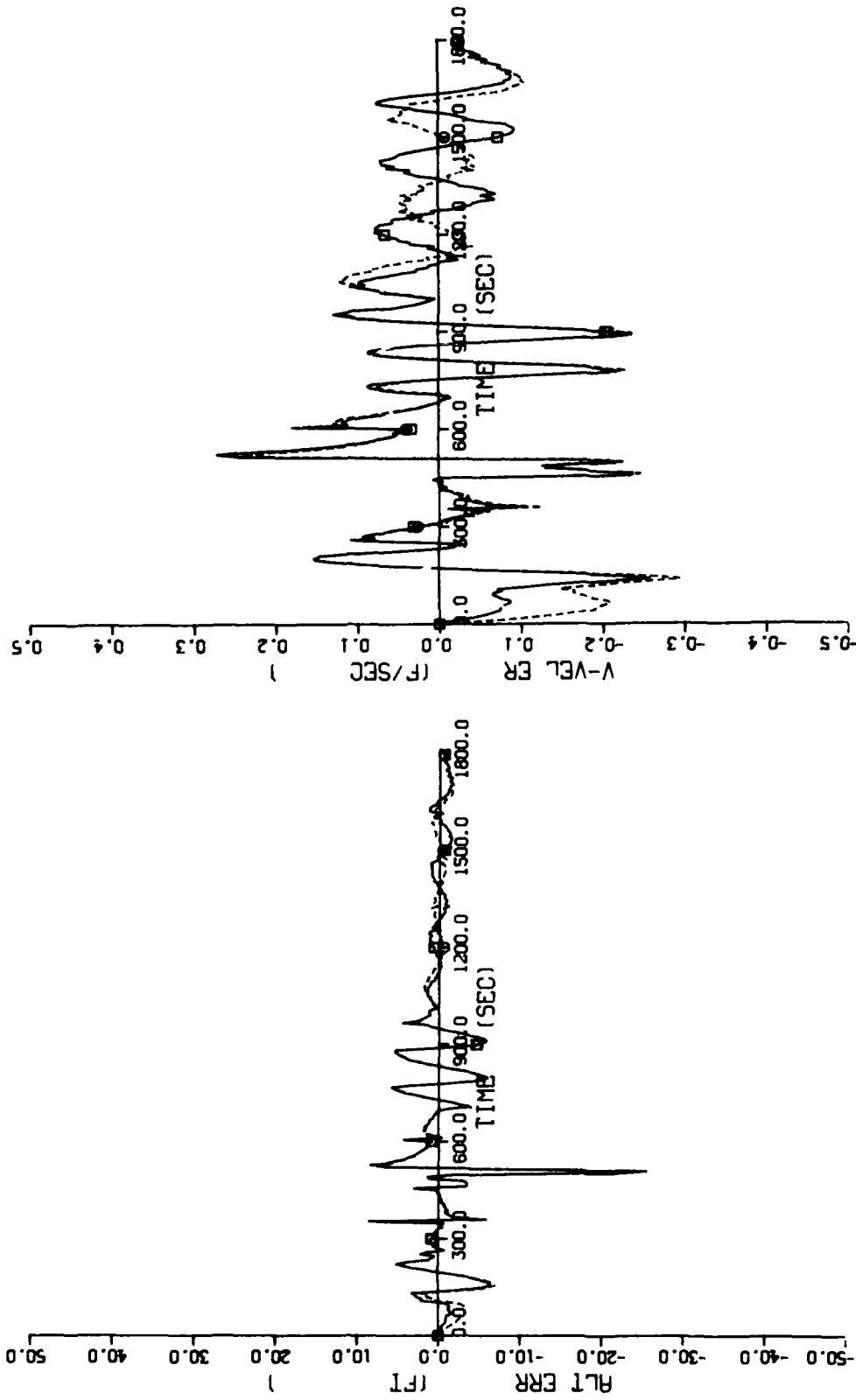
Figure 42. Altitude and Vertical Velocity Errors, With and
Without Least-Squares Averaging of Redundant
Accelerometer Data, For Configuration 1

One easily observable difference between performance of the two sensor configurations is the switch in channels (axes) of performance improvements. More decreases in latitude and X-axis velocity error resulted from Configuration 1 than from Configuration 2. The opposite effect can be observed for longitude and Y-axis velocity error.

The effects of the evasive maneuver at about 500 seconds are more evenly distributed between the X and Y velocity errors for Configuration 1 than they were for Configuration 2. As discussed previously, the change in error trend at this point is due primarily to the interaction of gyro misalignment errors with least-squares averaging.

Very little difference between the two configurations in altitude performance can be observed. The performance in vertical velocity is slightly better for Configuration 2 than for Configuration 1.

When least-square averaging of redundant accelerometer data is used, and all other parameters and dynamics remain the same, a significant difference in performance between Configuration 1 and Configuration 2 occurs. This difference is due primarily to the interaction of accelerometer misalignment errors with least-squares averaging.

A comparison of Figure 40 with Figure 31 shows the latitude error for Configuration 1 to be much smaller than for Configuration 2. However, the longitude error for Configuration 1 is much greater than for Configuration 2, and even worse, is significantly greater than without least-squares averaging of the redundant accelerometer data.

Similar changes occur in velocity errors as can be seen by comparing Figure 41 with Figure 32. In this case the evasive maneuver affected the performance of Configuration 1 considerably, but caused only minimal effects on Configuration 2. The loiter maneuver had similar effects on both configurations, but were switched to opposite axes.

Comparison of Figure 42 with Figure 33 shows very little difference in altitude and vertical velocity performance of the two configurations.

The previous discussion along with Figure 28 through Figure 42 were all concerned with no aircraft structural mode effects acting on the inertial sensors. However, the accelerometers were subjected to lever-arm effects. The navigation system performance, with an orthogonal-triad of sensors, during these simulation runs, and many simulation runs with different flight profiles and random selection of sensor parameters, was typically less than one and one-half nautical mile per hour error in position, less than five feet-per-second error in velocity, less than three-tenths feet-per-second error in vertical velocity, and less than twenty-five feet error in altitude.

The navigation system performance of the previously discussed cases using least-squares averaging of the redundant sensor data, was typically significantly better than that of an orthogonal-triad. However, this is not always true as was shown by one of the previously discussed cases. Other cases, to be discussed later in this section, will also show that least-squares averaging does not always improve the navigation system performance.

Figure 43 through Figure 50 show the navigation system errors when the inertial sensors are subjected to aircraft/structural modes. The simulated aircraft is an F-4 and the sensors are located at the same location (FS313) as for the previous cases. The same sensor parameters and dynamics are also used. The only difference is the addition of structural modes.

Comparison of Figure 43 with Figure 28 and Figure 44 with Figure 29 shows the effects of structural modes on navigation system performance, with and without least-squares averaging of the redundant gyro data for Configuration 2. Performance improvement is still realized with least-squares averaging. However, due to the structural mode effects, navigation system performance, with and without least squares averaging, has deteriorated approximately three to four times. The structural mode effects also tend to alter some effects of aircraft dynamic maneuvers.

Comparison of Figure 45 with Figure 37 and Figure 46 with Figure 38 show the effects of structural modes on sensor Configuration 1. These effects are comparable to those for Configuration 2.
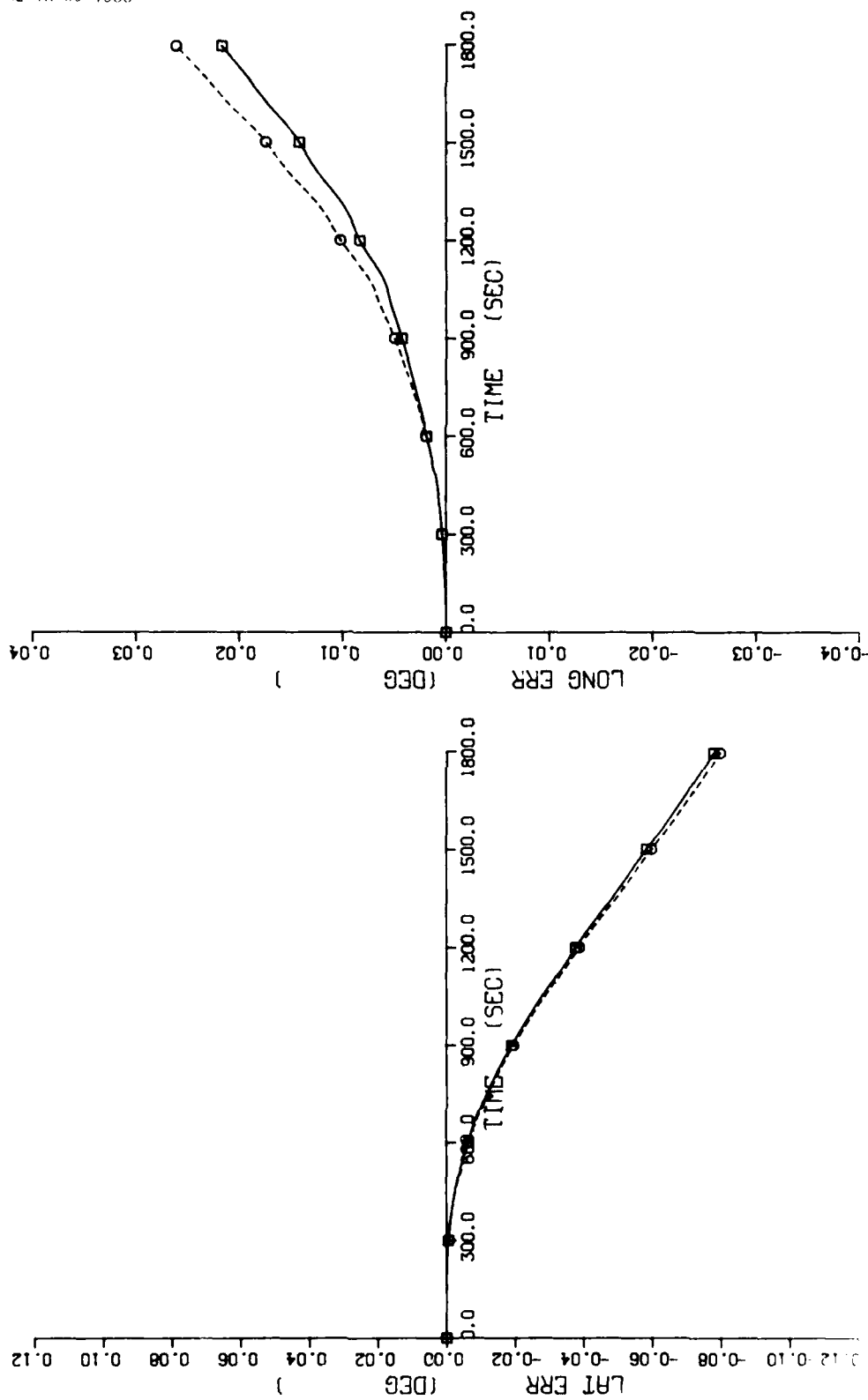
Figure 43. Latitude and Longitude Errors, With and Without Least-Squares Averaging of Redundant Gyro Data, For Configuration 2 With Structural Modes

Figure 44. X and Y Velocity Errors, With and Without Least-
Squares Averaging of Redundant Gyro Data, For
Configuration 2 With Structural Modes

Figure 45. Latitude and Longitude Errors, With and Without Least-Squares Averaging of Redundant Gyro Data, For Configuration 1 With Structural Modes
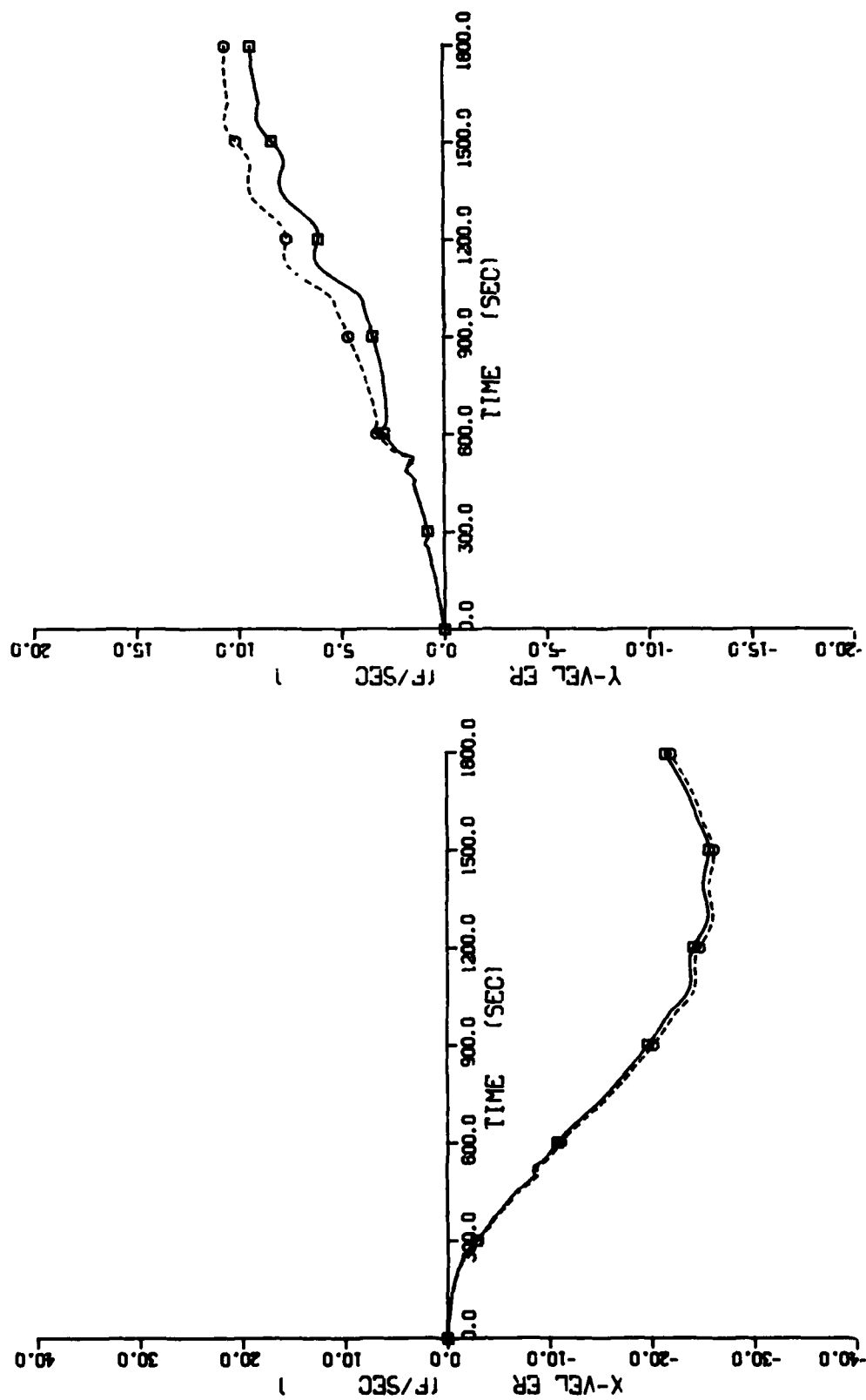
Figure 46. X and Y Velocity Errors, With and Without Least-Squares Averaging of Redundant Gyro Data, For Configuration 1 With Structural Modes

LONG ERR (DEG)

-0.010 -0.008 -0.005 -0.004 -0.002 0.000 0.002 0.004 0.005 0.008 0.010

TIME (SEC)

0.0 300.0 600.0 900.0 1200.0 1500.0 1800.0

LAT ERR (DEG)

-0.10 -0.08 -0.06 -0.04 -0.02 0.00 0.02 0.04 0.06 0.08 0.10

TIME (SEC)
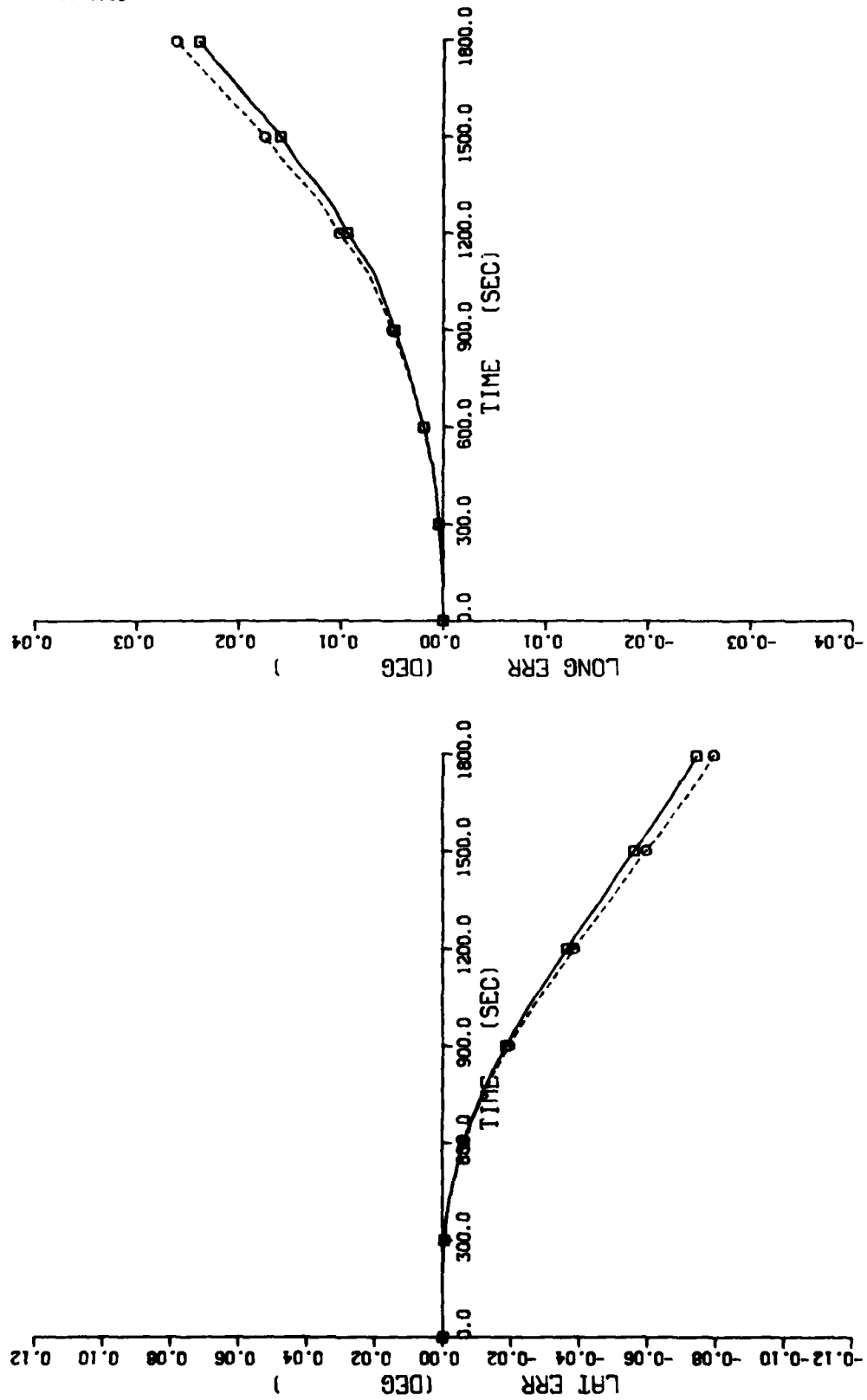
0.0 300.0 600.0 900.0 1200.0 1500.0 1800.0

Figure 47. Latitude and Longitude Errors, With and Without Least-Squares Averaging of Redundant Gyro Data, For Configuration 3 With Structural Modes

Figure 48. X and Y Velocity Errors, With and Without Least-Squares Averaging of Redundant Gyro Data, For Configuration 3 With Structural Modes

Figure 49. Latitude and Longitude Errors, With and Without Least-Squares Averaging of Redundant Gyro Data, For Configuration 4 With Structural Modes
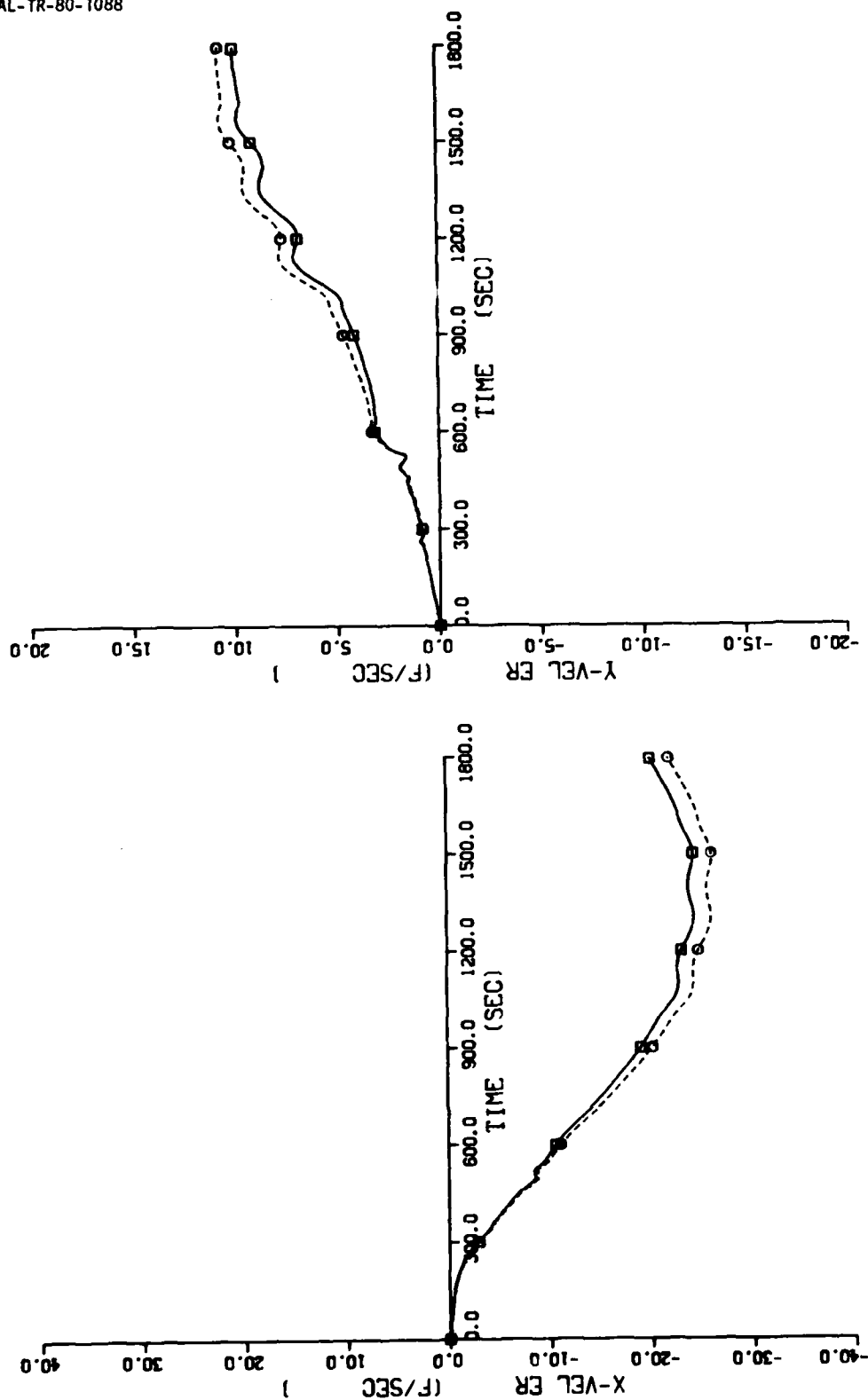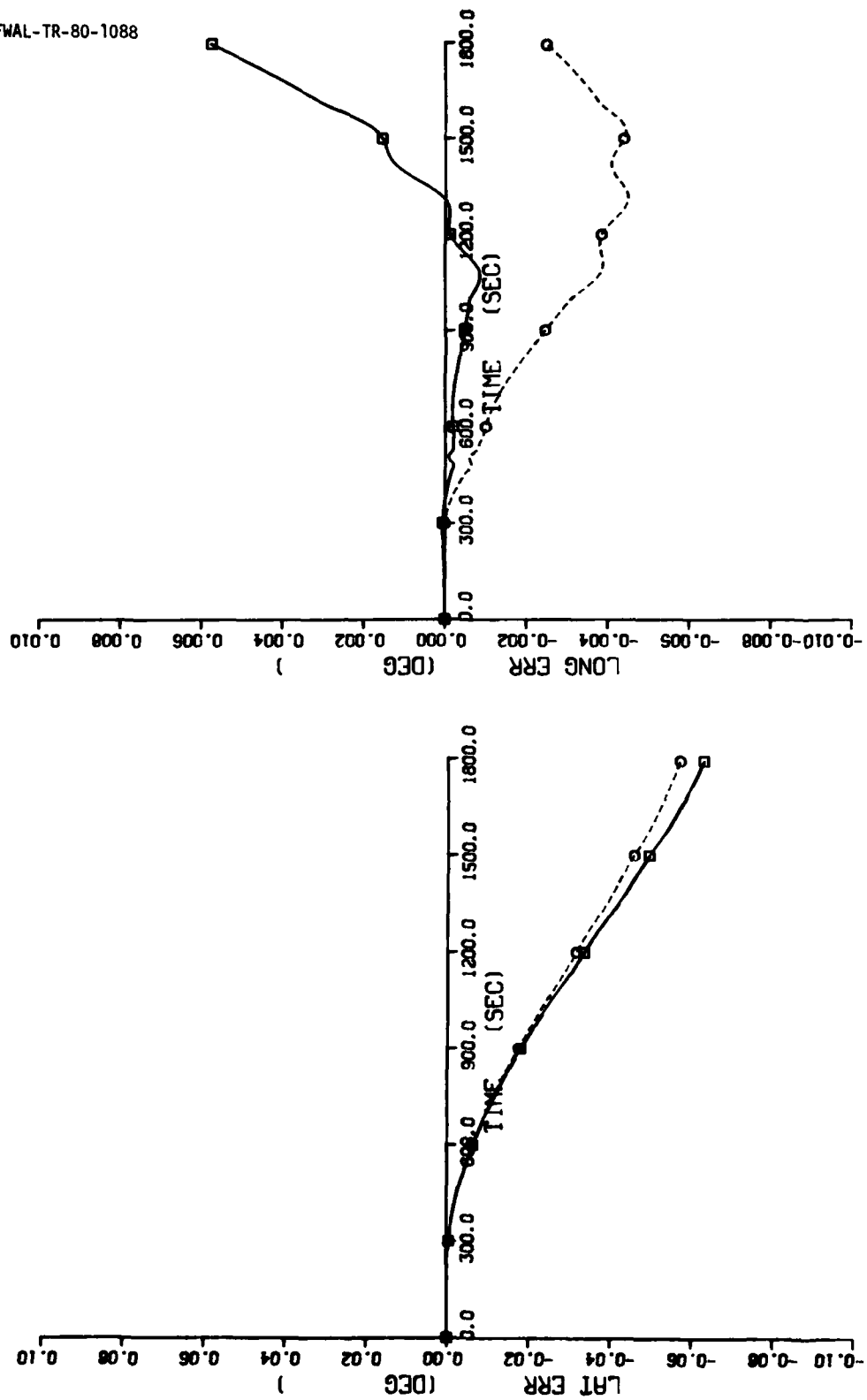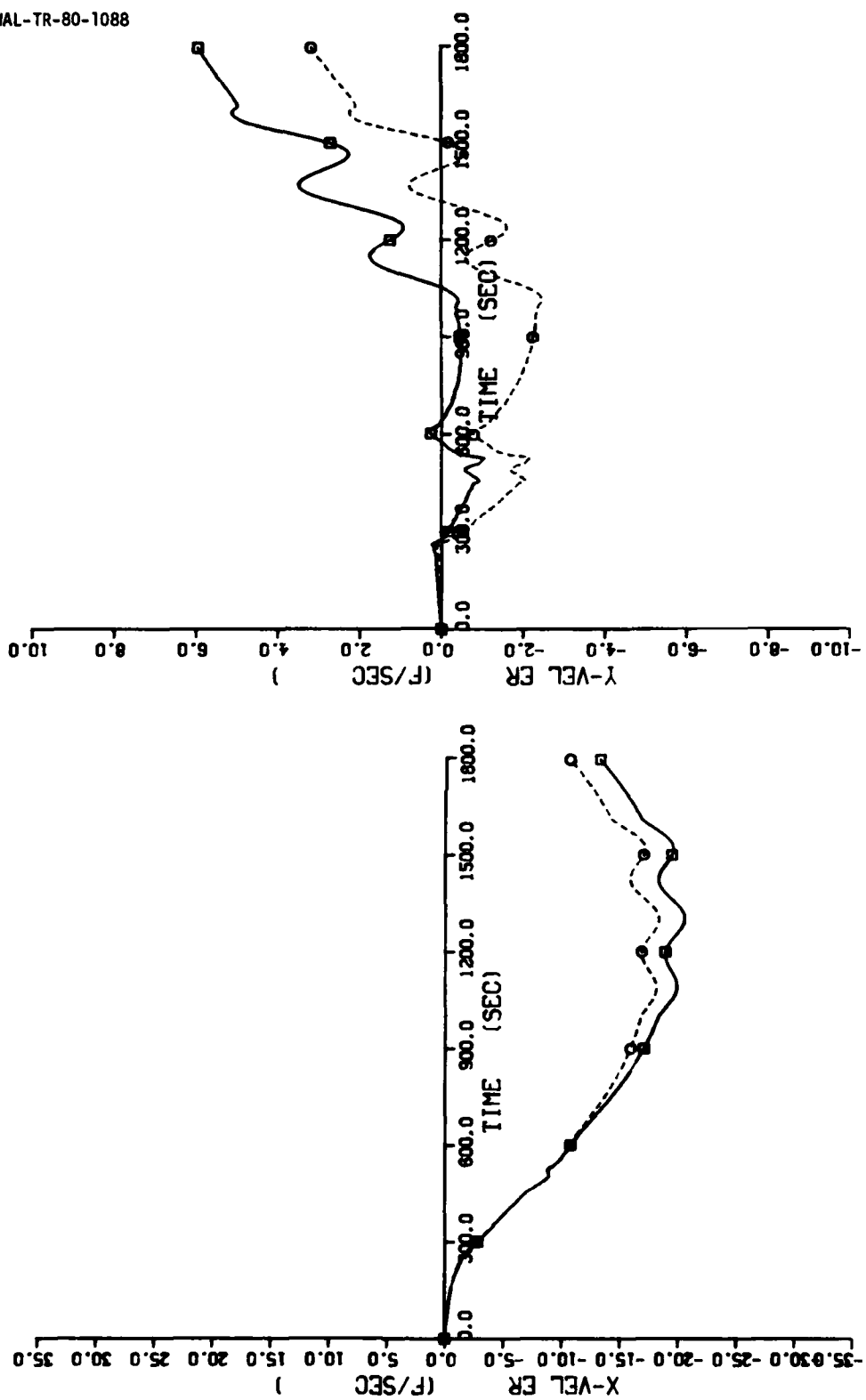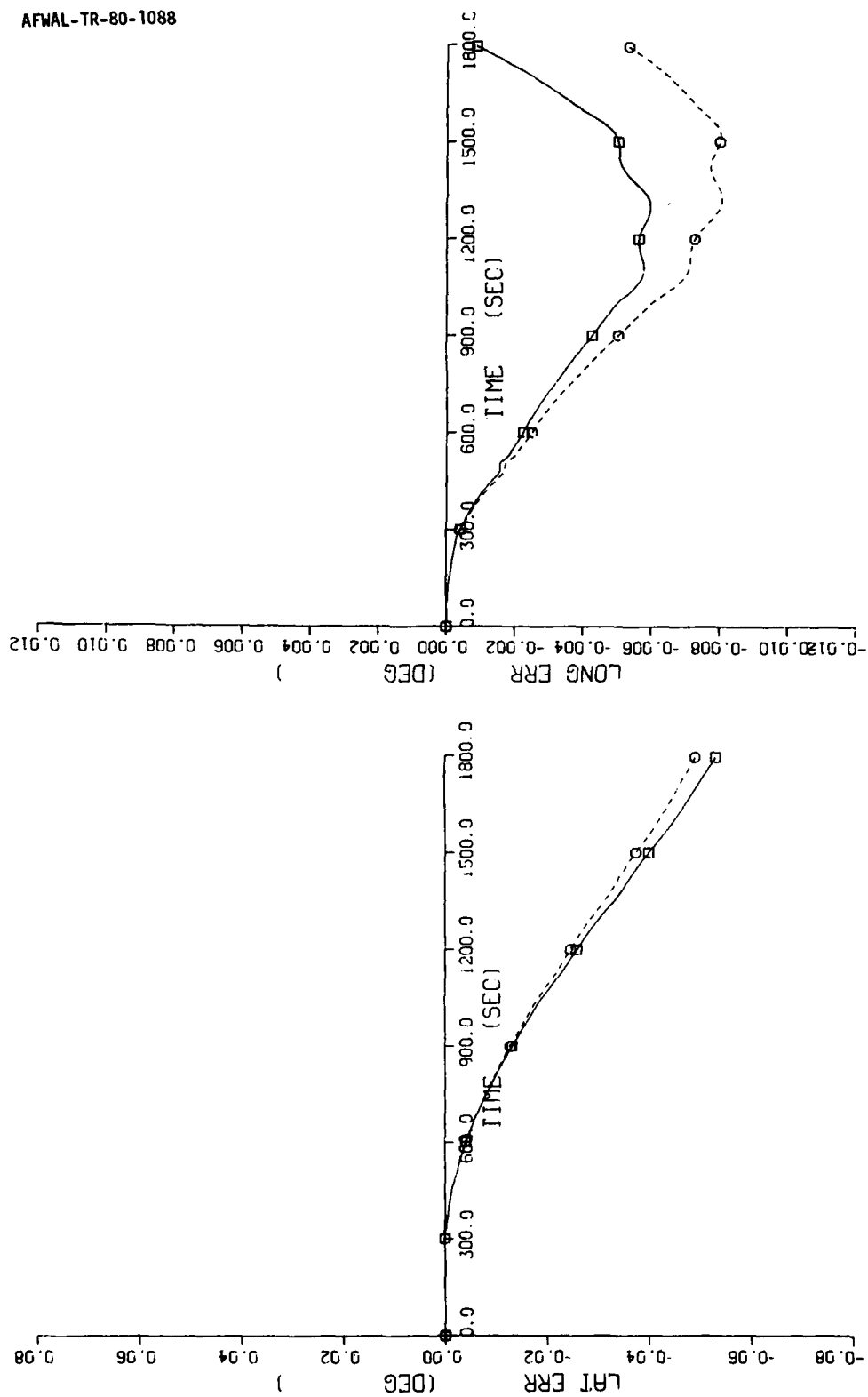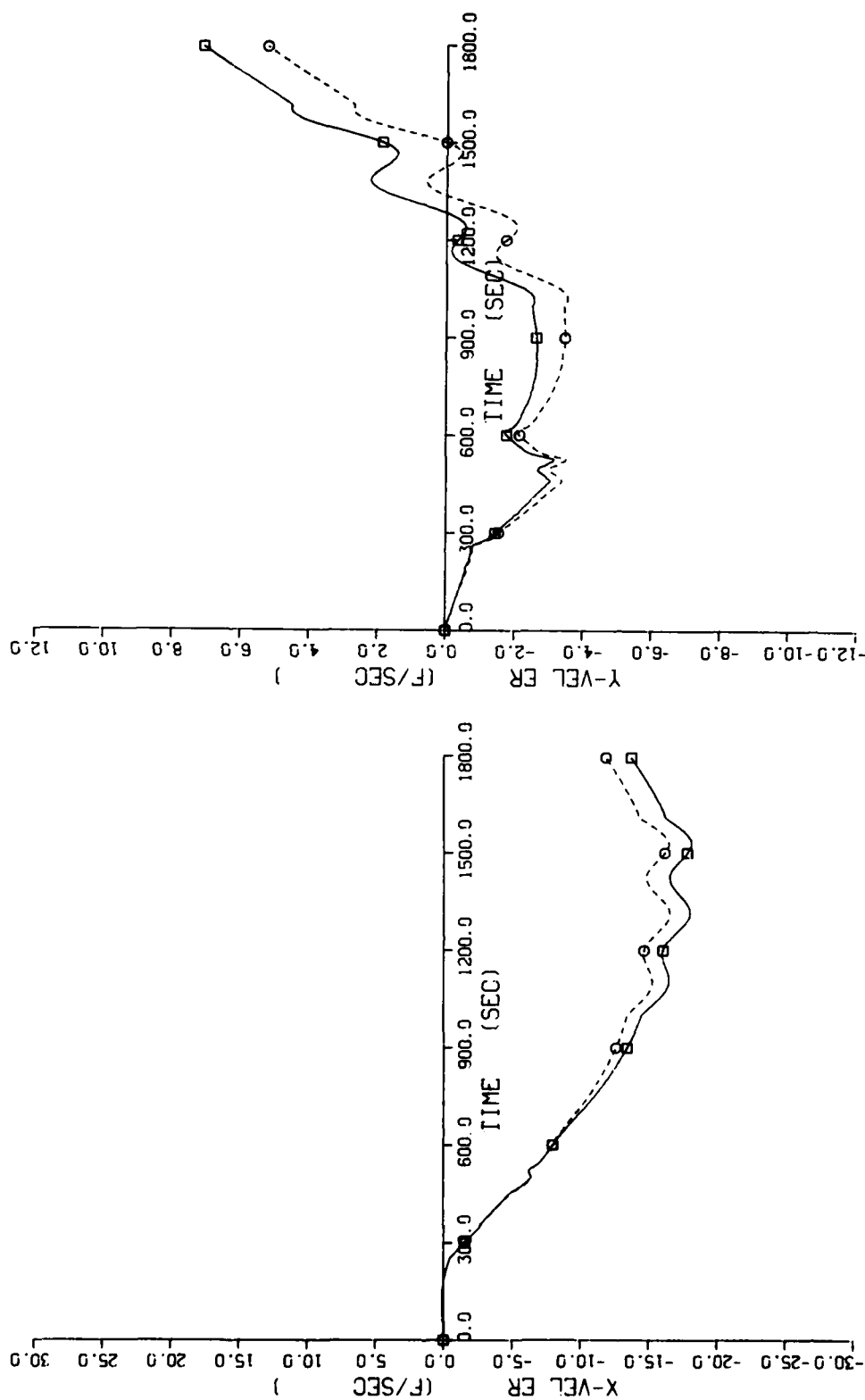
Figure 50. X and Y Velocity Errors, With and Without Least-Squares Averaging of Redundant Gyro Data, For Configuration 4 With Structural Modes

A comparison of navigation system performance for Configuration 1 through Configuration 4, with and without least-squares averaging of the redundant gyro data, is given by Figures 43, 45, 47, and 49 and by Figures 44, 46, 48, and 50. Configurations 1 and 2 give similar performance, with improved performance resulting from least-squares averaging of the redundant gyro data. Configurations 3 and 4 perform similar to each other but somewhat different than Configurations 1 and 2. These differences stem from the fact that the sensors of Configurations 3 and 4 are all skewed with respect to the aircraft cardinal axes.

Configurations 1 and 2 have one orthogonal-triad set of axes aligned with the aircraft and a second orthogonal-triad set of axes skewed with respect to the first triad. Configuration 1 is skewed to different angles than those of Configuration 2. Configuration 3 has one orthogonal-triad skewed with respect to another orthogonal-triad and both triads are skewed with respect to the aircraft cardinal axes. The sensor input-axes of Configuration 4 form a symmetrical cone about the vertical axis.

As can be observed in Figure 47 through Figure 50, the navigation system performance, for Configurations 3 and 4 using least-squares averaging of the redundant gyro data, is not as good as that given by an orthogonal-triad set of sensors skewed with respect to the aircraft cardinal axes. However, the performance, with and without least-squares averaging of the redundant gyro data, is better than that given by Configurations 1 and 2 for this set of parameters and dynamics.

Figure 51 through Figure 64 are time histories of navigation system errors showing the effects of individual error sources of nominal magnitude, typical of state-of-the-art inertial sensors, and algebraic sign used in previous simulation runs. Since these errors (with the exception of misalignment errors as previously discussed) are all random, this set of figures represent only one observation. However, they do give an insight into relative effects of the various sensor error sources on navigation system performance, with and without least-squares averaging of the redundant sensor data. No structural modes are sensed during these runs.

Figure 51. Latitude and Longitude Errors, With and Without Least-Squares Averaging of Redundant Gyro Data, and No Structural Modes - Gyro Bias Error

Figure 52. X and Y Velocity Errors, With and Without Least-Squares Averaging of Redundant Gyro Data, and No Structural Modes - Gyro Bias Error

Figure 53. Latitude and Longitude Errors, With and Without
Least-Squares Averaging of Redundant Gyro Data, and
No Structural Modes - Gyro Scale Factor Error

Figure 54. X and Y Velocity Errors, With and Without Least-
Squares Averaging of Redundant Gyro Data, and No
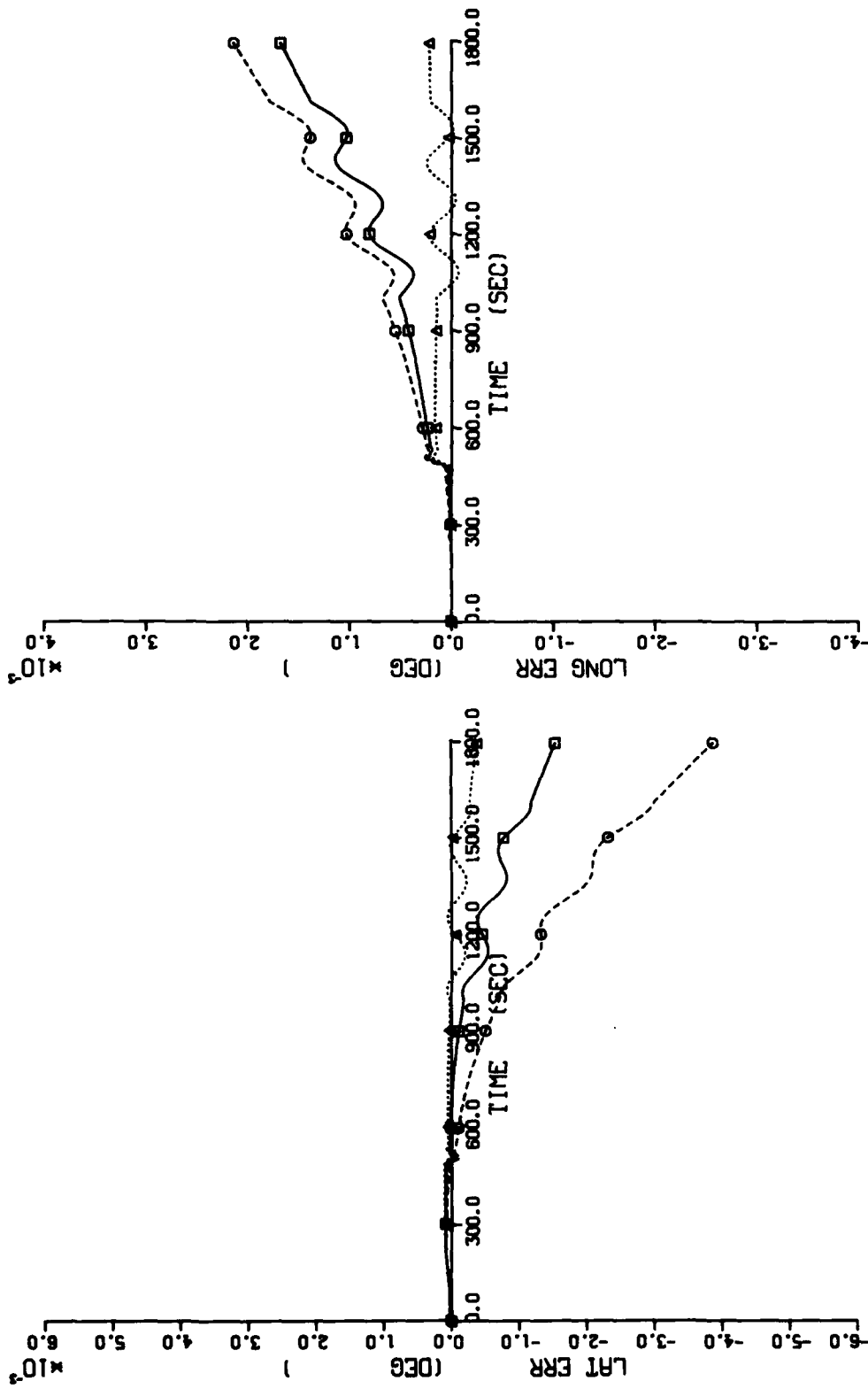Structural Modes - Gyro Scale Factor Error

96

Figure 55. Latitude and Longitude Errors, With and Without Least-Squares Averaging of Redundant Gyro Data, and No Structural Modes – Gyro Misalignment Error
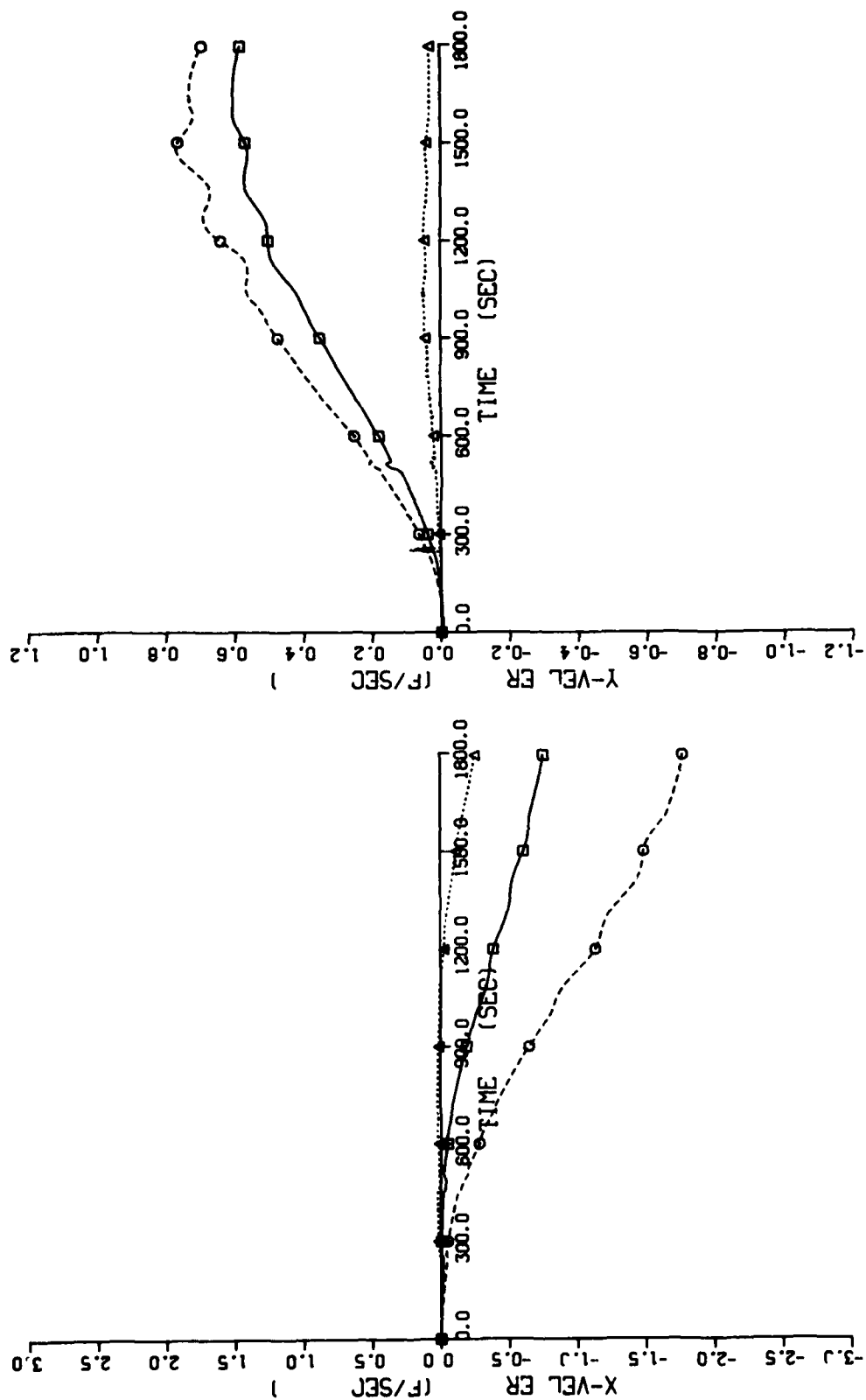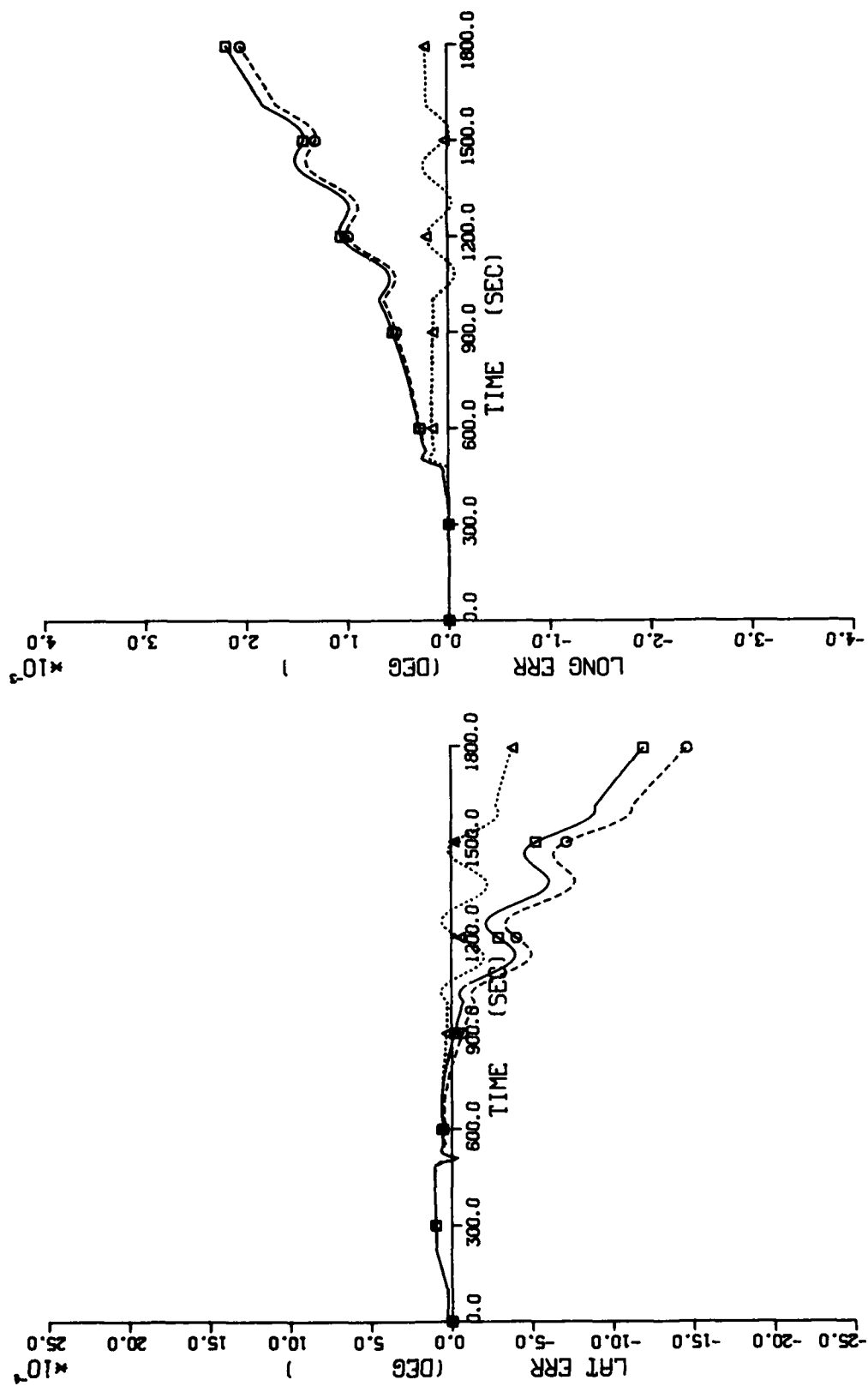
97

Figure 56. X and Y Velocity Errors, With and Without Least-Squares Averaging of Redundant Gyro Data, and No Structural Modes – Gyro Misalignment Error

Figure 57. Latitude and Longitude Errors, With and Without
Least-Squares Averaging of Redundant Accelerometer
Data, and No Structural Modes - Accelerometer Bias
Error

Figure 58. X and Y Velocity Errors, With and Without Least-
Squares Averaging of Redundant Accelerometer Data,
and No Structural Modes – Accelerometer Bias Error

Figure 59. Latitude and Longitude Errors, With and Without Least-Squares Averaging of Redundant Accelerometer Data, and No Structural Modes - Accelerometer Scale Factor Error
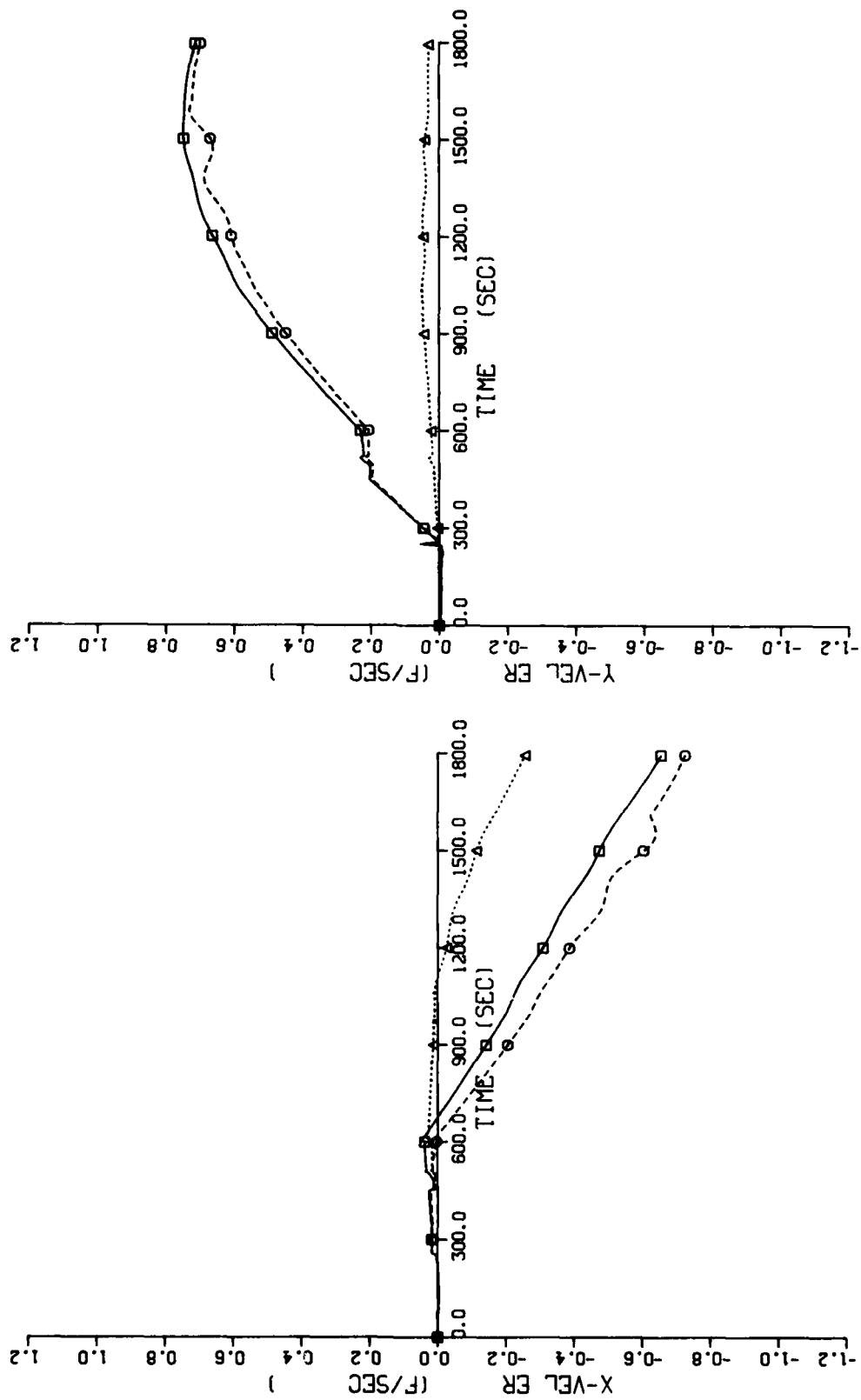
Figure 60. X and Y Velocity Errors, With and Without Least-Squares Averaging of Redundant Accelerometer Data, and No Structural Modes - Accelerometer Scale Factor Error

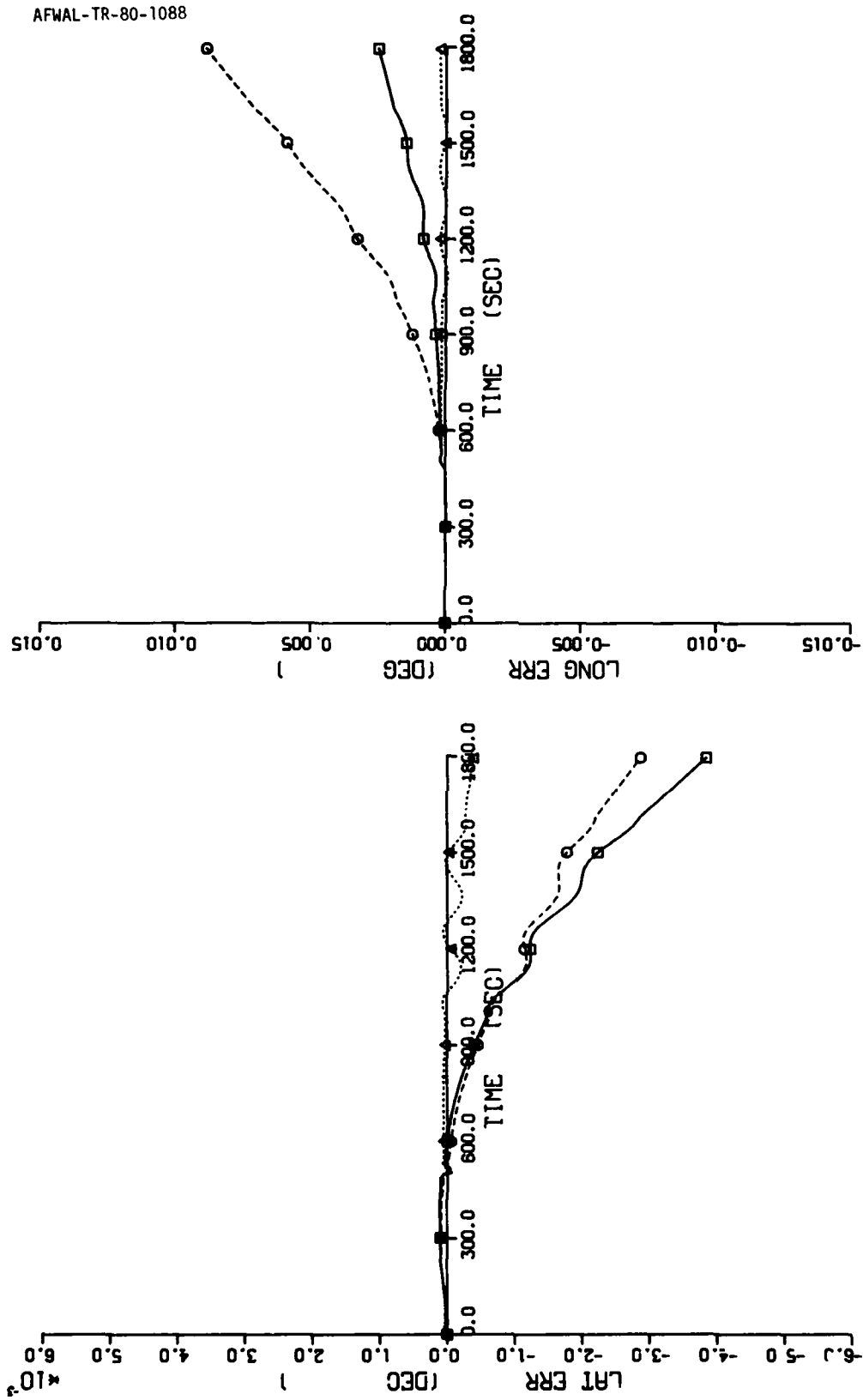Figure 6. Latitude and Longitude Errors, With and Without Least-Squares Averaging of Redundant Accelerometer Data, and No Structural Modes - Accelerometer Misalignment Error
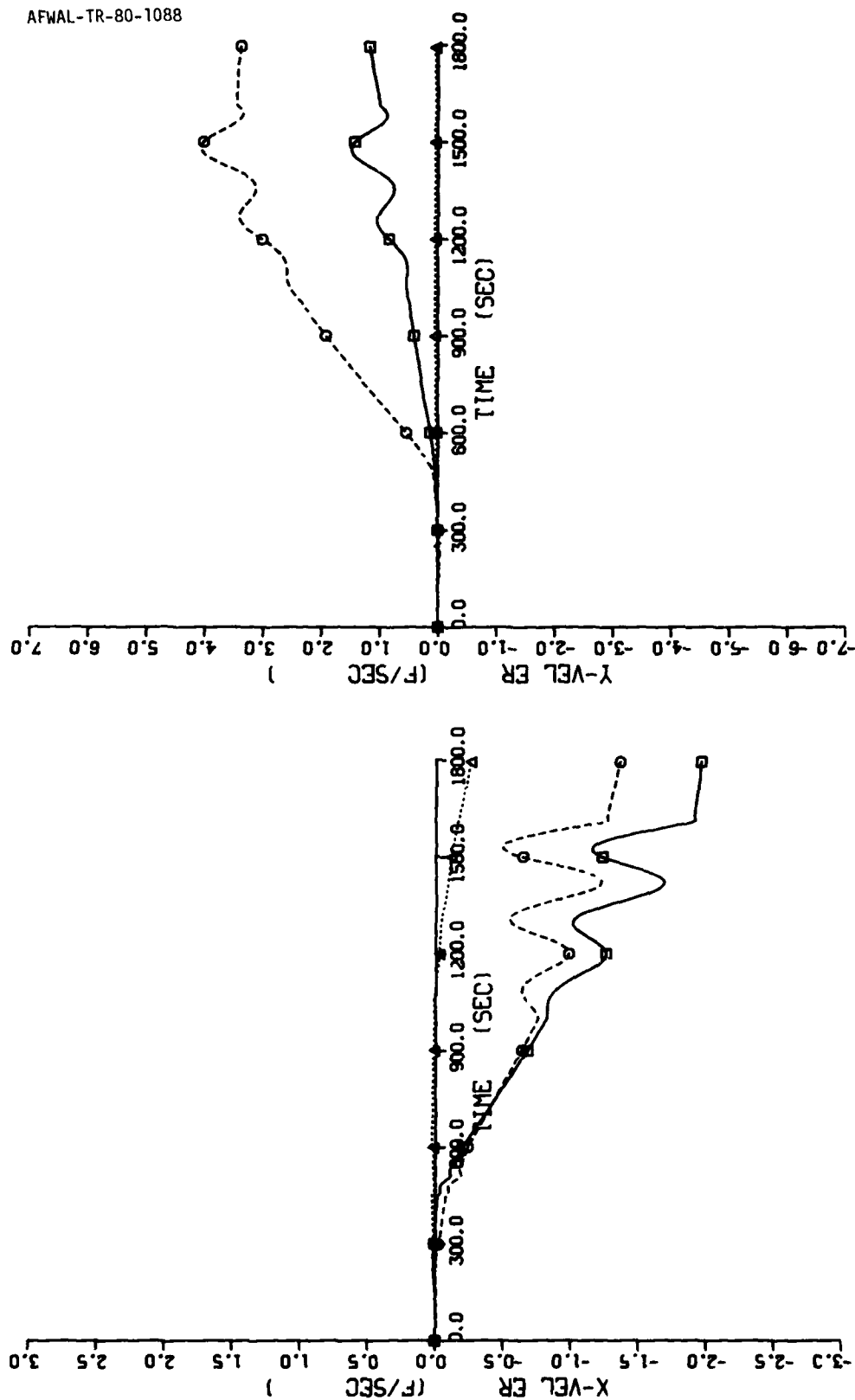
Figure 62. X and Y Velocity Errors, With and Without Least-Squares Averaging of Redundant Accelerometer Data, and No Structural Modes - Accelerometer Misalignment Error
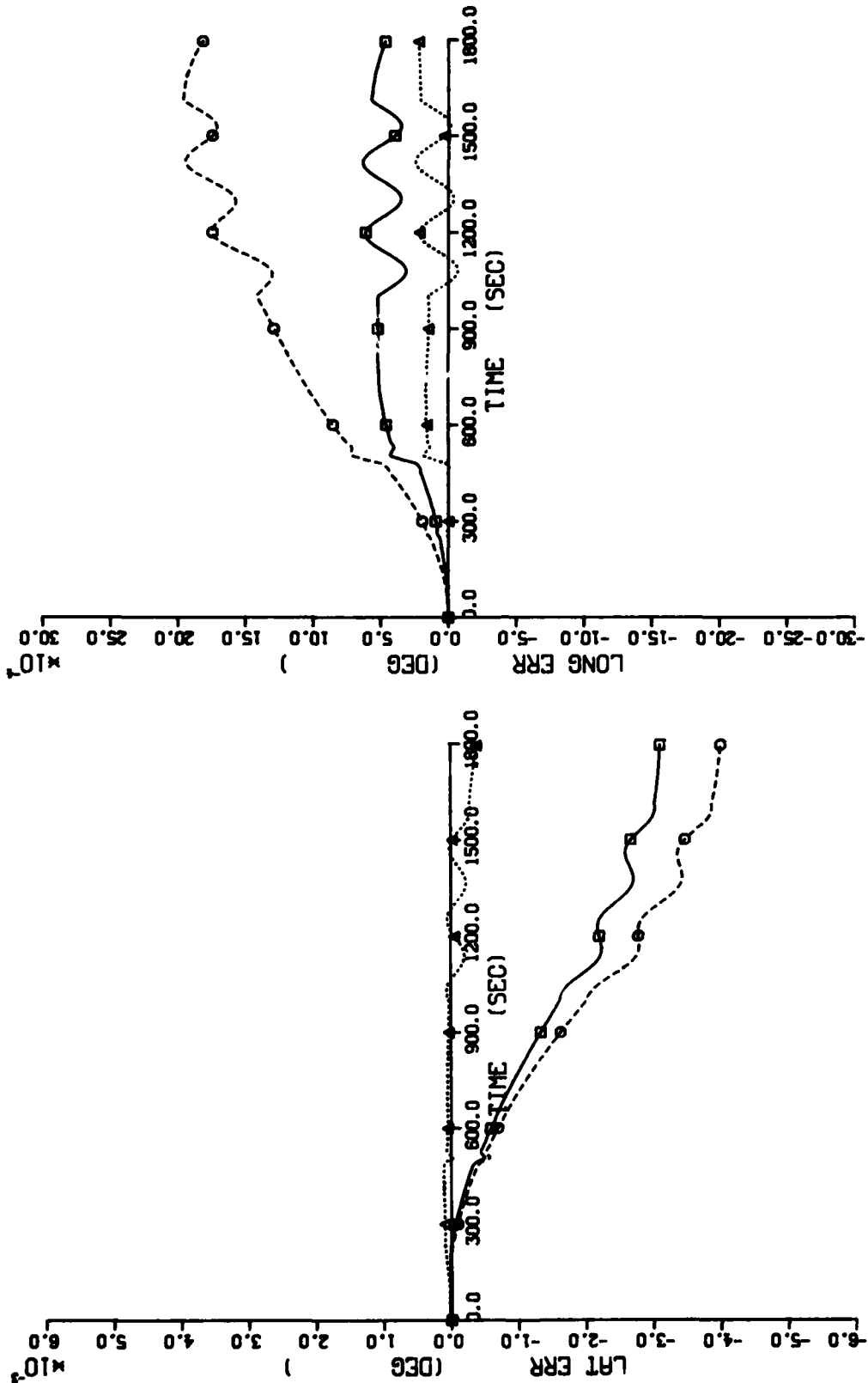
Figure 63. Latitude and Longitude Errors, With and Without Least-Squares Averaging of Redundant Accelerometer Data, and No Structural Modes - Accelerometer Lever-Arm Effects
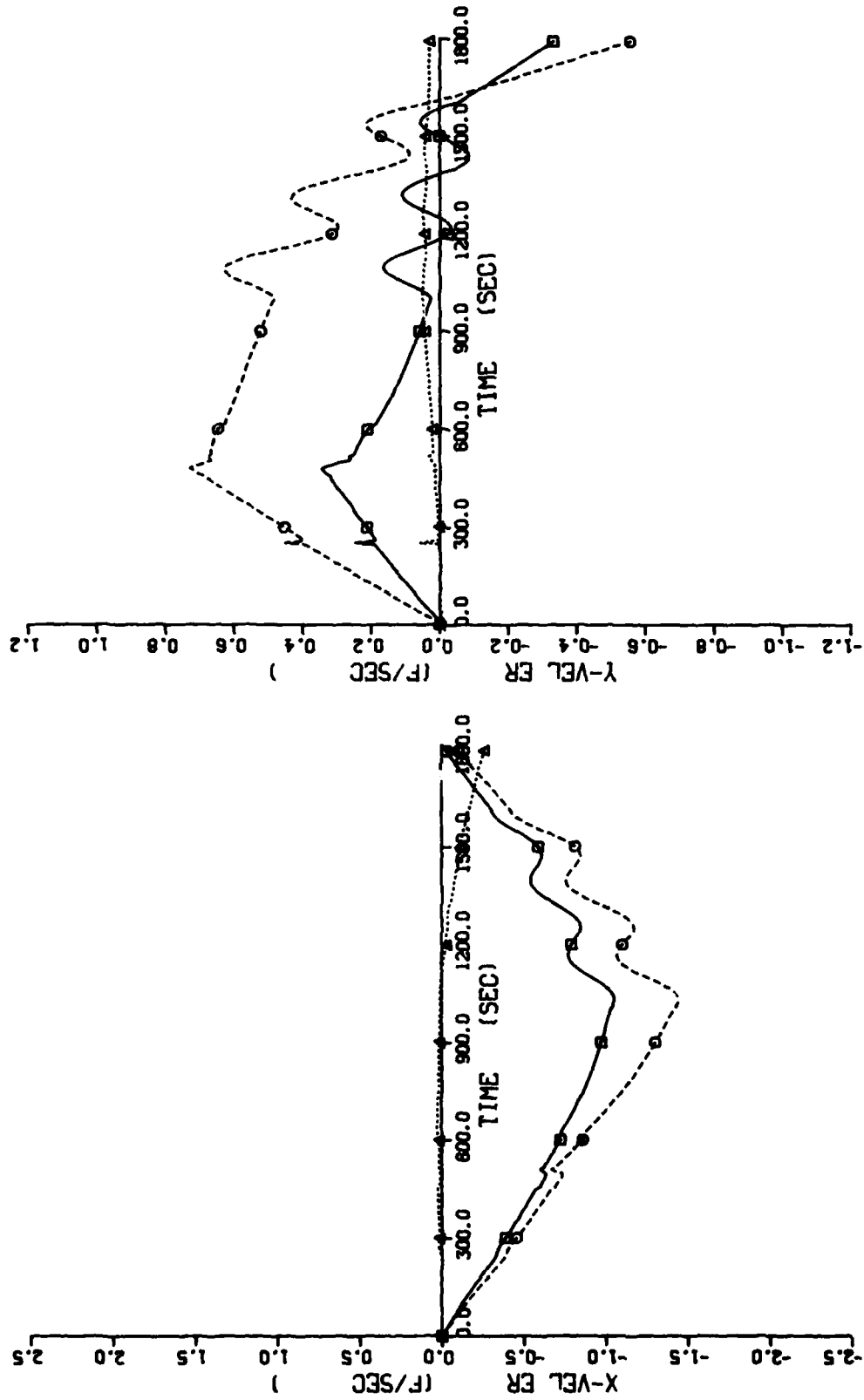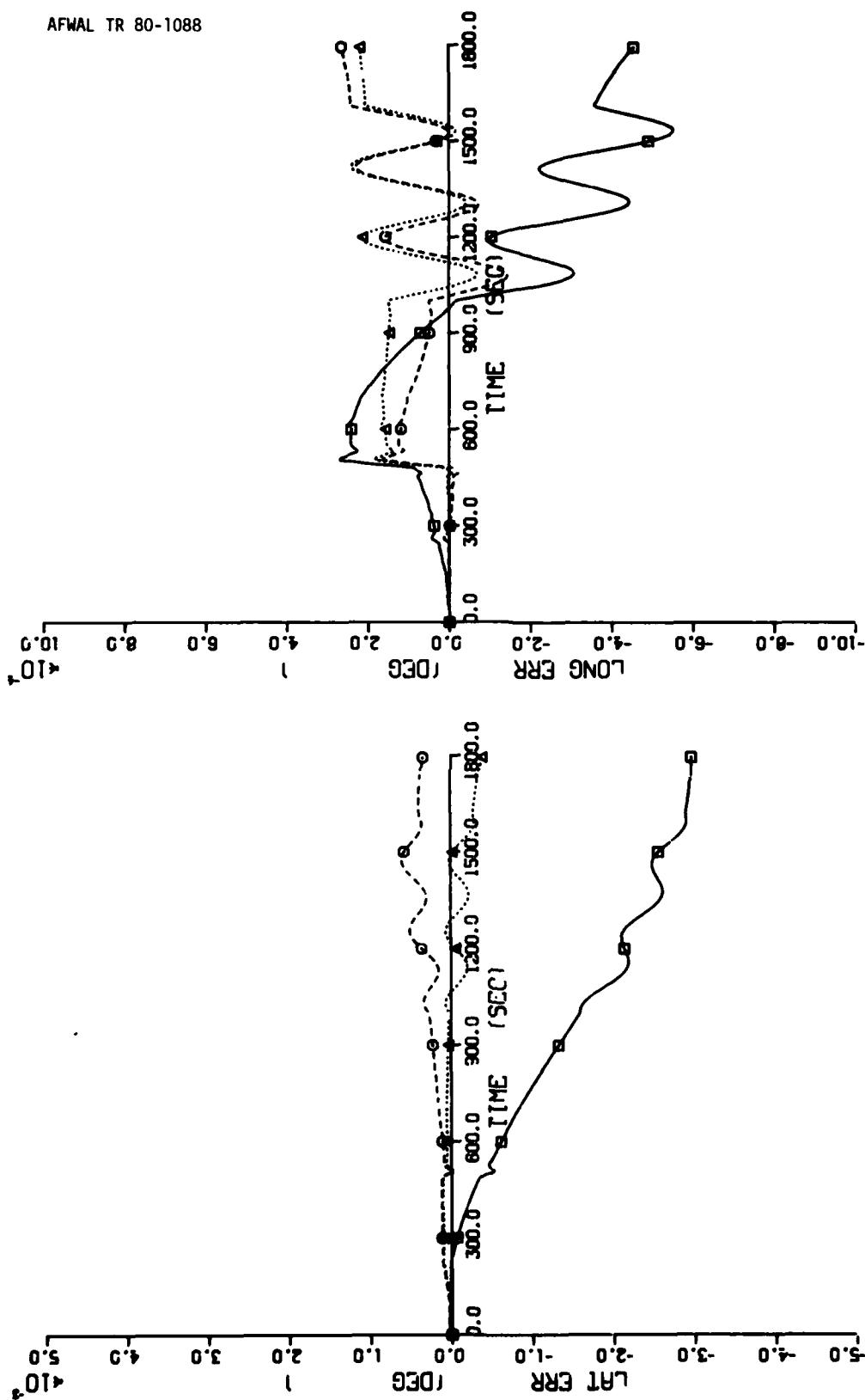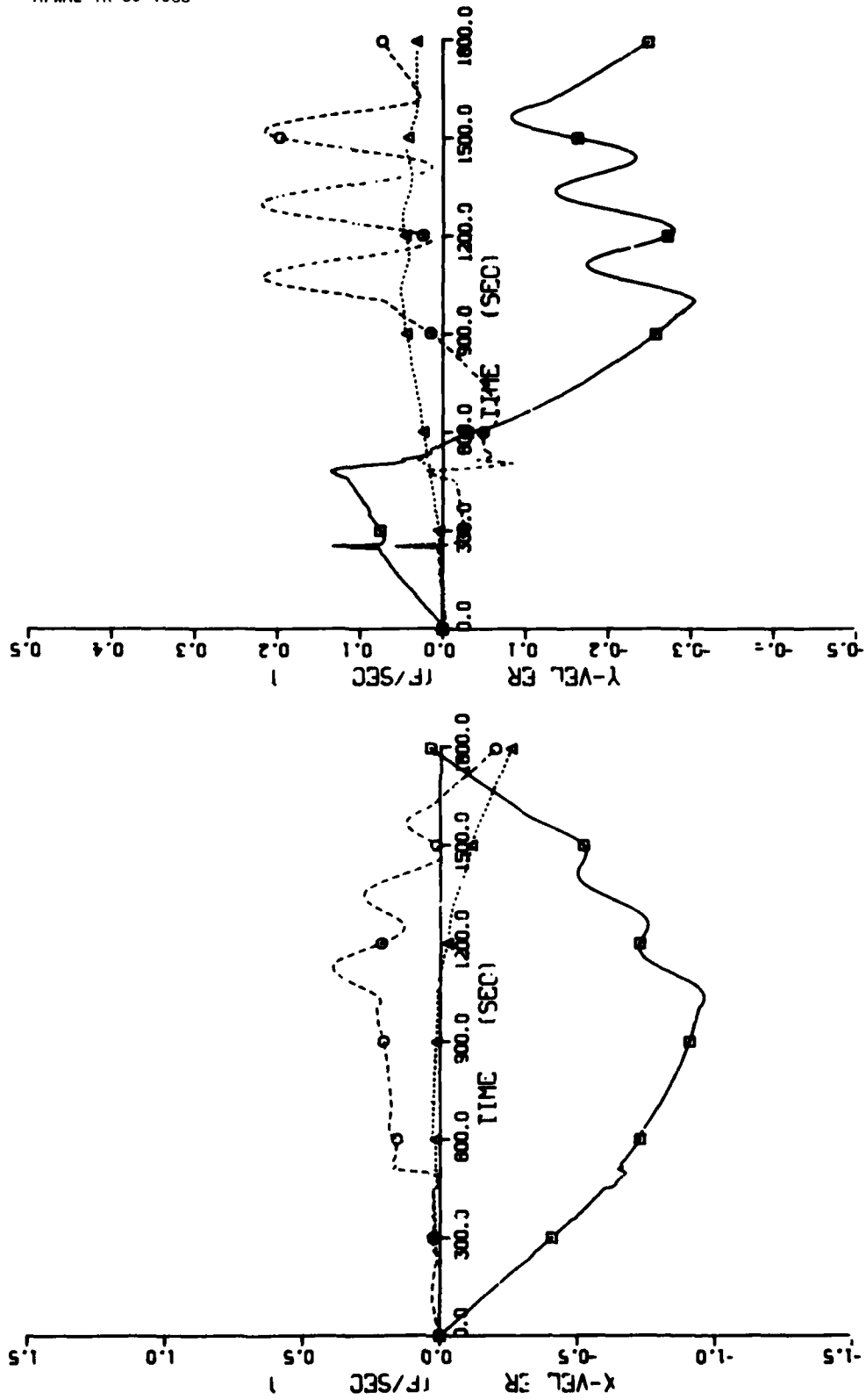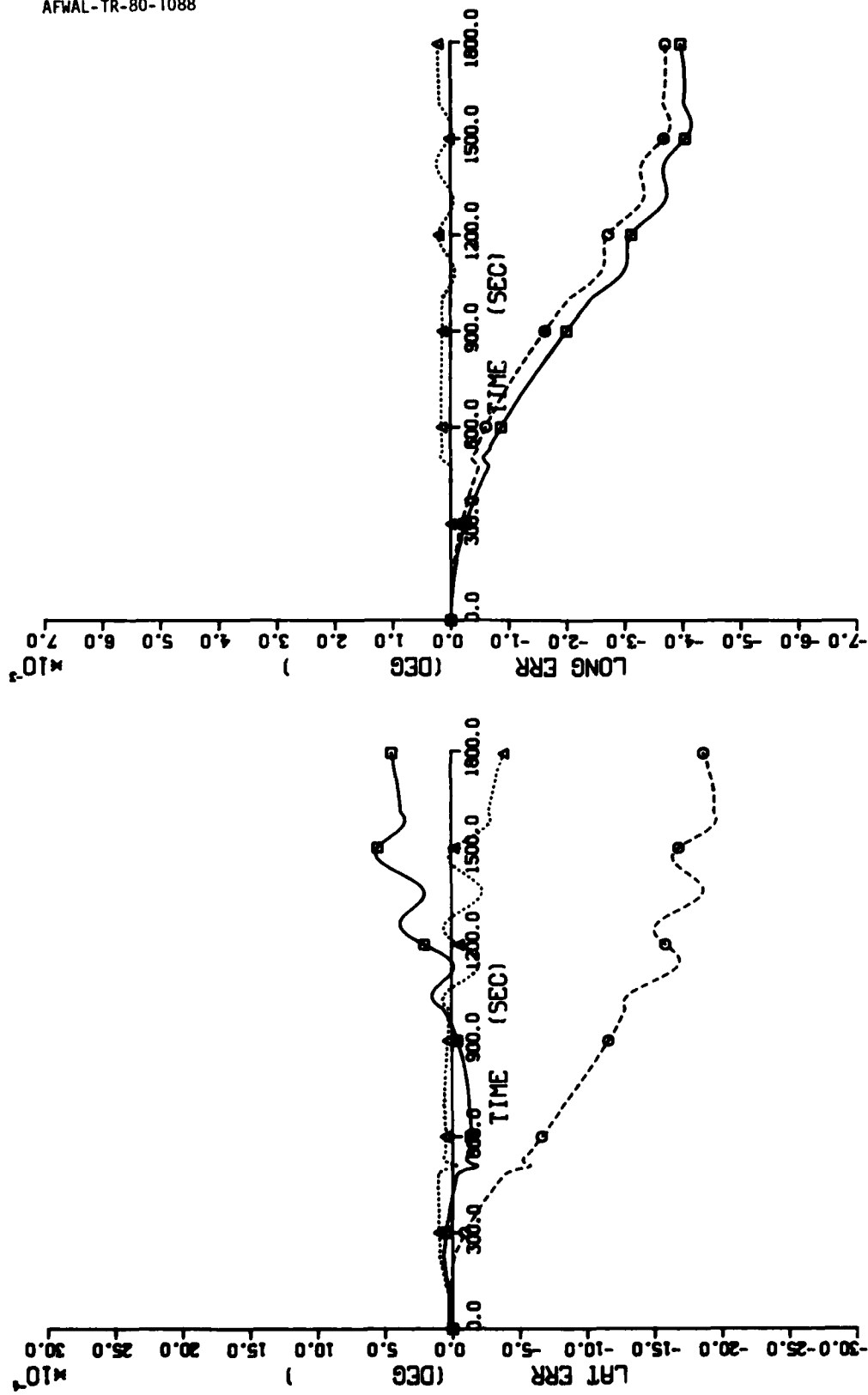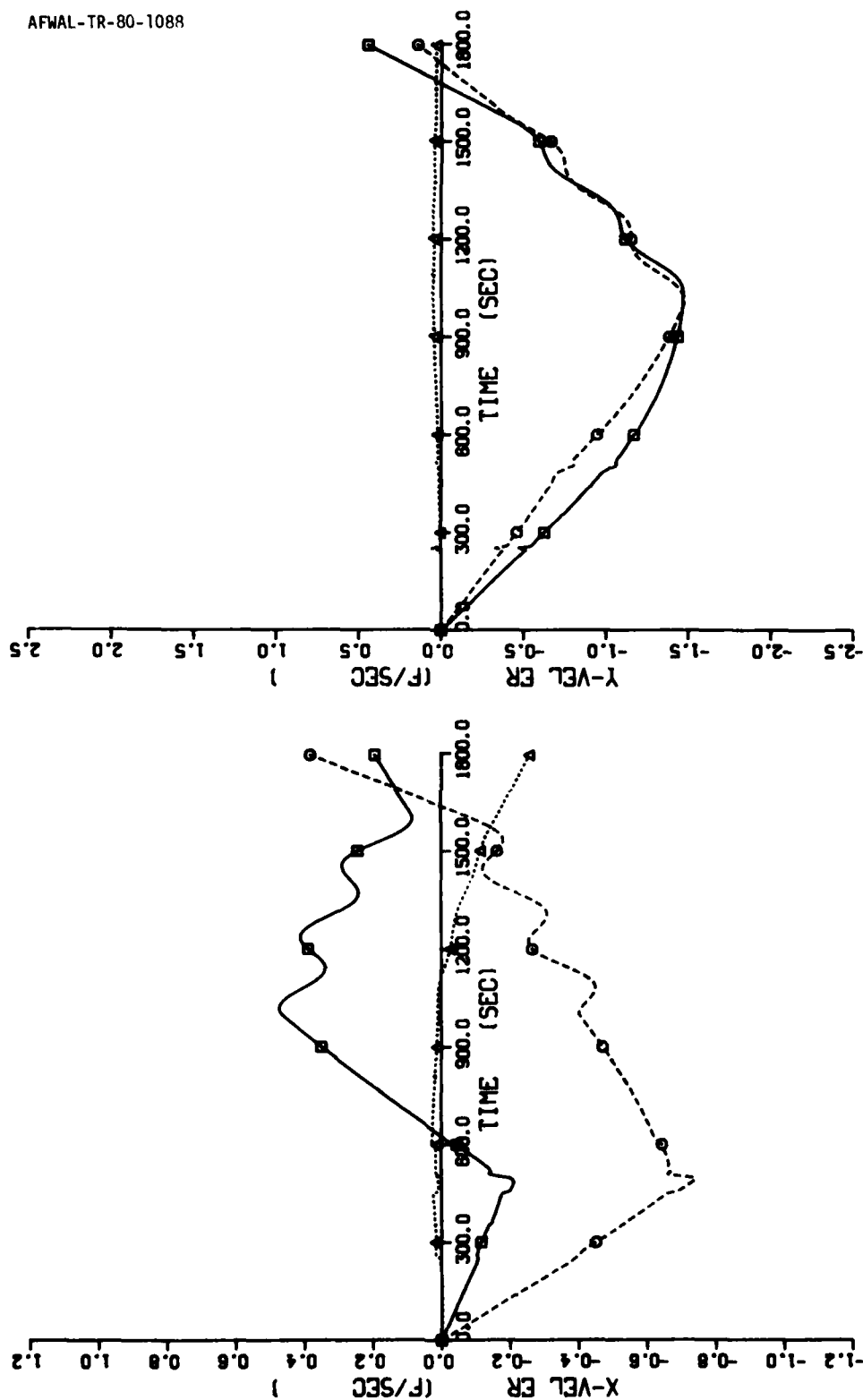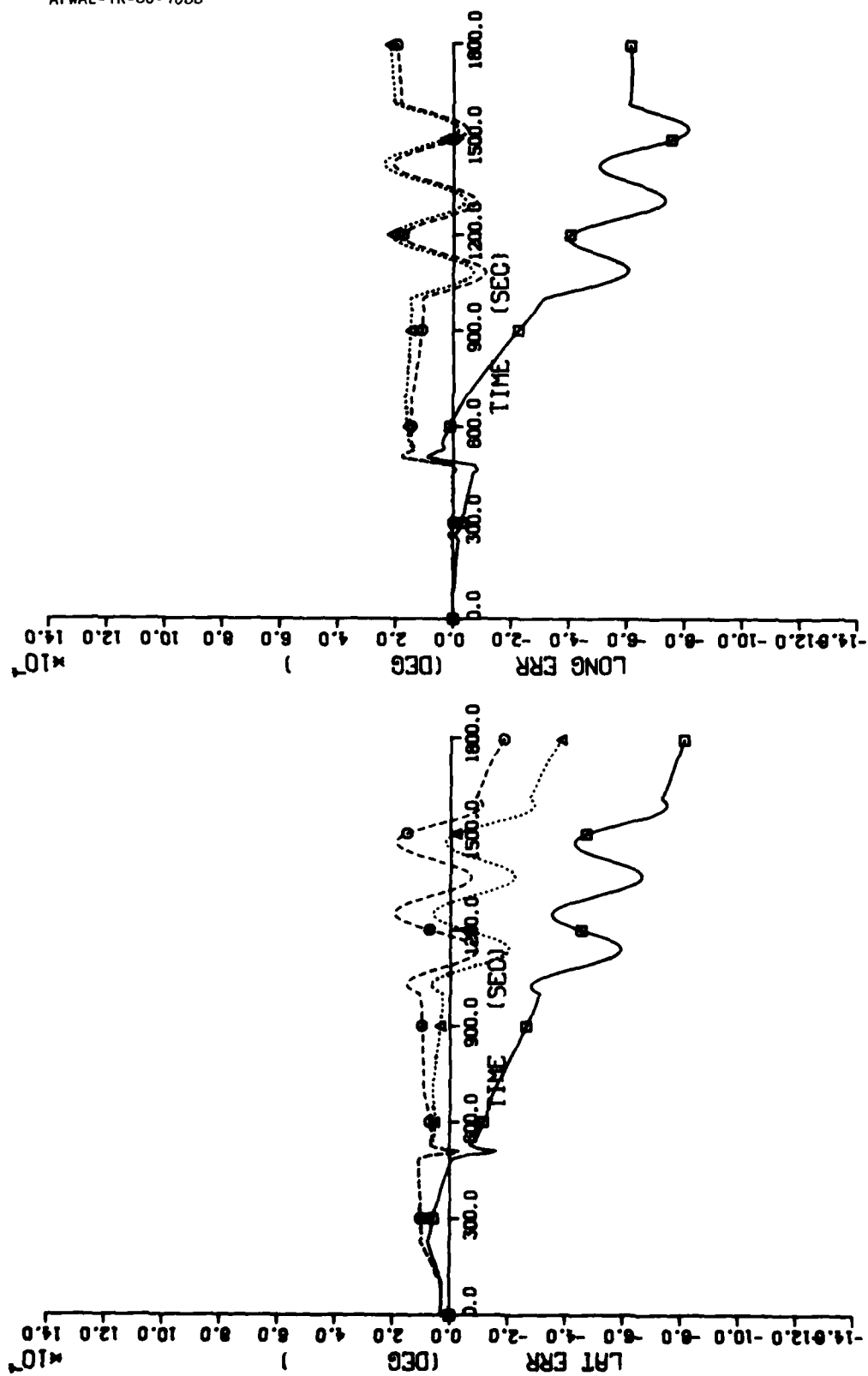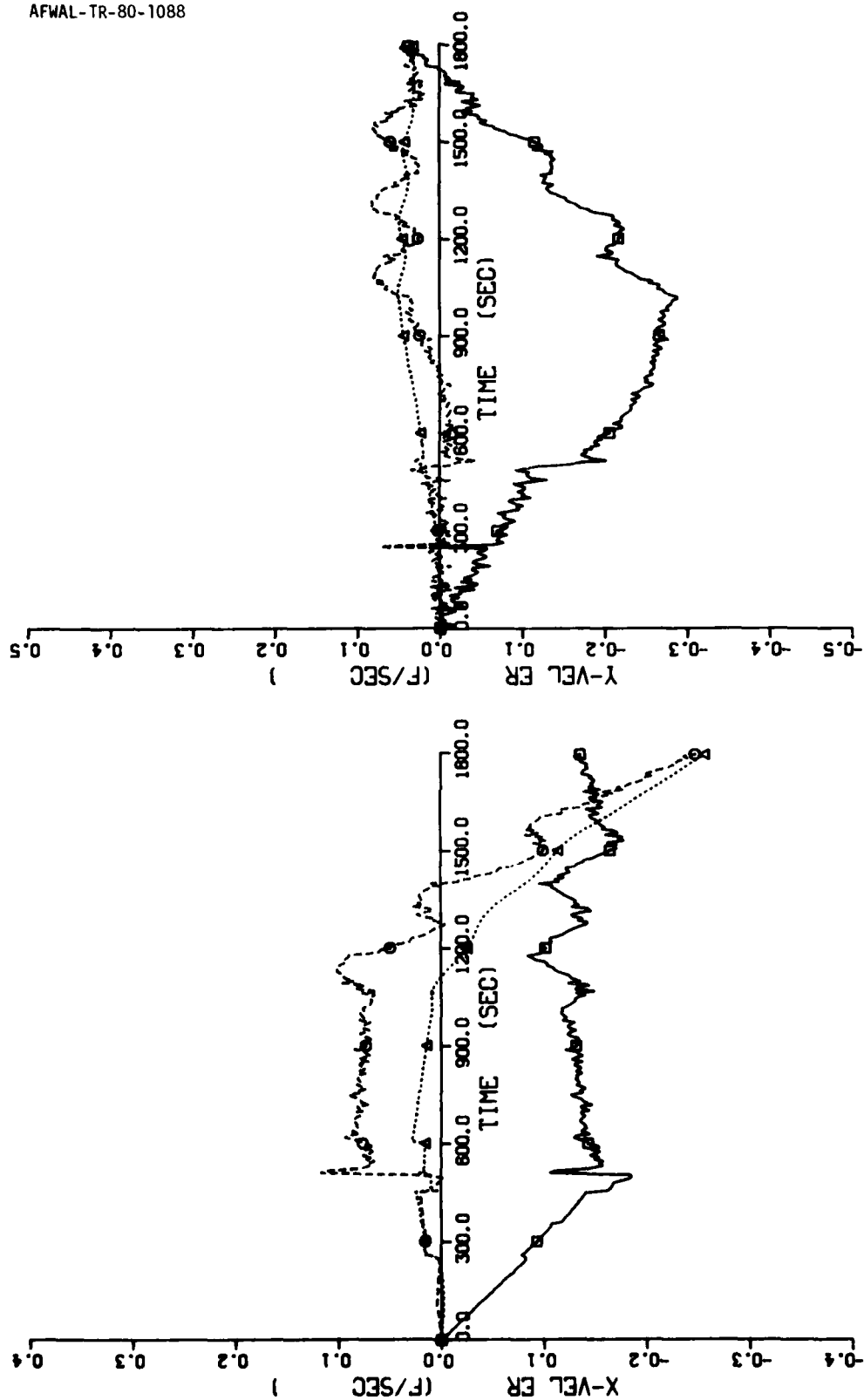
Figure 64. X and Y Velocity Errors, With and Without Least-Squares Averaging of Redundant Accelerometer Data, and No Structural Modes - Accelerometer Lever-Arm Effects

The dotted curve in the figures represents the navigation system error time histories when ideal gyros and accelerometers are used. Thus, these error curves represent computational error resulting, primarily, from attitude computation. They serve as a baseline reference for comparison with the time history error curves obtained for individual sensor errors.

Observation of Figure 51 through Figure 56 indicate that, of the gyro errors, misalignment errors contribute the most to navigate system errors. Figures 55 and 56 also show that least-squares averaging of the redundant gyro data can result in larger navigation system errors in some cases. In particular the X-velocity and latitude errors are larger with least-squares averaging than without. However, the Y-velocity error and position (CEP) error are significantly improved with least-squares averaging of the redundant gyro data.

The deterioration in performance noted above occurs as a result of least-squares averaging of data differing in algebraic sign. This is also true of the other error sources as can be seen for gyro scale factor error Figures 53 and 54 where longitude and Y-velocity errors are larger with least-squares averaging of the redundant gyro data than without.

Similar trends can be observed from Figure 57 through Figure 64 in which least-squares averaging of the redundant accelerometer data is used. However, for the accelerometers, misalignment errors are no longer dominant over the other accelerometer errors.

Fortunately, the cases when deterioration occurs with least-squares averaging of the redundant gyro and accelerometer data are in a minority. Typically, in a real application, the random nature of the error sources result in improved performance when least-squares averaging of the redundant inertial sensor data is used. However, care must be exercised to minimize the alignment error, particularly for the gyros, when the sensors are mounted initially and during any maintenance procedure. This is true because the misalignment errors are random only in the inability to repeatedly align the sensors upon removal and replacement. Once the sensors are mounted in the aircraft the misalignment errors remain constant until a sensor is removed and replaced.

107

In the case of gyro alignment, if the alignment errors happen to occur in a configuration which dominates all other sensor errors, then deterioration of navigation system performance with least-squares averaging can occur for all combinations of the other sensor errors. This situation is exemplified in Figure 65 through Figure 70.

Figures 65 and 66 serve as a reference for comparison with Figure 67 through Figure 70. Figure 65 and 66 represent simulation results using the same parameters and sensor configuration as used to obtain the results shown by Figures 43 and 44 respectively. The only difference is that the results from Figures 65 and 66 were obtained with a constant northerly heading flight profile. This flight profile was also used for the runs shown by Figure 66 through Figure 70.

The results of Figures 67 and 68 were obtained by changing the algebraic sign of one of the two misalignment errors of the number six gyro. The misalignment error magnitudes are all equal and remain the same as those used for Figures 65 and 66. No changes were made in any of the other error parameters nor the dynamics. As can be observed in Figures 67 and 68 there is little overall difference between the *navigation system performance, with and without* least-squares averaging of the redundant gyro data, when the above change in algebraic sign occurs with this particular set of error parameters.

In view of the above results the algebraic sign of one of the mis-alignment errors of a second gyro (gyro number five) was also reversed. Figures 69 and 70 show results for this set of sensor error parameters. In this case the longitude and Y-velocity errors are larger when least-squares averaging of the redundant gyro data is used than without the averaging.

These same characteristics hold true for least-squares averaging of the redundant accelerometer data. Thus, in the application of least-squares averaging of the redundant inertial sensor data, care must be exercised to minimize the dominant sensor errors; and in particular, the misalignment errors as discussed above.

Figure 65. Latitude and Longitude Errors, With and Without Least-Squares Averaging of Redundant Gyro Data, For Configuration 2 With Structural Modes

Figure 66. X and Y Velocity Errors, With and Without Least-
Squares Averaging of Redundant Gyro Data, For Con-
figuration 2 With Structural Modes

Figure 67. Latitude and Longitude Errors, With and Without Least-Squares Averaging of Redundant Gyro Data, For Configuration 2 With Structural Modes

111

Figure 68. X and Y Velocity Errors, With and Without Least-Squares Averaging of Redundant Gyro Data, For Configuration 2 With Structural Modes
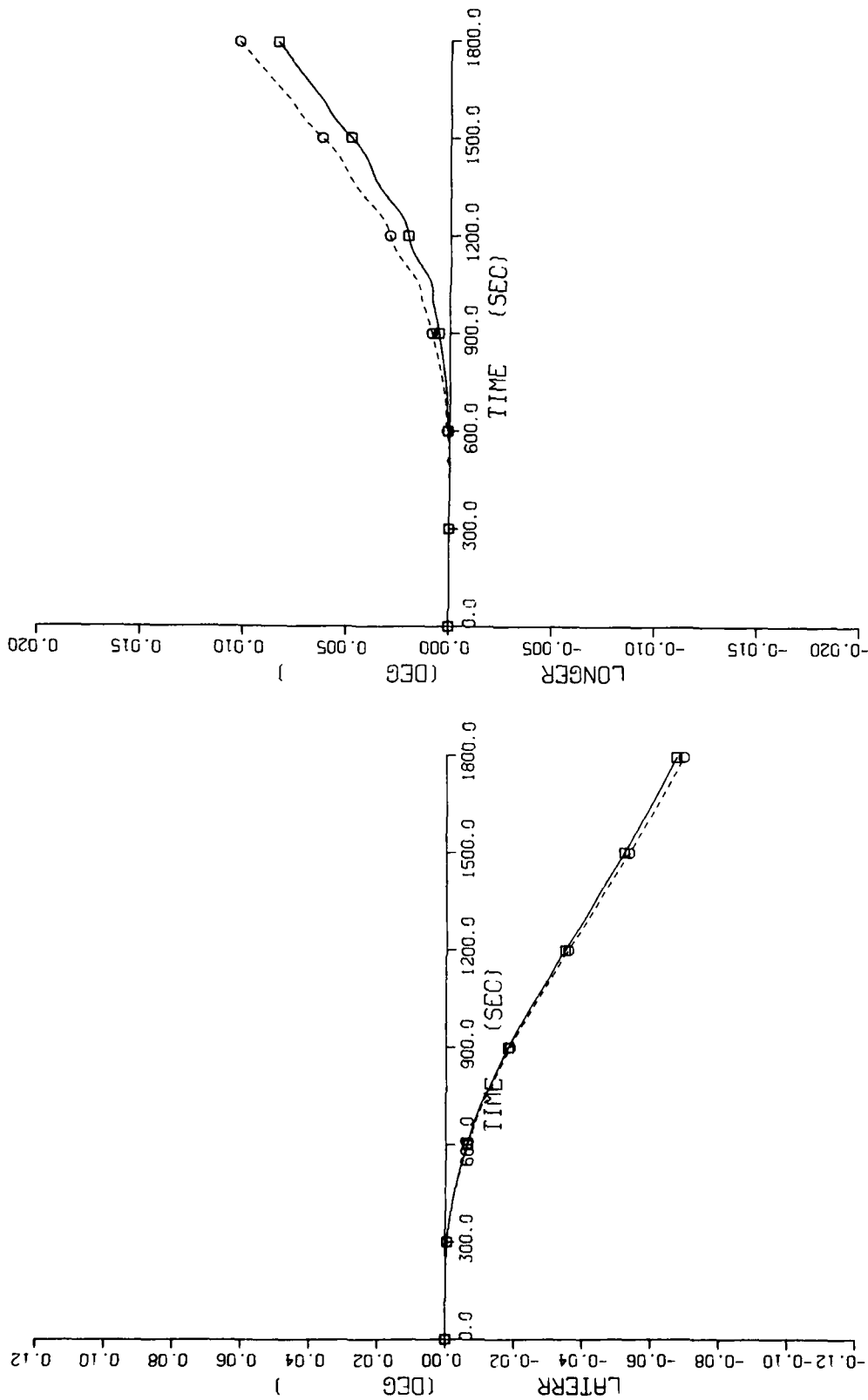
Figure 69. Latitude and Longitude Errors, With and Without
Least-Squares Averaging of Redundant Gyro Data,
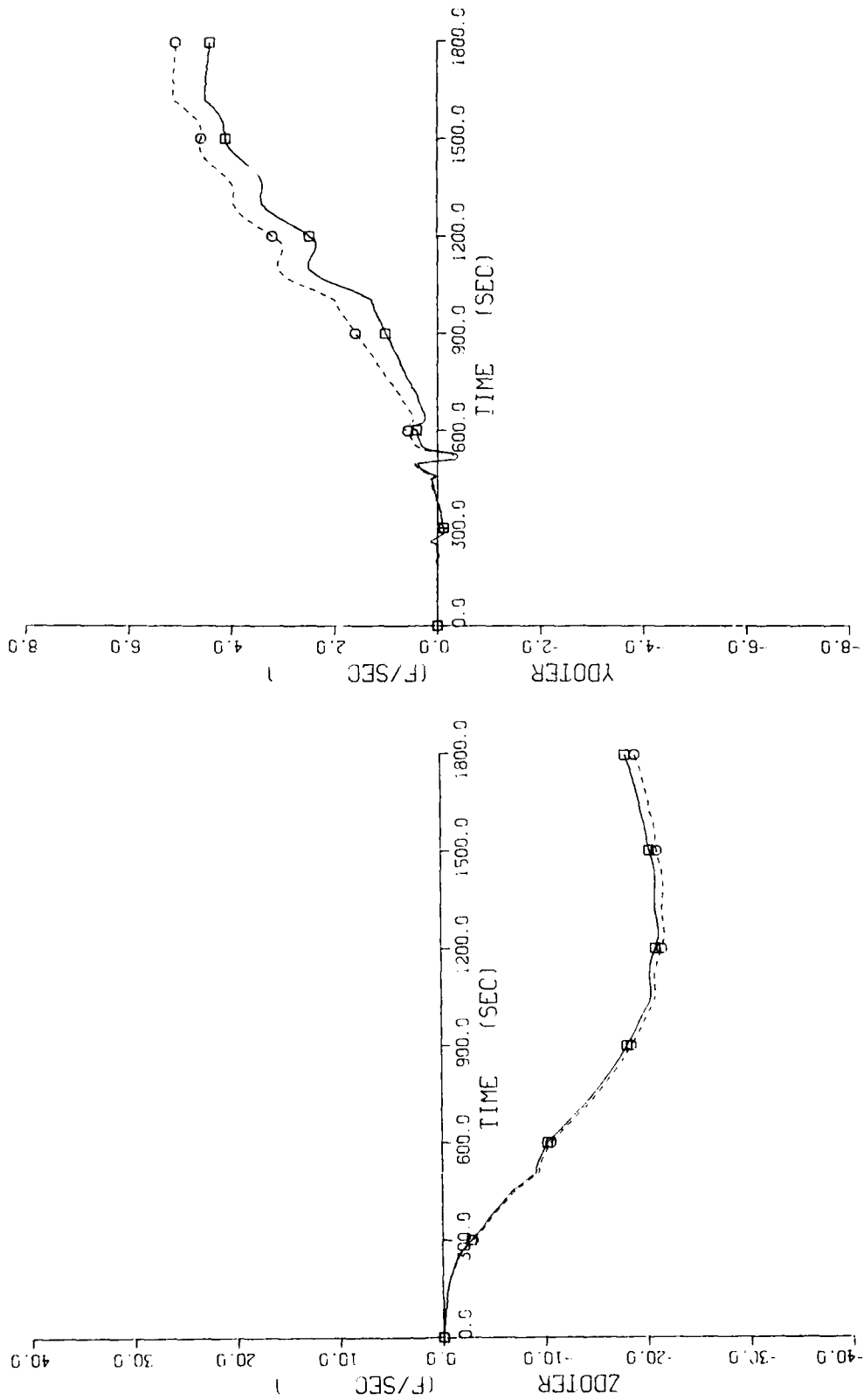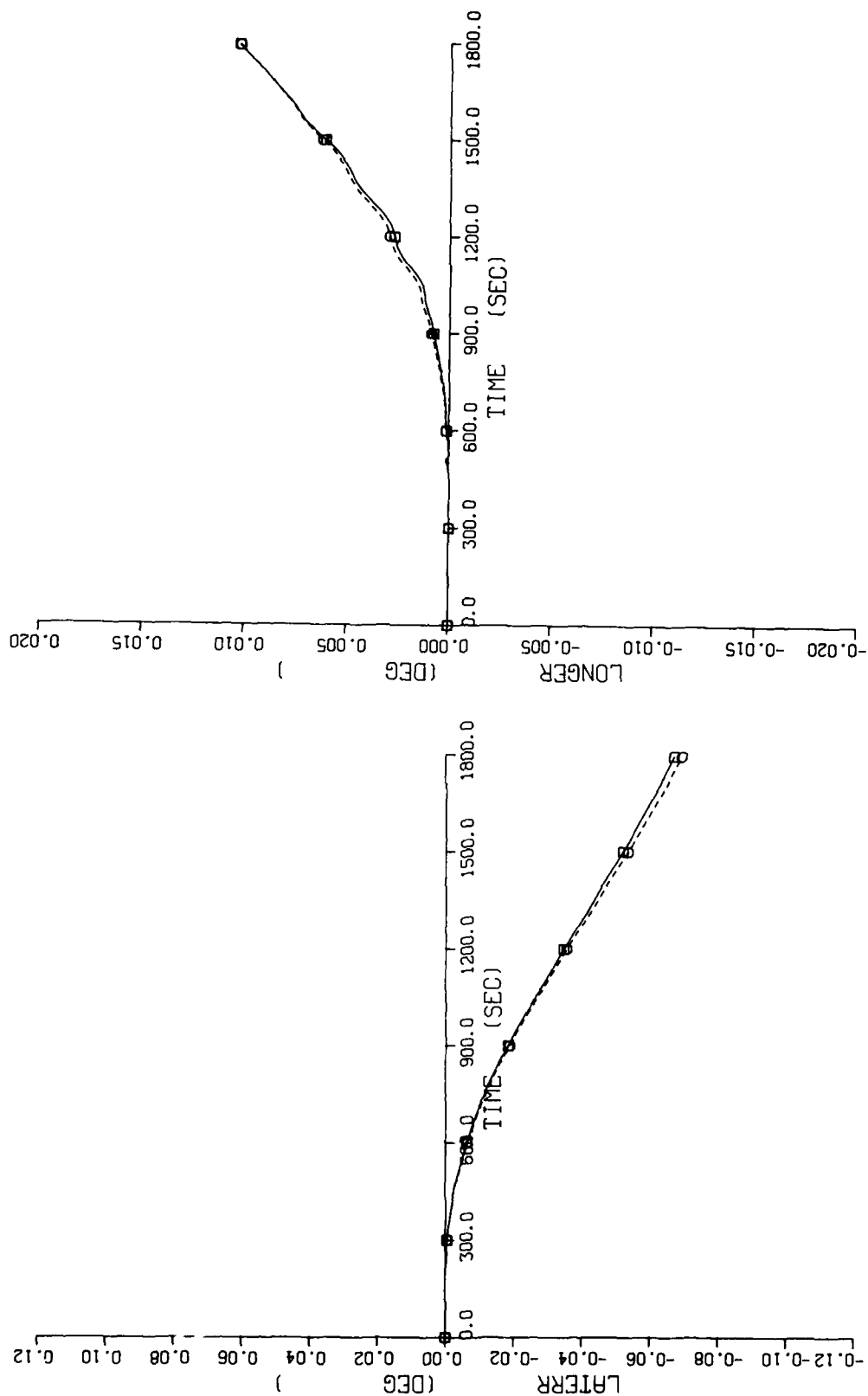For Configuration 2 With Structural Modes

113

Figure 70. X and Y Velocity Errors, With and Without Least-
Squares Averaging of Redundant Gyro Data, For
Configuration 2 With Structural Modes

As previously discussed, least-squares averaging is ideally suited
for utilization with redundancy management of the redundant inertial
sensor data. A simple look-up table for each possible failed sensor
configuration can be precomputed and stored in the system computer.
Thus, when a failed sensor is detected by an FDI algorithm, a new set of
least-squares transformation parameters can be initiated in one computer
iteration. The least-squares average of data from the reconfigured
set of redundant sensors, without the failed sensor(s), is then used for
navigation and flight control.

The effects of failed gyros are shown in Figure 71 through Figure 76.
The same sensor errors and system dynamics are used for these simulation
runs as those used on Figure 28 through Figure 42, and no structural modes
are present. In Figures 71 and 72, gyro number 1 is failed and the least-
squares average of the remaining five gyros is used in the navigation system
computation. In this case navigation system performance is even better
than that obtained in Figures 28 and 29 when all six gyros were used.

Figures 73 and 74 show the navigation system performance obtained
when gyro number 5 is failed and least-squares averaging of data from the
remaining five gyros is used. Again, for this set of sensor error para-
meters, the navigation system performance, with least-squares averaging,
is better than that obtained using all six gyros.

Figures 75 and 76 show the navigation system performance obtained
when both gyro number 1 and gyro number 5 are failed. In this case the
navigation system performance using least-squares averaging of the four
remaining is deteriorated from that using all six gyros. Further, the
performance is also deteriorated from that obtained with only an ortho-
gonal-triad of inertial sensors.

The variation in navigation system performance, upon failure of one
or more sensors, is dependent upon relative effects of the sensor random
errors with least-squares averaging at the redundant data. Consequently,
these effects must be considered if application of least-squares
averaging is contemplated. It is desirable to have all inertial sensor
errors as small as possible, but misalignment errors should be of
primary concern.

Figure 71. Latitude and Longitude Errors, With and Without Least-Squares Averaging of Redundant Gyro Data, For Configuration 2 With No Structural Modes - Gyro Number 1 Failed
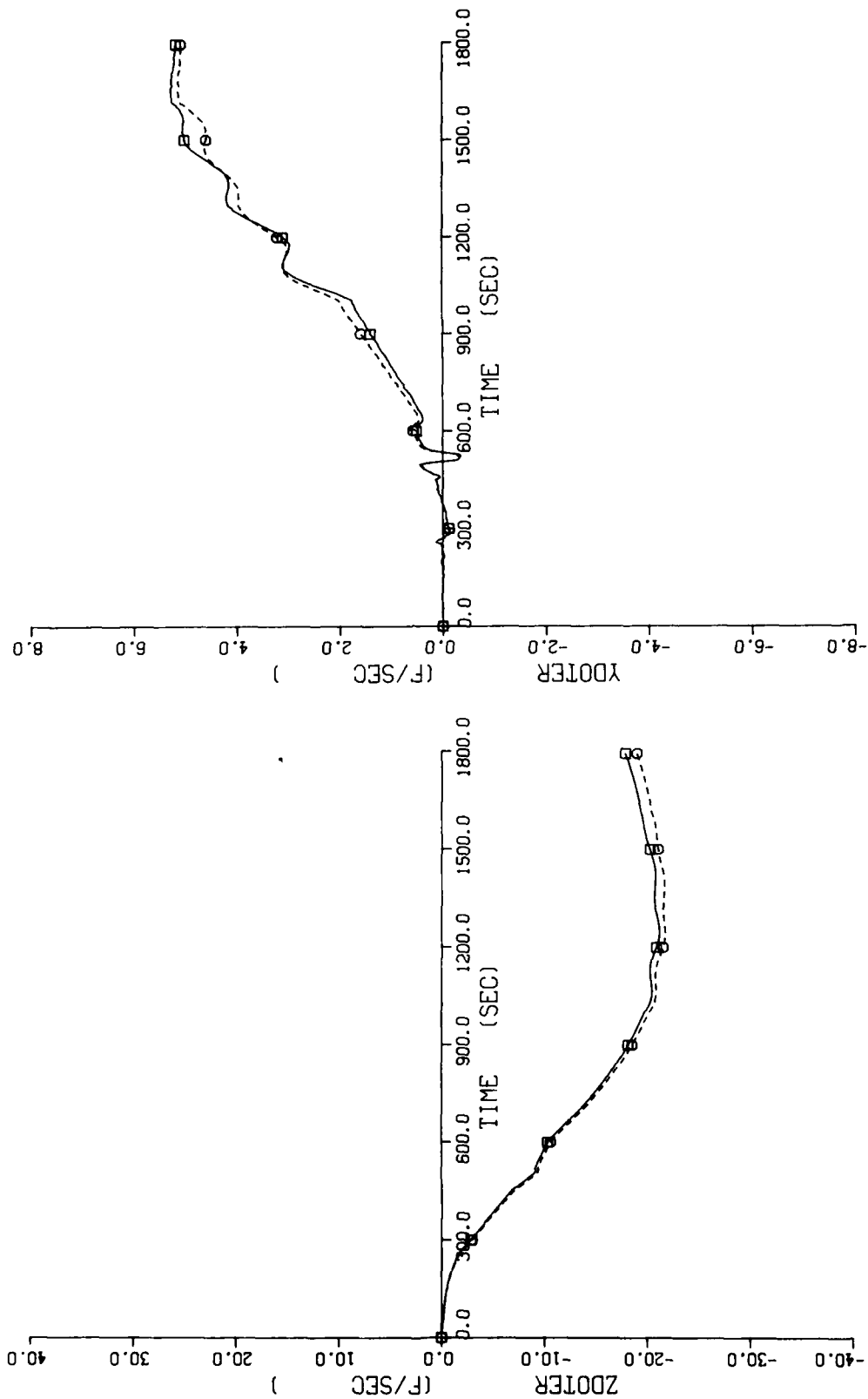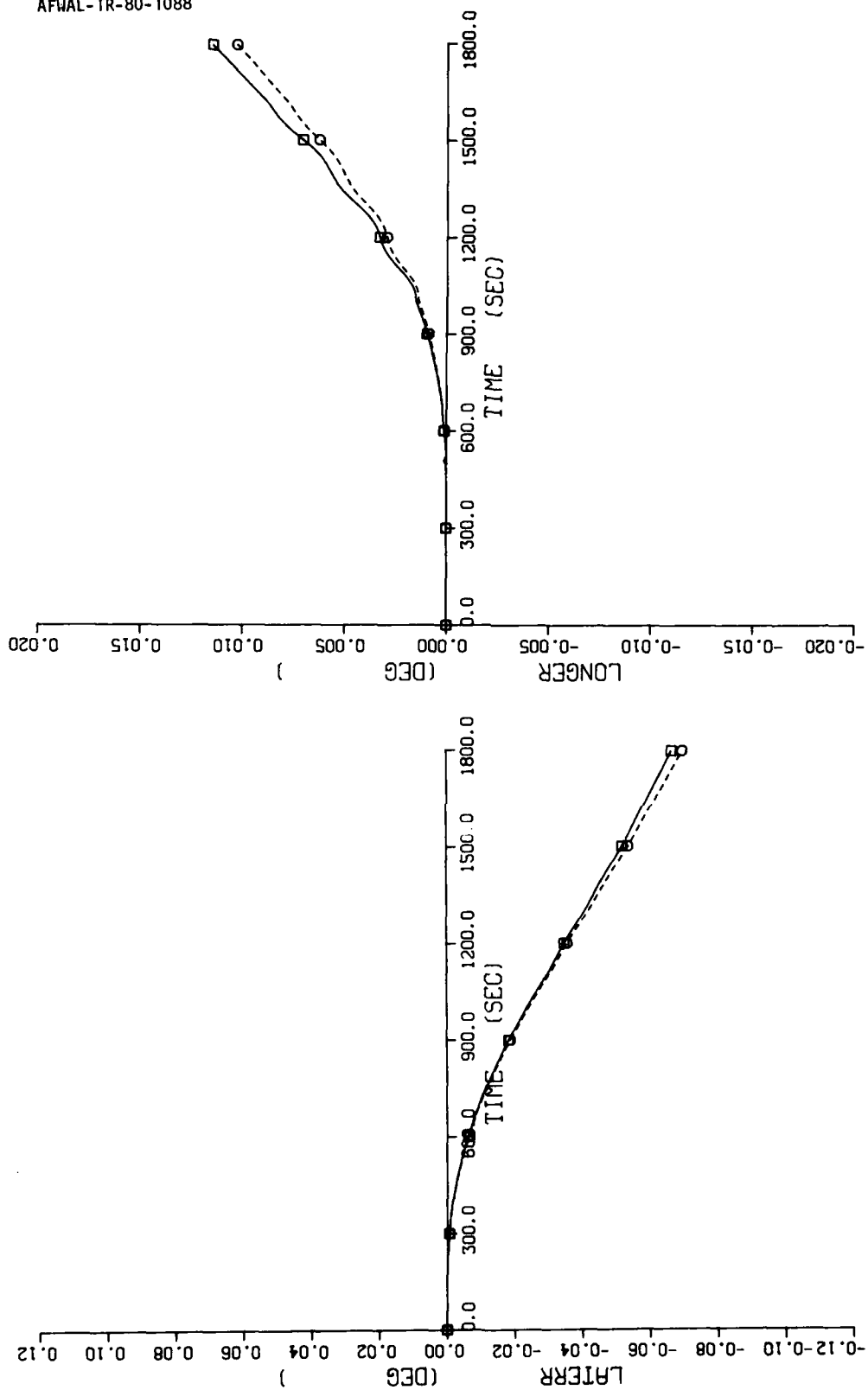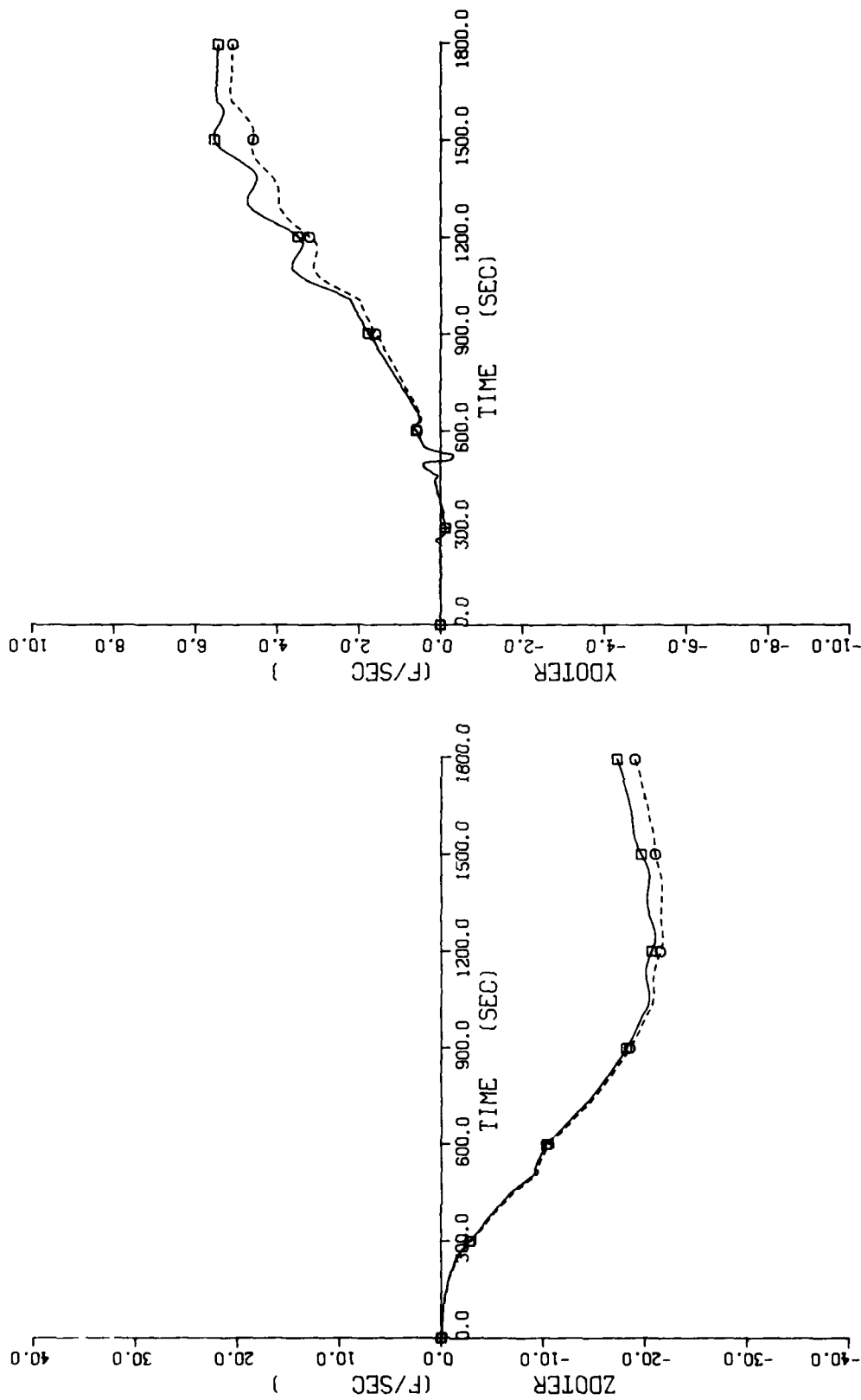
Figure 72. X and Y Velocity Errors, With and Without Least-Squares Averaging of Redundant Gyro Data, For Con-figuration 2 With No Structural Modes - Gyro Number 1 Failed

Figure 73. Latitude and Longitude Errors, With and Without Least-Squares Averaging of Redundant Gyro Data, For Configuration 2 With No Structural Modes – Gyro Number 5 Failed

Figure 74. X and Y Velocity Errors, With and Without Least-Squares Averaging of Redundant Gyro Data, For Configuration 2 With No Structural Modes – Gyro Number 5 Failed
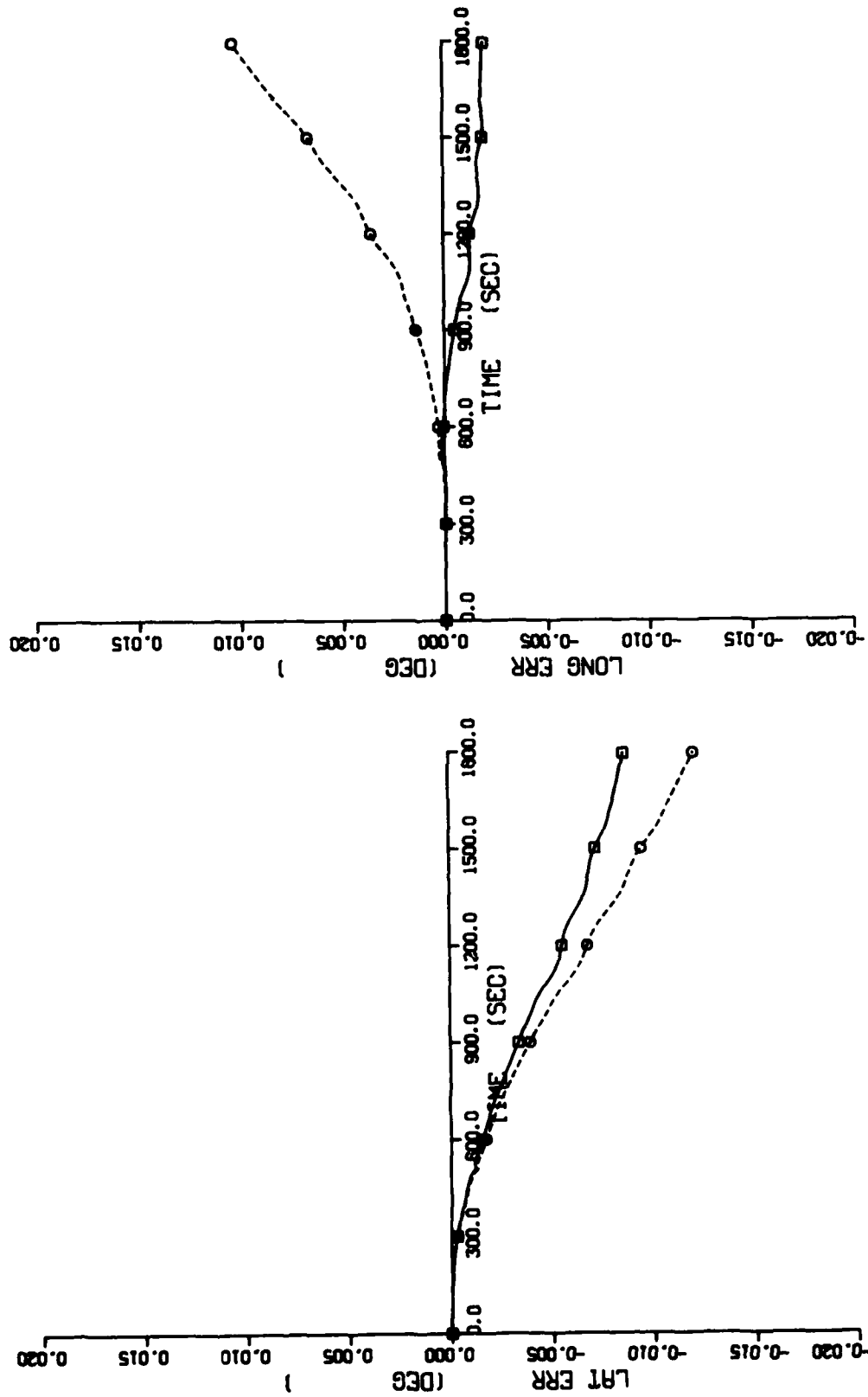
Figure 75. Latitude and Longitude Errors, With and Without Least-Squares Averaging of Redundant Gyro Data, For Configuration 2 With No Structural Modes - Gyro Numbers 1 and 5 Failed
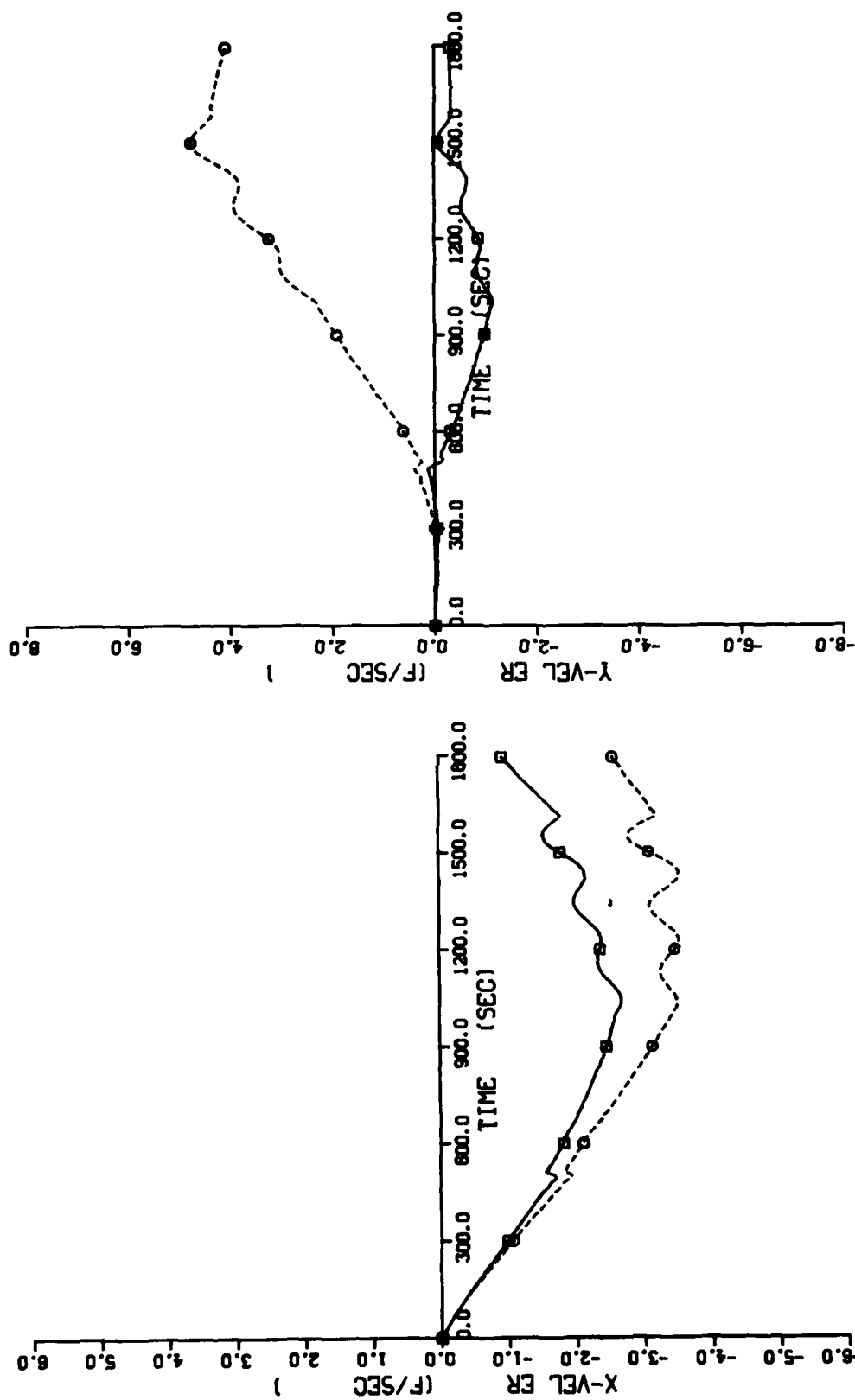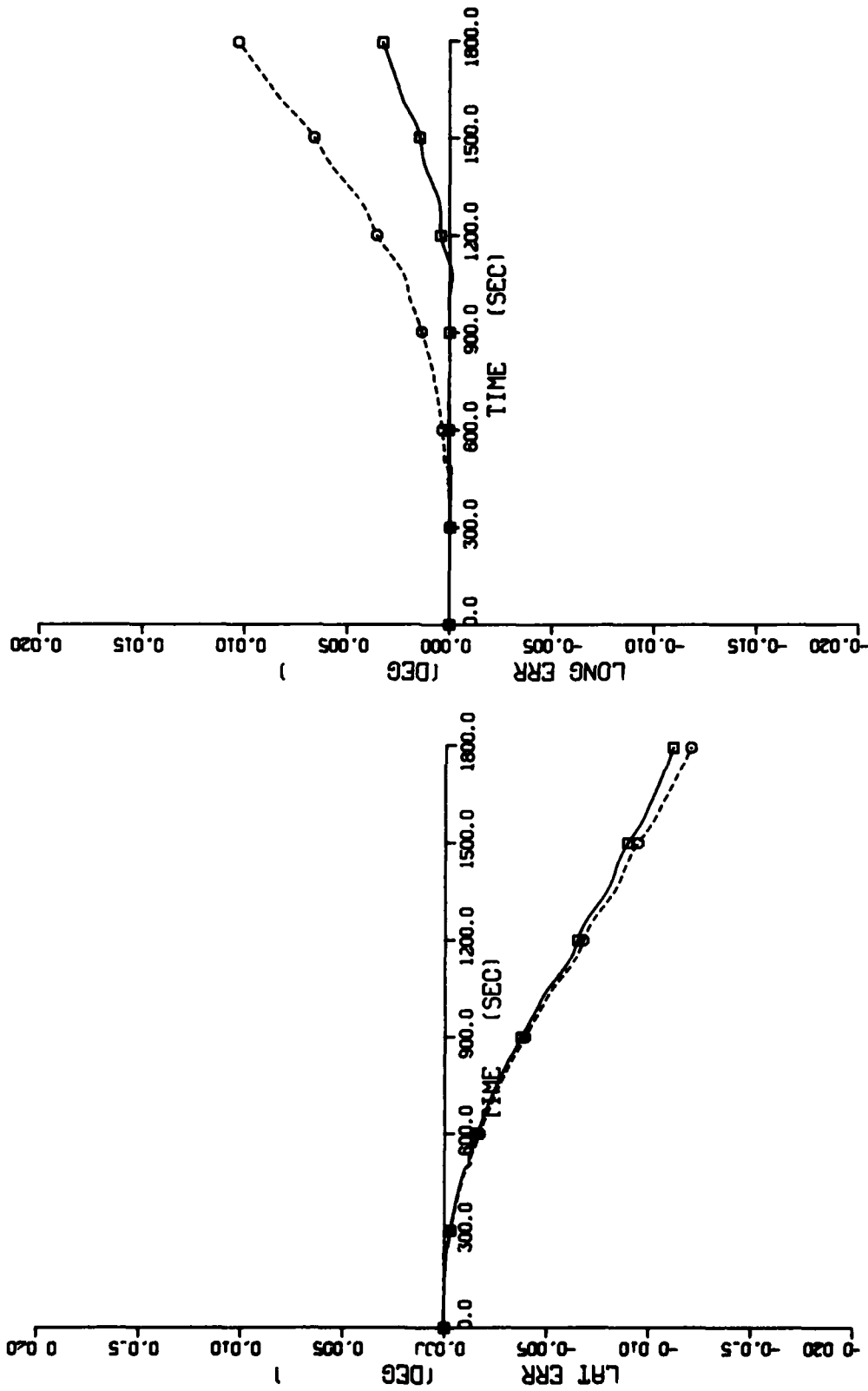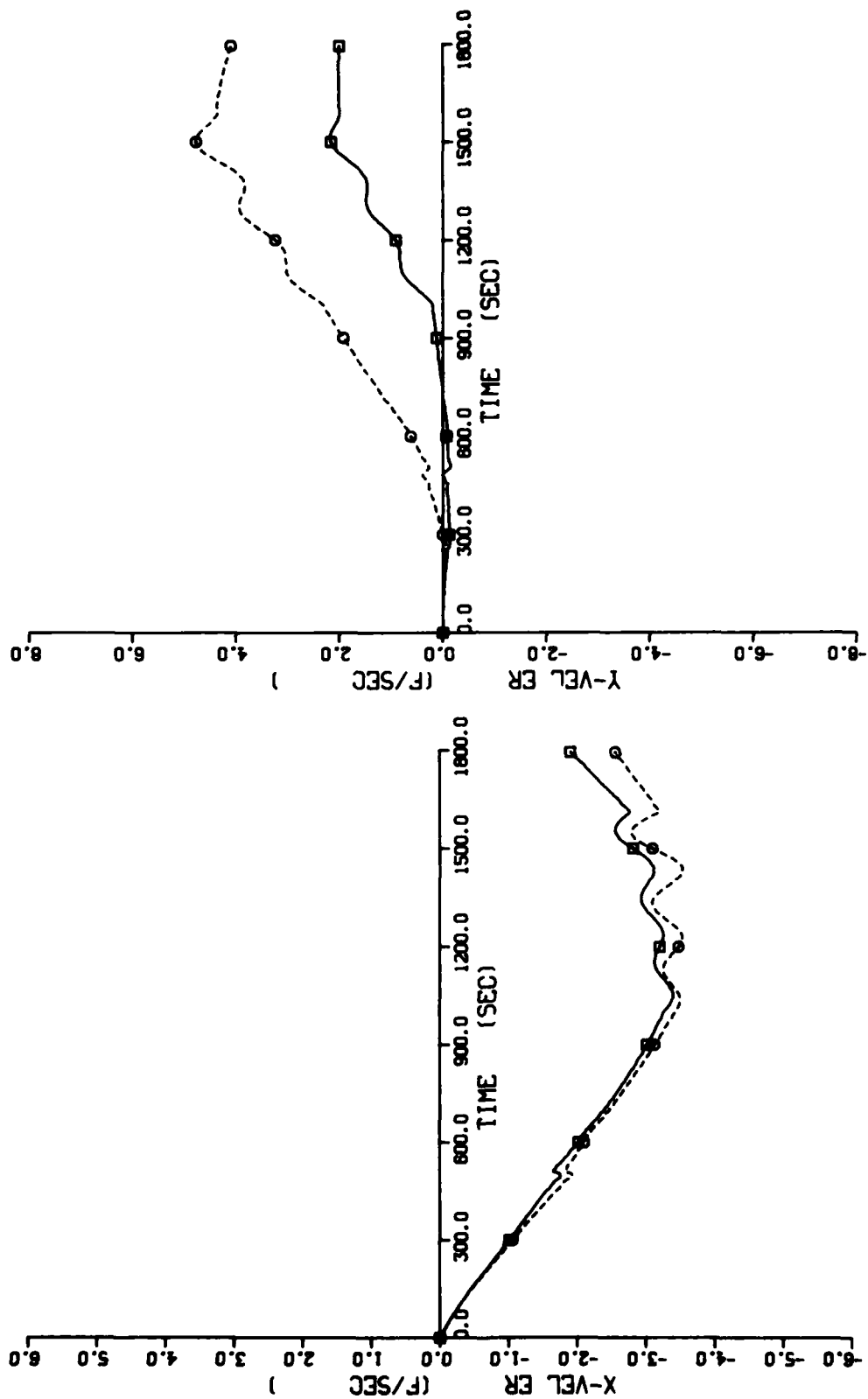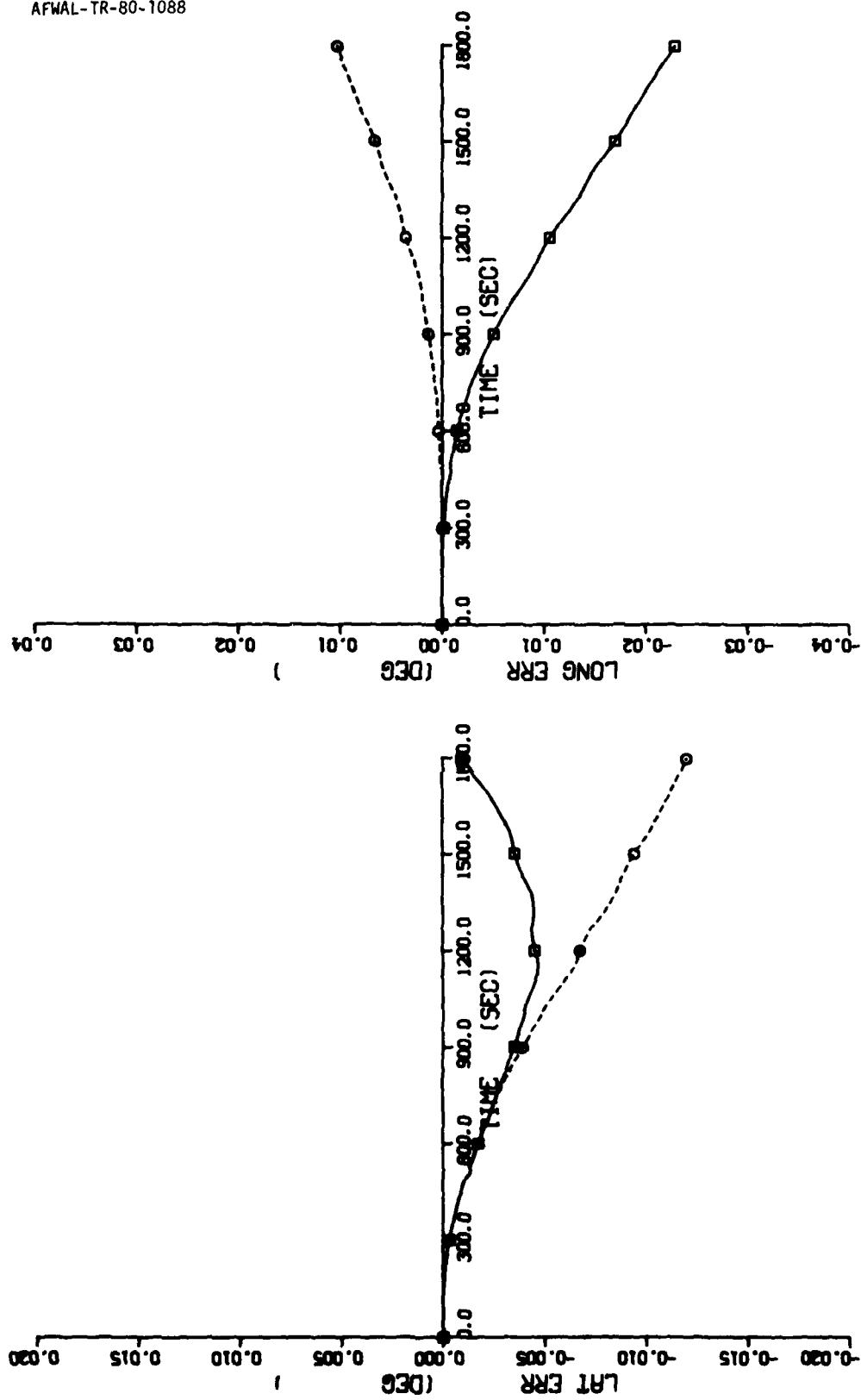
Figure 76. X and Y Velocity Errors, With and Without Least-
Squares Averaging of Redundant Gyro Data, For Con-
figuration 2 With No Structural Modes - Gyro Numbers
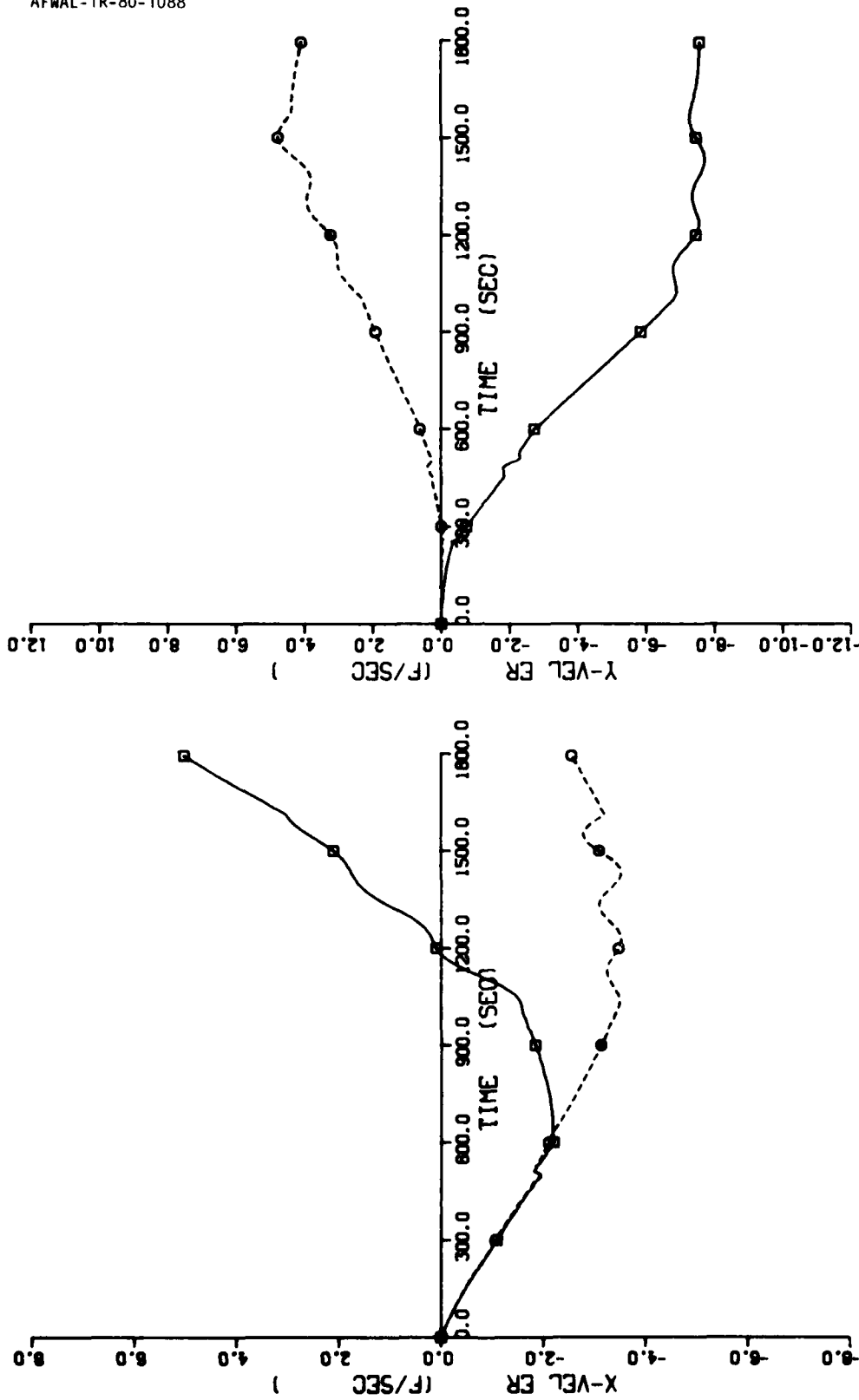1 and 5 Failed

4.   CONCLUSIONS

Least-squares averaging of the redundant inertial sensor data can significantly improve the performance of strapped down inertial reference systems employing redundant gyros and accelerometers. However, it should be recognized that sensor misalignment errors play a dominant roll in the performance achieved, and can in some instances, cause a degradation in performance rather than improvement. Thus, minimization of these errors should be of prime concern when application of least-squares averaging is considered.

A covariance analysis study effort should be accomplished to determine the extent each individual sensor error affects navigation system performance with least-squares averaging.

Weighted least-squares does not appear to add any benefits over least-squares averaging, for the types of sensors used, since accelerometer cross-coupling effects are minimal compared to the other errors. Thus, since ring laser gyros are not subject to cross-coupling effects, least-squares averaging without weighting is appropriate.

Estimation of the inertial sensor outputs and output rates can provide some measure of improvement for flight control, weapon delivery, and navigation. However, due to the additional computational requirements, this estimation is most beneficial when used in conjunction with failure detection/isolation (FDI) and redundancy management (RM) algorithms for redundant inertial sensor reference systems. The estimated sensor outputs can be used directly by the FDI algorithm for establishing and maintaining the variable failure thresholds necessary to perform reliable failure detection in the highly maneuvering environment of a fighter type aircraft.

When the inertial sensors were subjected to aircraft structural modes and lever arm effects, navigation system performance deteriorated significantly. The structural mode simulation was based upon theoretical analysis and vibration data for an F-4 aircraft. This data, while not being exact, was the best available for utilization in the simulation.

Based upon these results, navigation system performance is sensitive to location of the inertial sensors within the aircraft. The flight control system is also sensitive to inertial sensor location. However, utilization of compensation for the flight control system appears to be feasible. For navigation, the sensor errors need be reduced to reduce the effects of structural modes and lever arm. In particular, sensor misalignment errors need be reduced followed by bias and scale factor.

APPENDIX

RANDOM PROCESSES

Properties of several commonly used random processes are presented in this appendix. Only those processes used in this investigation are included. Specifically, the models are: random constant; random ramp; random walk; and exponentially correlated random variable.

1. RANDOM CONSTANT

A random constant, or random bias, can be represented by a state differential equation of the form

$$\dot{x} = 0 \tag{A.1}$$

with initial value

$$x(t_0) = \sigma \tag{A.2}$$

The mean square value for a random bias error source of magnitude σ is given by

$$E\left[x(t_0)x^T(t_0)\right] = \left[x^2(t_0)\right] = \sigma^2 \tag{A.3}$$

The Power Spectral Density (PSD) is given by

$$S(\omega) = 2\pi\sigma^2\delta(\omega) \tag{A.4}$$

A block diagram representation of this error source is given in Figure 77a. The initial conditions on the integrator being the rms error magnitude σ, which is the random quantity.

2. RANDOM RAMP

A random ramp is an error source which exhibits a linear growth rate with time. The random quantity for this error source is the growth rate. This error source can be described by two state differential equations of the form

$$\dot{x}_1 = x_2 \tag{A.5}$$
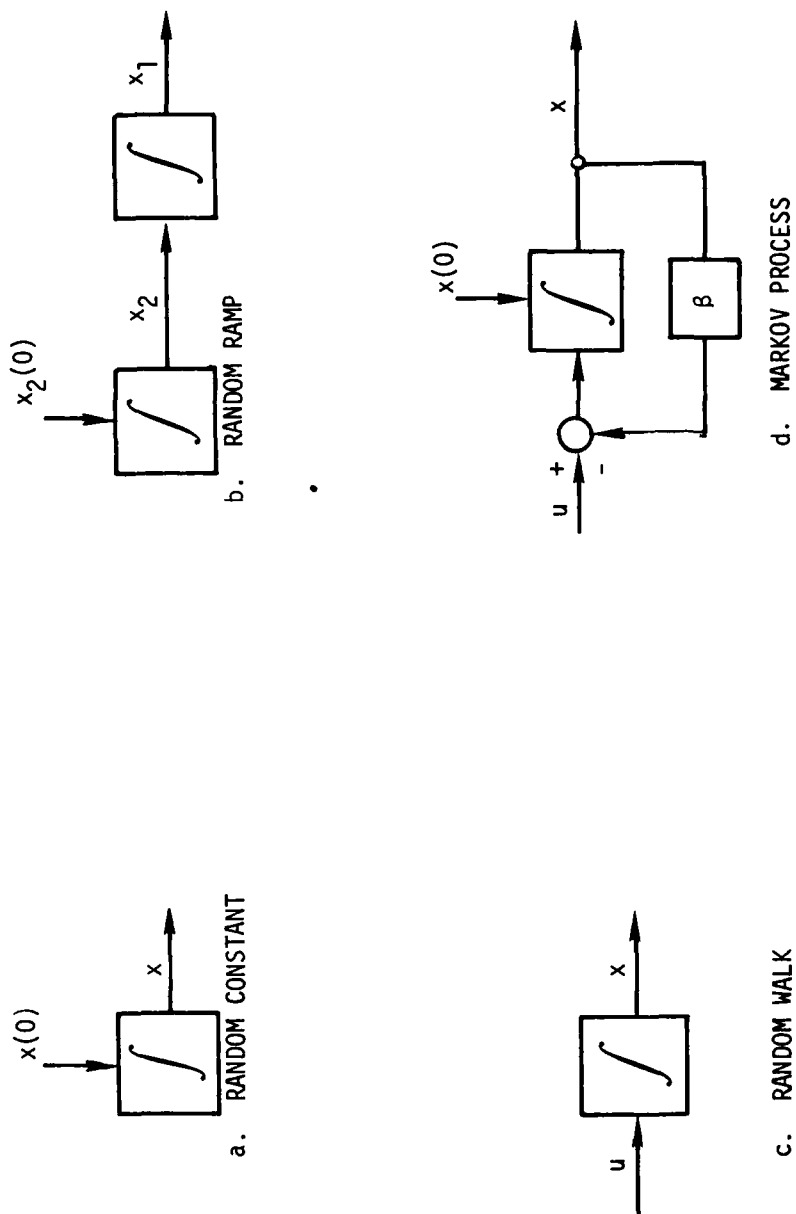
$$\dot{x}_2 = 0 \tag{A.6}$$

125

Figure 77. Common Random Process Model Block Diagrams

126

Thus, for this error source X_2 serves the roll of providing the random quantity. The randomness of the slope of the ramp, error state X_1, is established by the initial conditions of X_2, as did $X(t_0)$ in the random bias error case discussed above. Solving Equation A.5 gives

$$\dot{x}_1 = x_2 t \tag{A.7}$$

The mean-square value for a random ramp is given by

$$R(0) = E\left[x_1(t)x_1(t)\right] = E\left[x_2(t_0)t x_2(t_0)t\right]$$

$$R(0) = E\left[x_1^2(t)\right] = E\left[x_2^2(t_0)\right] t^2 \tag{A.8}$$

As in the random bias case

$$E\left[x_2(t_0)\right] = \sigma_2^2 \tag{A.9}$$

Thus

$$R(o) = \sigma_2^2 t^2 \tag{A.10}$$

A block diagram representation of the random ramp is shown in Figure 77b. The initial conditions on the integrators are

$$x_1(t_0) = 0$$

$$x_2(t_0) = \sigma_2 \tag{A.11}$$

3. RANDOM WALK

A random walk with error source can be represented by the state differential equation

$$\dot{x} = \sigma_1 u \tag{A.12}$$

where

$$\sigma_1 = \text{Constant}$$

$$u = \text{White noise with unity PSD}$$

and x has the initial value

$$x(t_0) = \sigma_2 \qquad\qquad (A.13)$$

Solving Equation A.12 for x gives

$$x(t) = \int_{t_o}^{t} \dot{x}(\tau)\, d\tau$$

$$= x(t_0) + \sigma_1 \int_{t_o}^{t} u(\tau)\, d\tau \qquad\qquad (A.14)$$

The autocorrelation function of white noise is a delta function. Thus, the autocorrelation function for a random walk error source is

$$
\begin{aligned}
R(t, t+\tau) &= E\left[x(t)x(t+\tau) \right] \\
&= E\left[x^2(0) \right] + E\left[x(0) \int_{t_o}^{t} \sigma_1 u(\zeta)\, d\zeta \right] \\
&\quad + E\left[x(o) \int_{t_o}^{t+\tau} \sigma_1 u(\zeta)\, d\zeta \right] \\
&\quad + E\left[\int_{o}^{t} \sigma_1 u(\xi)\, d\xi \int_{o}^{t+\tau} \sigma_1 u(\zeta)\, d\zeta \right] \qquad (A.15)
\end{aligned}
$$

In this case, $u(t)$ is white noise with zero mean. Also, $u(t)$ and $x(0)$ are uncorrelated. Thus, the two inner terms of Equation A.16 vanish and the equation is

$$R(t,t+\tau) = \sigma_2^2 + \sigma_1^2 \int_{t_o}^{t} \int_{t_o}^{t+\tau} \delta(\zeta-\xi) d\zeta d\xi$$

$$= \sigma_2^2 + \sigma_1^2 \int_{o}^{t} 1 \cdot d\xi$$

$$= \sigma_2^2 + \sigma_1^2 t \tag{A.16}$$

Typically, the initial value $x(t_0)$ is set equal to zero. This results in the autocorrelation function

$$R(\tau) = \sigma_1^2 t \tag{A.17}$$

A block diagram of the random walk error source is shown in Figure 77c. The initial conditions on the integrator are shown to be zero, which relates to Equation A.17.

4. EXPONENTIALLY CORRELATED RANDOM VARIABLES

An exponentially correlated random variable, or first order Markov process, can be represented by the differential equation

$$\dot{x}+\beta x = w \tag{A.18}$$

where

w = White noise

β = $1/t$

t = Correlation time

The initial conditions are given by

$$x(t_0) = \sigma \tag{A.19}$$

The autocorrelation function is given by

$$R(\tau) = \sigma^2 e^{-\beta|\tau|} \tag{A.20}$$

and the PSD is given by

$$s(\omega) = \int_{-\infty}^{\infty} \sigma^2 e^{\beta|\tau|} \cos(\omega\tau) d\tau \tag{A.21}$$

This integral can be represented by the sum of two integrals

$$s(\omega) = \int_{-\infty}^{0} \sigma^2 e^{\beta\tau} \cos(\omega\tau) d\tau + \int_{0}^{\infty} \sigma^2 e^{-\beta\tau} \cos(\omega\tau) d\tau$$

$$= 2 \int_{0}^{\infty} \sigma^2 e^{-\beta\tau} \cos(\omega\tau) d\tau \tag{A.22}$$

which integrates to

$$s(\omega) = \frac{2\sigma^2\beta}{\beta^2+\omega^2} \tag{A.23}$$

The resulting white noise spectral density necessary to generate the exponentially correlated random noise process is given in terms of the correlation time and variance. Thus, the exponentially correlated random variable is given by the state differential equation

$$\dot{x} = -\beta x + \sqrt{2\beta} \, \sigma u \tag{A.24}$$

where

u = White noise with unity PSD

A block diagram of the exponentially correlated random variable is shown in Figure 77d.

130

REFERENCES

1. Burns, R.C., "Multifunction Inertial Reference Assembly (MIRA)," McDonnell Douglas Corporation. Final Technical Report, Air Force Flight Dynamics Laboratory Report No. AFFDL-TR-78-105, Sept 1978.

2. Harrington, E.V., Bell, J.W., and Raroha, G. H., "A New Concept in Integrated Reference Systems," Proceedings of the AIAA Symposium on Integrated Systems, Los Angeles, California, Nov 1977.

3. Kubatt, Dr. Wolgang, J., "A Multifunctional Guidance and Control System," Proceedings of the IEEE 1977 National Aerospace and Electronics Conference, NAECON '77.

4. Elson, B.M., "Boeing Investigating New Sensor Types," Aviation Week and Space Technology, 18 October 1976, pp. 83-87.

5. Johnson, L. B., and Harrison, J.V., "Multifunction Inertial Sensing," Advanced Inertial Technologies, Air Force Avionics Laboratory Technical Report AFAL-TR-73-124, Volume II, November 1974.

6. Lipscomb, M.L., and Smith, F.D., "Inertial System Enhancement of Flight Control," Proceedings of the IEEE 1974 National Aerospace and Electronics Conference, NAECON '74.

7. Reynolds, R.H., "Deterministic Analysis of the Effects of Sensor Errors on Strapped-Down INS Performance," Air Force Institute of Technology Thesis, GE/EE/79-30, December, 1979.

8. Daly, K.C., Gai, E., and Harrison, J.V., "Generalized Likelihood Test for FDI in Redundant Sensor Configurations," Journal of Guidance and Control, Vol. 2, No. 1, Jan-Feb 1979, pp. 9-17.

9. Motyka, P.R., and Bell, J.W., "Failure Detection and Isolation for Tactical Aircraft Using the Generalized Likelihood Test," Proceedings at the IEEE 1980 National Aerospace and Electronics Conference, NAECON '80.

10. Britting, K.R., Inertial Navigation Systems Analysis, Wiley-Interscience, New York, 1971.

11. Wauer, J.C., "Practical Considerations in Implementing Kalman Filters," AGARD Lecture Series No. 82, March 1976.

12. Kalman, R.E., and Bucy, R.S., "New Results in Linear Filtering and Prediction Theory," Transactions of American Society of Mechanical Engineers, Series D, Journal of Basic Engineering, Vol. 83, March 1961, pp. 95-108.

13. Jazwinski, A.H., "Filtering for Nonlinear Dynamical Systems," IEEE Transactions on Automatic Control, Vol. AC-11, Nov 1966, pp. 765-766.

REFERENCES (CONCLUDED)

14. Sage, A.P., and Melsa, J.L., Estimation Theory with Application to Communications and Control, McGraw-Hill, New York, 1971.

15. Meditch, J.S., Stochastic Optimal Linear Estimation and Control, McGraw-Hill, New York, 1969.

16. Papoulis, A., Probability, Random Variables, and Stochastic Processes, McGraw-Hill, New York, 1965.

17. Gelb, A., Applied Optimal Estimation, The M.I.T. Press, Cambridge, Massachusetts, 1974.

18. Bell, J.W., Optimal Estimation Applied to Redundant Strapped Down Inertial Sensors For Navigation and Flight Control, Ph.D. Dissertation, University of Dayton, 1979.

19. Friedland, B., "Estimating Angular Velocity From Output of Rate-Integrating Gyro," IEEE Transactions on Aerospace and Electronic Systems, Vol. AES-11, No. 4, July 1975, pp. 551-555.

DATE
ILMED
—8